Distribution Agreement

In presenting this thesis or dissertation as a partial fulfillment of the requirements for an advanced degree from Emory University, I hereby grant to Emory University and its agents the non-exclusive license to archive, make accessible, and display my thesis or dissertation in whole or in part in all forms of media, now or hereafter known, including display on the world wide web. I understand that I may select some access restrictions as part of the online submission of this thesis or dissertation. I retain all ownership rights to the copyright of the thesis or dissertation. I also retain the right to use in future works (such as articles or books) all or part of this thesis or dissertation.

Signature:

_____ _____

Santiago Archila Date

Experimental and computational evidence for regulation of synaptic conductance via graded homeostasis of post-synaptic chloride concentration

By

Santiago Archila

Doctor of Philosophy

Graduate Division of Biological and Biomedical Science

Neuroscience

_____	_____
Astrid A. Prinz, Ph.D. Advisor	Dieter Jaeger, Ph.D. Committee Member
_____	_____
Ronald Calabrese, Ph.D. Committee Member	Andrew Jenkins, Ph.D. Committee Member
_____	_____
Jorge Golowasch, Ph.D. Committee Member	Peter Wenner, Ph.D. Committee Member

Accepted:

_____
Lisa A. Tedesco, Ph.D.
Dean of the James T. Laney School of Graduate Studies

_____
Date

Experimental and computational evidence for regulation of synaptic conductance via graded homeostasis of post-synaptic chloride concentration

By

Santiago Archila

B.S., Georgia Institute of Technology, 2006

Advisor: Astrid A. Prinz, Ph.D.

An abstract of

A dissertation submitted to the Faculty of the

James T. Laney School of Graduate Studies of Emory University

in partial fulfillment of the requirements for the degree of

Doctor of Philosophy

Graduate Division of Biological and Biomedical Science

Neuroscience

2013

Abstract

Experimental and computational evidence for regulation of synaptic conductance via graded homeostasis of post-synaptic chloride concentration

By Santiago Archila

Neuronal networks often alter the strength of their synaptic connections in response to activity perturbations. The general understanding is that these responses exist to compensate for the perturbation and recover normal activity, though the dynamics of this synaptic plasticity, how it affects ongoing network activity, and how such regulation might be mediated are unclear. In this work, I aimed to answer these questions by monitoring the conductance dynamics of a single identified synapse – the inhibitory lateral pyloric (LP) to pyloric dilator (PD) synapse in the stomatogastric ganglion of the crab *Cancer borealis* – in response to a post-synaptic voltage perturbation. Though the voltage perturbation affected activity and triggered a change in synaptic conductance, I show that the synapse did not appear to influence any attribute of network activity. Instead, by matching the experimental results with those of a computational model, I found that the response was consistent with homeostatic regulation of post-synaptic internal chloride, the primary permeant ion through these synaptic channels. Finally, I show experimentally that direct disruption of chloride levels alone – by targeting an iontophoretic injection of chloride into PD without disrupting network activity – can trigger a change in synaptic conductance, uncovering experimental evidence consistent with a graded regulation of synaptic conductance driven by post-synaptic chloride homeostasis.

Experimental and computational evidence for regulation of synaptic conductance via graded homeostasis of post-synaptic chloride concentration

By

Santiago Archila

B.S., Georgia Institute of Technology, 2006

Advisor: Astrid A. Prinz, Ph.D.

A dissertation submitted to the Faculty of the

James T. Laney School of Graduate Studies of Emory University

in partial fulfillment of the requirements for the degree of

Doctor of Philosophy

Graduate Division of Biological and Biomedical Science

Neuroscience

2013

TABLE OF CONTENTS

FIGURES

TABLES

CHAPTER 1 :

GENERAL INTRODUCTION

Stability from variable underlying parameters

Neural circuits produce reliable and consistent electrical output throughout life despite developmental growth, environmental changes, and cellular molecules that turn over with a time scale of minutes to weeks (Marder and Prinz 2002, Bucher, Prinz et al. 2005). The fact that network activity is maintained within a functional range over such long time scales while the underlying cellular components are turned over relatively quickly (Bucher, Prinz et al. 2005) suggests that regulatory mechanisms may exist in these circuits to constrain neuronal parameters, such as "cell-intrinsic" membrane conductances or synaptic conductances, to produce this reliable, consistent activity (Marder and Goaillard 2006). Interestingly, theoretical and experimental studies show that the cell-intrinsic and synaptic parameters underlying this network stability can be (and often are) variable (Prinz, Bucher et al. 2004, Bucher, Prinz et al. 2005, Marder and Goaillard 2006, Goaillard, Taylor et al. 2009, Roffman, Norris et al. 2012). These findings have led to the idea that neurons need not set their cellular and synaptic parameters to necessarily achieve some constrained channel density, subunit composition, synaptic release probability, etc. This variability provides evidence that underlying neuronal parameters may be plastic, adaptable, and variable but could be regulated with a homeostatic target of stable network activity.

The term homeostatic here refers to the concept of biological self-regulation, as coined by Walter Cannon over eighty years ago (Cannon 1932). He observed that

many parameters of the human body (e.g. body temperature, pH, internal balance of salts) were remarkably stable throughout life and that the body had mechanisms to self-regulate these parameters to within functional bounds.

In the last twenty years, Cannon's concept of homeostasis has been extended into neuronal circuits to explain the reliability and consistency that is observed in neuronal network electrical activity. Theoretical work demonstrated that a computational crustacean stomatogastric neuron model whose ionic membrane currents had maximal conductances that were dependent on internal calcium concentrations (and so were indirectly dependent on electrical activity) could achieve stable levels of target neuronal activity (LeMasson, Marder et al. 1993). Ignoring the synaptic input for now, Figure 1.1 represents how activity homeostasis could occur by activity-dependent regulation of cell-intrinsic membrane conductances. If neuronal activity becomes too high, it could be due to a high level of depolarizing channels or a low level of hyperpolarizing channels. This imbalance is sensed by the neuron as an increase in the intracellular concentration of calcium (Figure 1.1, right panel). In order to recover the target activity level, the neuron must downregulate depolarizing channels, upregulate hyperpolarizing channels, or both. The converse is true for recovery from a situation where its activity is too low.

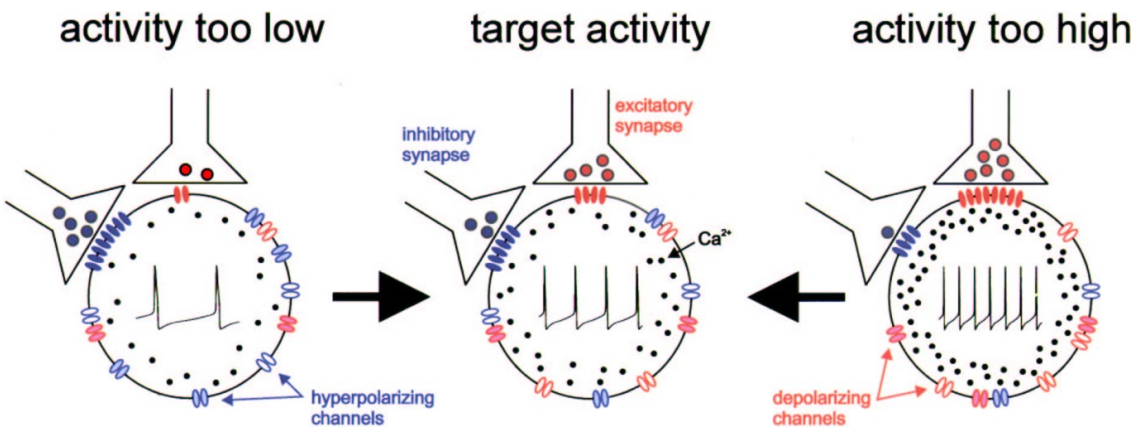

Figure 1.1 Schematized concept of activity homeostasis in neurons

Theory of activity dependent homeostatic regulation is that regulation mechanisms constrain neuronal electrical activity to a target level, shown at center. If activity is sensed as being too high by the increased concentration of Ca^{2+} in the cell, it is likely due to either a high number of depolarizing channels, a low number of hyperpolarizing channels, high excitatory synaptic drive, or low inhibition (right). The cell can adjust these membrane or synaptic conductances to return to target activity (see transition from right back to center). The opposite is hypothesized for when activity is lower than the target level (left). Figure from (Marder and Prinz 2002)

Soon after this form of cell-intrinsic membrane conductance regulation was theorized, Turrigiano et al. demonstrated experimentally that when an individual crustacean stomatogastric neuron that normally fires bursts of action potentials within its network was removed and cultured in isolation, the neuron was capable of transitioning from an acute silent or tonic spiking activity pattern to recovering a bursting activity pattern similar to that which it produced in the connected network (Turrigiano, Abbott et al. 1994) (Figure 1.2). This study was among the first to show experimental evidence for the idea that a neuron's electrical activity is itself a parameter regulated to stay within a homeostatic target level; one that, when perturbed outside of functional bounds (in this case by acute isolation in culture), can initiate homeostatic regulation mechanisms in the neuron to compensate and recover normal activity levels.

Stability may be achieved through regulation mechanisms that target cell-intrinsic or synaptic properties

Neural circuit dynamics rely on interactions between cell-intrinsic membrane currents and synaptic currents (Marder and Calabrese 1996, Marder 1998). Therefore, regulation mechanisms that induce compensatory changes in either of these properties have the ability to control circuit output.

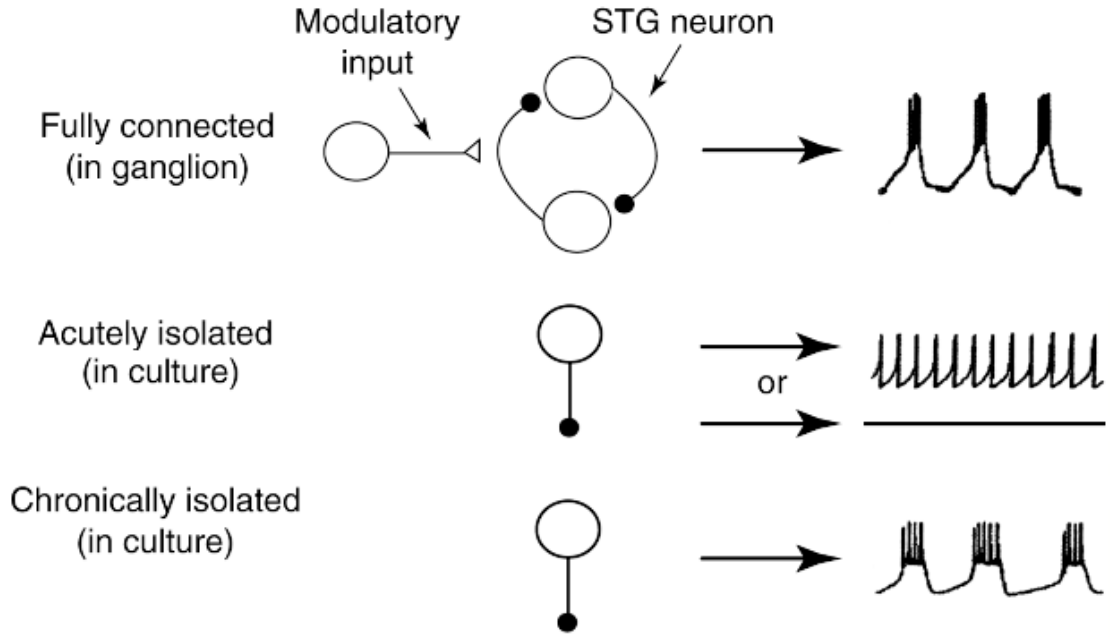

Figure 1.2 Activity homeostasis in cultured neurons.

Crustacean stomatogastric ganglion (STG) neurons display behavior consistent with homeostatic regulation of spiking activity after chronic isolation in culture. In situ with synaptic connections and modulatory inputs intact, the stomatogastric neuron fires bursts of action potentials (top panel). When acutely isolated in culture, the neuron spikes tonically or goes silent (center panel). After several days isolated in culture, the neuron regains the ability to fire bursts of action potentials (bottom panel). The modulatory input shown represents the entire complement of inputs that modulate all the crustacean stomatogastric neurons. Figure adapted from (Turrigiano 1999).

Regulation of cell-intrinsic membrane currents, such as the up-regulation or down-regulation of hyperpolarizing or depolarizing channels as shown in Figure 1.1, has now been shown in many systems in response to perturbations of normal activity levels using pharmacological agents or manipulation in the amount of neuromodulatory, excitatory, or inhibitory input.

For example, in the aforementioned cultured crustacean stomatogastric neurons (Figure 1.2), the activity deprivation that occurred when stomatogastric neurons were isolated in culture led to an overall increase in cellular excitability (Turrigiano, Abbott et al. 1994) that was mediated by increases in inward currents and decreases in outward currents (Turrigiano, LeMasson et al. 1995). Ever since these seminal studies, many others have found that activity-dependent regulation of cell-intrinsic membrane currents can lead to stability of network activity as well as recovery of normal activity levels following an activity perturbation (Desai, Rutherford et al. 1999, Golowasch, Abbott et al. 1999, Golowasch, Casey et al. 1999, Haedo and Golowasch 2006, Pratt and Aizenman 2007, Wilhelm, Rich et al. 2009, Bergquist, Dickman et al. 2010, Ransdell, Nair et al. 2012). Though the investigation of homeostatic changes to cell-intrinsic membrane currents is an interesting topic of study, this dissertation focuses on the complementary avenue of homeostatic regulation: that of synaptic transmission.

Like cell-intrinsic membrane currents, synaptic currents are also adaptable, a phenomenon known as synaptic plasticity (Turrigiano 2012). Therefore, besides

modulating the balance of membrane currents within each cell, neuronal networks may exhibit synaptic plasticity mechanisms to affect activity (as demonstrated in Figure 1.1).

There is a rich body of literature on synaptic plasticity, but until about 15 years ago, much of the work on synaptic plasticity had focused on Hebbian plasticity (such as long-term potentiation and long-term depression) at hippocampal or cerebellar excitatory synapses (Turrigiano, Leslie et al. 1998). In Hebbian plasticity, an excitatory synapse is strengthened according to the ability of an action potential in the pre-synaptic neuron to cause an action potential in the post-synaptic neuron (Hebb 1949). If a pre-synaptic spike reliably triggers a post-synaptic spike, the connection is potentiated. If a pre-synaptic event is consistently unable to trigger a post-synaptic action potential, the connection is weakened.

The need for a stabilizing negative-feedback form of plasticity was recognized after it was found that Hebbian synaptic plasticity inherently destabilized network activity (Abbott and Nelson 2000). Alone, it would lead to a positive feedback loop in which strong synapses become increasingly more likely to get strengthened while weak synapses become more likely to get weakened (Turrigiano 1999, Abbott and Nelson 2000).

Homeostatic synaptic plasticity

Due to a more clear understanding of the destabilizing effects of Hebbian plasticity, recently there has been an explosion of interest in a converse form of synaptic plasticity: homeostatic synaptic plasticity (HSP). In HSP, synapses change in strength and number to stabilize neuronal and circuit activity (as in the synaptic connections depicted in Figure 1.1). Currently evidence for HSP has been observed in many different networks such as cultured cortical (Turrigiano, Leslie et al. 1998, Kilman, van Rossum et al. 2002) and hippocampal neurons (Burrone, O'Byrne et al. 2002, Hartman, Pal et al. 2006, Stellwagen and Malenka 2006), rat visual cortex (Desai, Cudmore et al. 2002), *Drosophila* neuromuscular junction (Davis and Goodman 1998), the developing chick embryo (Gonzalez-Islas and Wenner 2006), and the tadpole optic tectum (Deeg and Aizenman 2011).

One way HSP is expressed functionally in a neuron is through synaptic scaling (Turrigiano, Leslie et al. 1998, Turrigiano 1999). In synaptic scaling, a neuron will globally scale its input synaptic currents up or down by a common multiplicative factor to regulate its own excitability and total synaptic input while preserving relative synaptic weights.

The study that introduced synaptic scaling induced scaling in rat visual cortical cultures by either bath-applying tetrodotoxin (TTX, a sodium channel blocker) or 6-cyano-7-nitroquinoxaline-2,3-dione (CNQX, an AMPA receptor

antagonist) (Turrigiano, Leslie et al. 1998). Both of these perturbations blocked spiking activity throughout the entire cultured network. Following several days bathed in TTX or CNQX, miniature excitatory post-synaptic current (mEPSC) amplitudes within the network increased proportionally. The opposite effect was observed when GABA-mediated inhibition was blocked throughout the network by bath-applied bicuculine. The reduced inhibition in the network led to an acute increase in spiking activity, but over two days in culture, mESPC amplitudes decreased proportionally and spiking returned to near control values. This study pioneered the concept that HSP mechanisms like synaptic scaling are triggered by changes in activity and act primarily to regulate spiking toward a target activity level (Turrigiano 1999).

Inhibitory homeostatic synaptic plasticity

Most studies of HSP demonstrate changes in excitatory synaptic currents. Though not as well characterized as HSP of excitatory synapses, HSP of inhibitory synapses has also been observed. In a paradigm similar to that which induced synaptic scaling of excitatory currents, cultured pyramidal neurons were treated with TTX to block all spiking activity for 2 days. Much like the scaled increase in mEPSCs observed after activity deprivation, miniature inhibitory post-synaptic currents (mIPSCs) exhibited a scaled decrease, an effect that was mediated by a decrease in the number of post-synaptic GABA-A receptors (Kilman, van Rossum et al. 2002). Other work from cultured rat hippocampal neurons demonstrated that,

though network-wide activity blockade does reduce mIPSCs, the mechanism appears to be through a reduction in pre-synaptic vesicle filling (Hartman, Pal et al. 2006).

Interestingly, work in the developing chick embryo has shown that activity deprivation by lidocaine infusion *in ovo* can scale GABAergic miniature post-synaptic currents up (Gonzalez-Islas and Wenner 2006). This is the opposite direction than was previously observed for GABAergic scaling after activity block, but at this early stage in development, GABA is depolarizing due to an increased level of intracellular chloride accumulation in immature neurons (Ben-Ari, Khalilov et al. 2012). For this reason, the increase in GABAergic current amplitude did have the effect of increasing excitability following activity deprivation (Gonzalez-Islas and Wenner 2006). Unlike previous studies of GABAergic scaling, no evidence was found for changes in either the amount of post-synaptic GABA receptors or the amount of pre-synaptic vesicle filling; instead the scaling up of GABAergic currents in the developing chick was mediated by a shift in the chloride reversal potential (Gonzalez-Islas, Chub et al. 2010).

Other potential mechanisms exist for HSP of inhibitory synapses, such as stimulation of release of circulating factors, e.g. endogenously synthesized neurosteroids that increase GABAergic transmission (Belelli and Lambert 2005).

The work presented in this dissertation focuses on characterizing the role of synaptic plasticity at a specific inhibitory synapse and how that plasticity might be mediated.

Central pattern generators display highly stable network activity

To characterize how effective plasticity at an inhibitory synapse can be in regulating activity, it is imperative to establish quantifiable measures of neuronal or network activity. This is simplified if the neuronal network produces a stable, stereotyped pattern of activity, making it feasible to determine, in measureable quantities, how a perturbation changes electrical activity and how that network activity changes dynamically over time. In few other networks are the outputs as stable and as stereotyped as in central pattern generators. Central pattern generators (CPGs) are neuronal networks that can produce coordinated rhythmic output for patterned tasks such as walking, chewing, swimming, and breathing without the need for descending input (Marder and Calabrese 1996).

CPGs are useful for characterizing network homeostasis because the circuits that drive this rhythmic behavior – even when isolated from their muscle targets – often display a "fictive motor pattern" in which the network will fire a rhythmic pattern of electrical activity *in vitro* or *in situ* that would lead to the rhythmic muscle activation in the live animal (Marder and Calabrese 1996). Thus, the target electrical activity of a CPG can be clearly defined and highly consistent. For these

reasons, perturbing a CPG's output in order to trigger a homeostatic change is feasible, and the responses to such perturbations are readily quantifiable.

The pyloric central pattern generator as a model system

One way to begin to characterize the effects of complex synaptic interactions on activity in biological circuits is to study them in a simpler invertebrate model, such as the aforementioned crustacean stomatogastric ganglion (STG) neurons. The STG is a cluster of neurons located in the stomatogastric nervous system (STNS) of crabs and lobsters (decapod crustaceans) that control the movements of the animal's stomach musculature (Harris-Warrick, Marder et al. 1992, Marder and Bucher 2007) (see Figure 1.3a-c for a depiction of the STNS in the crab *Cancer borealis*). This system is ideal for studying network function because it has a small number of consistently identifiable neurons with well-characterized membrane conductances and synaptic connections (Marder and Bucher 2007). The *Cancer borealis* STG contains 25 or 26 neurons (variable from animal to animal) whose cell bodies are located in the posterior section of the ganglion with their neurites occupying the anterior section in a densely packed neuropil region (Kilman and Marder 1996). In addition to the STG, the stomatogastric nervous system also includes two commissural ganglia (CoG) and one esophageal ganglion (OG) that provide descending neuromodulatory input to the neurons of the STG through the stomatogastric nerve (stn) (Figure 1.3c).

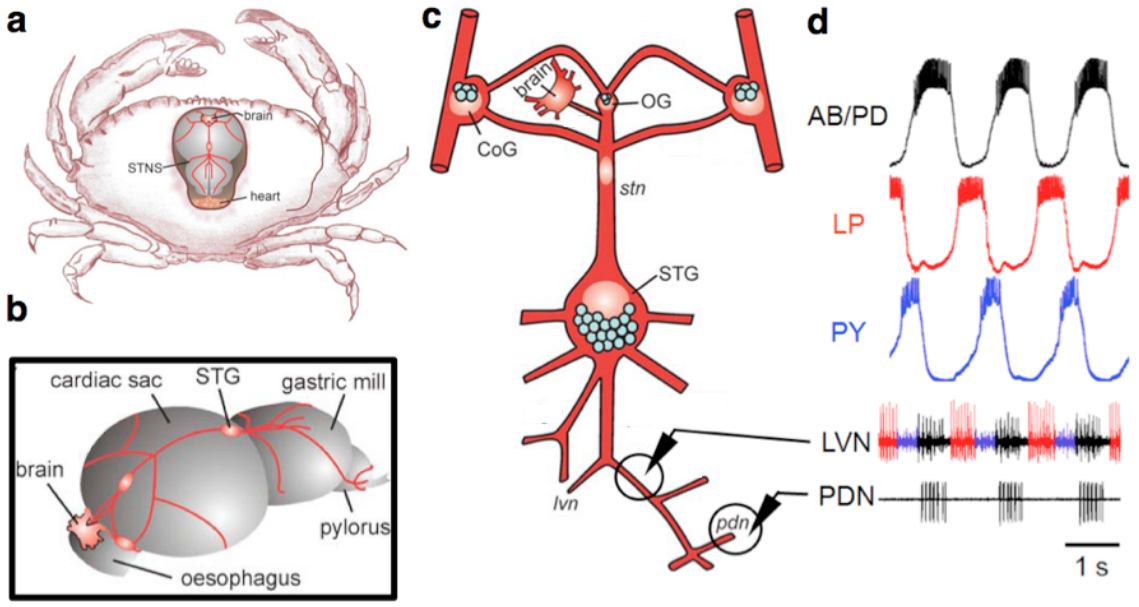

Figure 1.3 The *Cancer borealis* stomatogastric nervous system and the characteristic activity of the crustacean pyloric network.

(a) The stomatogastric nervous system is situated dorsomedially in the crab Cancer borealis. (b) The nervous system wraps around and controls the muscles of the crab's stomach. (c) Pyloric network neurons are located in the stomatogastric ganglion (STG) and project their axons bilaterally down the lateral ventricular nerves (lvns). In vivo and in situ, STG neurons receive descending modulatory input via the stomatogastric nerve (stn). Pale blue circles represent cell bodies. (d) Coordinated bursting activity can be observed intracellularly or extracellularly from nerve recordings. Ganglia – CoG: commissural ganglion (bilateral pair); OG: oesophageal ganglion; STG: stomatogastric ganglion. Nerves – stn: stomatogastric nerve; lvn: lateral ventricular nerve; pdn: pyloric dilator nerve. Neurons - AB: anterior burster; PD: pyloric dilator; LP: lateral pyloric; PY: pyloric constrictor. (a-c) adapted from (Stein 2009) (d) adapted from (Prinz, Bucher et al. 2004)

There are two CPGs whose component neurons are housed in the crustacean STG: a gastric mill CPG that controls a set of teeth that grind food particles within the stomach, and a pyloric CPG that controls the rhythmic constriction and dilation of the animal's foregut. In this work, we focus only on neurons of the pyloric network.

The crustacean pyloric circuit can be separated into 3 functionally distinct nodes. The neurons that comprise these neuronal nodes fire in successive bursts and, through mutual inhibition, give rise to the characteristic triphasic pyloric firing pattern with a network cycle period that ranges from 0.5–1.5 s in *Cancer borealis* (Figure 1.3d) (Goaillard, Taylor et al. 2009). The anterior burster/pyloric dilator (AB/PD) node, which consists of one AB neuron that is electrically coupled to two PD neurons through gap junctions, is considered the circuit pacemaker and often referred to collectively as the pacemaker complex. When descending neuromodulatory inputs from the CoGs and OG are intact, AB displays an oscillatory membrane potential and drives the two PD neurons to oscillate in synchrony through gap junctions (Harris-Warrick, Marder et al. 1992). In the crab, the AB neuron of the pacemaker complex sends glutamatergic inhibitory synapses to the single lateral pyloric (LP) neuron and the three-to-five pyloric constrictor (PY) neurons (Figure 1.4), creating the staggered periodic bursting in those two circuit nodes that follows the pacemaker complex burst (Figure 1.3d).

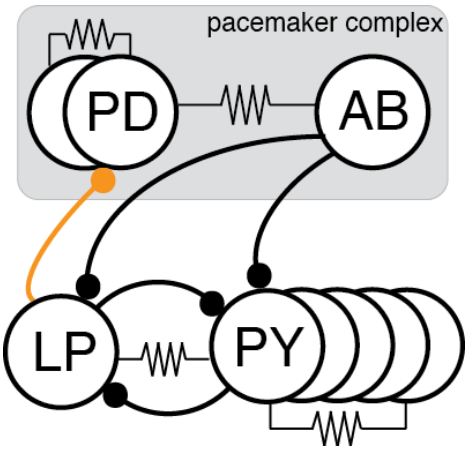

Figure 1.4 Connectivity diagram of the *Cancer borealis* pyloric circuit.

Schematized pyloric network of the crab with the synapse of interest highlighted in orange. All chemical synapses are glutamatergic inhibitory synapses. Resistor symbols represent electrical connections through gap junctions. Neurons - AB: anterior burster; PD: pyloric dilator (2); LP: lateral pyloric; PY: pyloric constrictor (3-5).

The neurons of the crustacean pyloric circuit are referred to as conditional bursters because if the stn that carries neuromodulatory inputs to the STG is cut or action potential conduction is blocked in the nerve by building a petroleum jelly well that includes tetrodotoxin (TTX, a sodium channel blocker) around the nerve, the triphasic rhythm is quickly abolished. The acute response to this form of neuromodulator block is that each cell in the circuit falls silent or spikes tonically (Thoby-Brisson and Simmers 1998, Golowasch, Casey et al. 1999). In the STG literature, this technique of modulatory input block is known as decentralization.

Importantly for this work, crustacean STG neurons have been shown to exhibit long-term activity homeostasis and are able to recover their characteristic bursting pattern in the face of activity perturbations. As mentioned previously, isolation of a crustacean stomatogastric neuron in culture led to an acute loss of rhythmic bursting activity, which was subsequently regained after several days in isolation (Turrigiano, Abbott et al. 1994) (Figure 1.2). STG pyloric neurons are also able to recover functional triphasic network activity several days after falling silent by decentralization *in situ* (Thoby-Brisson and Simmers 1998, Golowasch, Casey et al. 1999, Thoby-Brisson and Simmers 2000, Thoby-Brisson and Simmers 2002, Luther, Robie et al. 2003, Khorkova and Golowasch 2007) (Figure 1.5). Because these neurons have the ability to restore their characteristic activity pattern after perturbation, there is a solid history of work in the STG devoted to studying cellular and network homeostasis.

Much of this work has gone into characterizing the changes in cell-intrinsic membrane currents that these neurons undergo and the implications these changes have for network stability (Marder and Goaillard 2006), but less is known about the role of synaptic homeostasis mechanisms in the pyloric circuit. Of note, one modeling study indicated that synaptic regulation mechanisms could potentially support stability of the triphasic pyloric bursting pattern (Soto-Trevino, Thoroughman et al. 2001). This model predicted that if one were to clamp a post-synaptic STG neuron at a depolarized or hyperpolarized voltage, it would trigger a respective increase or decrease in inhibitory synaptic strength; but the synaptic

regulation rules used in the study lacked experimental basis and have not been directly tested in the living system since then.

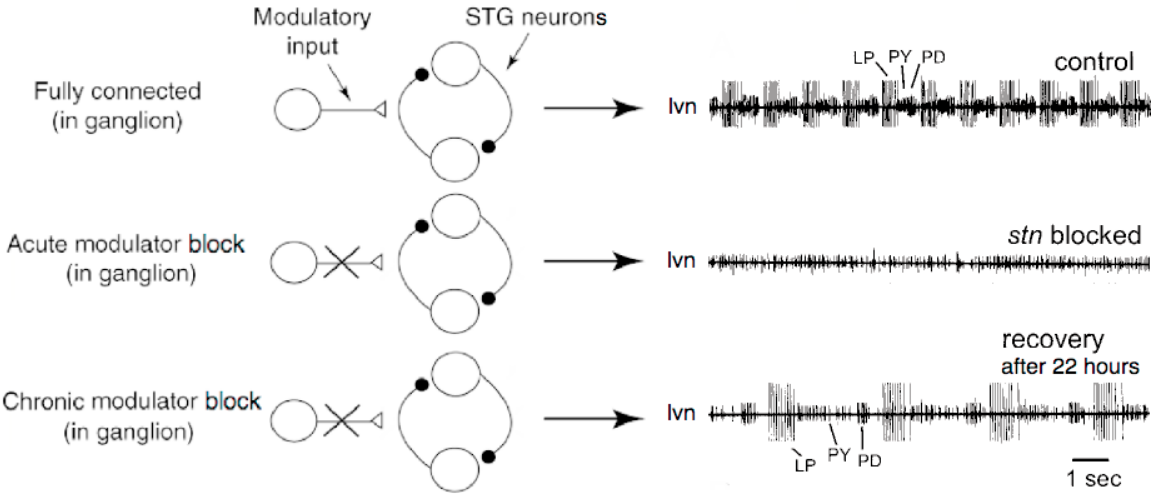

Figure 1.5 Activity homeostasis in the pyloric circuit following decentralization.

Crustacean STG neurons display behavior consistent with homeostatic regulation of network activity after chronic neuromodulatory block in situ. The modulatory input shown represents all descending inputs via the stomatogastric nerve (stn) that modulate the crustacean STG neurons. With neuromodulatory inputs intact, the pyloric neurons fire bursts of action potentials that can be observed through lateral ventricular nerve (lvn) recordings (top panel). Following acute neuromodulator block by either cutting the stn or by blocking electrical conduction with a sucrose and TTX well around the stn, the neurons spike tonically or go silent (center panel). After several days, the pyloric neurons regain the ability to fire bursts of action potentials and recover the characteristic triphasic bursting pattern (bottom panel). Neurons - PD: pyloric dilator; LP: lateral pyloric; PY: pyloric constrictor. Figure adapted from (Golowasch, Casey et al. 1999) and (Turrigiano 1999)

The LP-to-PD pyloric synapse

The synaptic connection I focus on in this dissertation is the synapse from the LP neuron to one of the PD neurons in the pacemaker complex (Figure 1.4, in orange). In the crustacean STG, this synaptic connection is known to be an inhibitory glutamatergic synapse. Although early on, the inhibitory glutamatergic response in STG neurons was examined in a related crab species, *Cancer pagurus* (Marder and Paupardin-Tritsch 1978), most systematic analyses of crustacean inhibitory glutamatergic receptor properties have been performed in lobster (Eisen and Marder 1982, Marder and Eisen 1984, Cleland and Selverston 1995, Cleland and Selverston 1997, Cleland and Selverston 1998). Agonist and antagonist profiles among inhibitory glutamatergic receptors in crabs (*Cancer*) and lobsters (*Panulirus* and *Homarus*) show no differences in sensitivity, suggesting that they are related (Table 1.1). Glutamatergic transmission is blocked by picrotoxin *in situ* (Marder and Eisen 1984) as well as in culture (Cleland and Selverston 1998) in both crabs and lobsters. Thus, properties of inhibitory glutamatergic receptors in crab are assumed to be similar to those reported in studies of lobster neurons.

In one potential difference between these species, lobster inhibitory glutamatergic receptors increase conductance primarily to chloride but also to potassium (Eisen and Marder 1982, Cleland and Selverston 1995) while in *Cancer pagurus*, evidence for separate potassium-dependent and chloride-dependent responses was found (Marder and Paupardin-Tritsch 1978).

Table 1.1 Agonist and antagonist sensitivity of L-glutamate-activated inhibitory channels

Agonist sensitivity

Species	L,D-α-amino adipate	L,D-α-amino pimelate	D-Glu	Cysteate	Homo-cysteate	NMDA	Glycine	GABA	β-GP	QA	Ibotenate
Cancer		N	N					N	N		
Panulirus						N	N	N		N	Y
Homarus	N	N	N	N	N	N		N	N	N	

Antagonist sensitivity

Species	PTX	Bicuculline	Strychnine	Niflumate & flufenamate	GDEE	Curare
Cancer	Y	N				
Panulirus	Y		N	Y		
Homarus	Y	N	N		N	N

N represents receptor/channel displayed no sensitivity to agonist or antagonist. Y represents receptor/channel was sensitive to agonist or antagonist. Blank boxes are untested. Information in this table was gathered from information presented in (Cleland 1996). NMDA: N-Methyl-D-aspartate; GABA: gamma-aminobutyric acid; β-GP: beta-glycerophosphate; QA: quisqualate; PTX: picrotoxin; GDEE: Glutamic acid diethylester.

This synapse is of particular importance in the pyloric circuit because it serves as the only feedback of network function to the pacemaker complex (Nadim, Zhao et al. 2011). It is also well suited for study because there is only one LP neuron, so any chemical synaptic input to the PD neuron is known to be from one single cellular source.

Though this synapse is in a prime location to affect attributes of network activity (Manor, Nadim et al. 1997), whether it actually homeostatically regulates network activity on a cycle-to-cycle basis is not known. One study in lobster found that the inhibitory synapses in the pyloric network show a significant reduction in strength several days after decentralization (Thoby-Brisson and Simmers 2002), but it was not clear whether this was a homeostatic synaptic response in order to recover from the acute loss of coordinated network activity that accompanies decentralization (Figure 1.5, acute response) or if it was related to the loss of neuromodulators.

In addition, it appears unclear whether the LP-to-PD synapse can reliably influence network performance enough to serve as an effective homeostatic regulator of activity. Across different crustacean species, some have found that increasing the strength of this synapse (which provides stronger inhibition onto the pacemaker) slows the rhythm and increases the cycle period (Weaver and Hooper 2003, Weaver and Hooper 2003).

Others have found that the timing of when the LP neuron inhibits the PD neurons occurs at a time in the pacemaker oscillation cycle that minimizes its effect on the next pacemaker cycle. Using phase response analysis in experimental and computational studies, it was shown that the phase (timing within the cycle period) in which LP inhibits PD is critical for determining how the inhibition will affect the subsequent cycle period. In these studies, the oscillation cycle was defined by the pacemaker cycle, so the beginning of a PD burst is considered phase=0 and the beginning of the next PD burst is considered phase=1. If LP inhibition onto PD is initiated early in the oscillation cycle (early phase), the effect of inhibition is to shorten the cycle period; if the pacemaker is inhibited late in phase, the inhibition lengthens the cycle period; and middle phases (phase values 0.4-0.6) have little effect on the pacemaker cycle period (Ayers and Selverston 1977, Ayers and Selverston 1979, Prinz, Thirumalai et al. 2003, Mamiya and Nadim 2004, Oprisan, Prinz et al. 2004, Thirumalai, Prinz et al. 2006). It was also determined using dynamic clamp that in this middle phase, even large increases to inhibitory synaptic strength would not appreciably affect the cycle period of PD and that the effects of this inhibition in the early and late phases saturate after a certain point where further increases to inhibition strength have little effect on pacemaker cycle period (Prinz, Thirumalai et al. 2003, Thirumalai, Prinz et al. 2006).

Interestingly, during the ongoing pyloric rhythm *in situ*, the LP neuron consistently bursts in the middle phase range of the PD cycle period in both lobster (Bucher, Prinz et al. 2005) and crab (Goaillard, Taylor et al. 2009) pyloric networks,

suggesting that even large increases to LP-to-PD synaptic strength may not influence the cycle period during ongoing network activity. Indeed, it was found in the American lobster *Homarus americanus* that when the neuromodulator red pigment concentrating hormone (RPCH) is introduced to the network, a modulator that increases the LP-to-PD synaptic strength several-fold, there is little effect on the cycle period despite the strong increase in inhibition onto PD (Thirumalai, Prinz et al. 2006).

Recent work in *Cancer borealis* has found that acutely removing the feedback inhibition onto PD by strongly hyperpolarizing LP, preventing LP-to-PD transmitter release, has no significant effect on pacemaker cycle period, but does seem to increase cycle period variability (Nadim, Zhao et al. 2011, Zhao, Sheibanie et al. 2011, Nadim, Zhao et al. 2012). Phase response analysis suggests that when present, rather than actively alter the cycle period, the LP-to-PD synapse may act primarily to stabilize the ongoing rhythm from external perturbation, thus limiting variability (Mamiya and Nadim 2004, Nadim, Zhao et al. 2011, Nadim, Zhao et al. 2012).

Still, a recent study in the California spiny lobster *Panulirus interruptus* shows that the LP-to-PD synapse does alter the cycle period when strengthened by the presence of the neuromodulator octopamine (Johnson, Brown et al. 2011). Therefore, it is still inconclusive if and how the strength of this feedback synapse

dynamically affects ongoing pyloric activity on a cycle-to-cycle basis over the course of several hours *in situ*.

Of note, the LP neuron exhibits graded release of neurotransmitter where the cell will release glutamate onto PD as a graded function of its membrane potential, not exclusively during spiking events (Manor, Nadim et al. 1997). This was shown by demonstrating that in the presence of TTX, which eliminates spiking activity but does not eliminate the slower oscillatory membrane potential waveforms in each of the pyloric neurons, PD was still inhibited by the slower non-spiking depolarizations in LP (Graubard, Raper et al. 1980, Graubard, Raper et al. 1983). At present, it is not known if the graded and spike-mediated responses represent different structural components or what machinery is present to sequester neurotransmitter at these synaptic sites and how this process is affected by compound graded and spike- mediated transmitter release.

In this work, I focused on changes in spike-mediated input from LP to PD and systematically investigated how such changes might affect the stereotyped aspects of network activity during the ongoing pyloric rhythm.

Is electrical activity the true target of homeostatic synaptic plasticity?

Though the general understanding is that HSP acts to achieve a target level of network activity, the evidence for this theory is mostly circumstantial.

Perturbations to network activity are capable of inducing compensatory changes in synaptic currents, but these synaptic changes have not been shown experimentally to be necessary or sufficient for recovery after activity blockade. In fact in STG neurons, bursting activity can recover when isolated even in the absence of network synaptic connections (Turrigiano and Marder 1993, Turrigiano, Abbott et al. 1994) (Figure 1.2).

More recent work has begun to cast doubt on the assumption of a target level of spiking activity. Aside from one study in dissociated rat neuronal cultures that found that blocking somatic spiking alone triggers synaptic scaling, while local synaptic blockade does not (Ibata, Sun et al. 2008), most studies have not targeted activity perturbations to a single post-synaptic neuron, instead blocking global activity e.g. (Lissin, Gomperts et al. 1998, O'Brien, Kamboj et al. 1998, Turrigiano, Leslie et al. 1998, Kilman, van Rossum et al. 2002, Gonzalez-Islas and Wenner 2006, Hartman, Pal et al. 2006, Stellwagen and Malenka 2006). Several studies that have targeted activity manipulations to a single post-synaptic neuron have found that altering post-synaptic electrical activity alone does not trigger synaptic scaling (Burrone, O'Byrne et al. 2002, Hartman, Pal et al. 2006, Pratt and Aizenman 2007).

Notably for the work presented in this dissertation (as it relates to inhibitory homeostatic synaptic plasticity), it was found that though network wide activity deprivation could induce GABAergic scaling, selective hyperpolarization (and thus abolishment of spiking activity) of a single pre-synaptic or single post-synaptic

neuron in rat hippocampal cultures does not trigger changes in mIPSCs (Hartman, Pal et al. 2006). Also, in the developing chick embryo, GABAergic (as well as AMPAergic) scaling was induced by blocking GABA transmission for 2 days, during which network activity remained relatively unchanged (Wilhelm and Wenner 2008).

Indeed, ceasing all network activity with a global perturbation such as bath-applied TTX not only blocks spiking activity; it also stops spike-evoked synaptic transmission at every terminal. Therefore, it is conceivable that in studies that induced synaptic scaling by chronically blocking all spiking activity in a neuronal network (such as those mentioned previously), it may have been the local reduction in synaptic transmission at every synapse that triggered many local synaptic changes in post-synaptic currents, not a global reduction in spiking activity triggering a cell-wide scaling mechanism. In other words, it is possible that HSP is induced in a synapse-specific manner, as with Hebbian synaptic plasticity, and in such a way as to regulate the amount of transmission through synaptic channels, not global spiking activity.

Evidence that HSP is an input- or synapse-specific mechanism has been found in many studies (Davis and Goodman 1998, Sutton, Ito et al. 2006, Sutton and Schuman 2006, Hou, Zhang et al. 2008, Kim and Tsien 2008, Jakawich, Nasser et al. 2010, Beique, Na et al. 2011, Deeg and Aizenman 2011, Henry, McCartney et al. 2012), casting doubt on the general understanding that HSP is primarily a cell-wide

mechanism to regulate cellular excitability. Thus, more research is needed to determine whether a target level of electrical activity is the true target of HSP.

Objectives of this dissertation

The primary objectives of this work were to elucidate the role of HSP, if any, at a particular glutamatergic inhibitory connection (the LP-to-PD synapse) of the pyloric circuit in the crab *Cancer borealis* and to determine how such regulation might be mediated. This objective was pursued using both experimental as well as computational approaches.

In the second chapter of this dissertation, I use a computational network model database to determine the expected effect of a change in this synapse's strength on several quantifiable attributes of the stereotyped pyloric network activity. Next, I test experimentally whether this synapse changes in strength in response to an activity perturbation. I show that this synapse does change strength markedly in response to a perturbation of the post-synaptic PD membrane potential, a manipulation that affects global pyloric network activity. By tracking the long-term dynamics of synaptic strength before, during, and after the post-synaptic voltage perturbation, I systematically analyze the effect of the changes in synaptic strength on these quantifiable attributes of pyloric activity. I provide evidence that the change in synaptic strength is not consistent with homeostatic regulation of any attribute of network activity; instead, the synapse seems to

respond in a manner consistent with homeostatic regulation of peak synaptic current or synaptic reversal potential.

Because transmission at this synapse is primarily mediated by chloride, I show that a computational model of synaptic regulation by post-synaptic chloride homeostasis can qualitatively match the experimental observations from the voltage perturbation study and can explain the apparent homeostasis of peak synaptic current and synaptic reversal potential. Lastly, I show experimentally that a targeted post-synaptic chloride concentration perturbation by iontophoretic injection can alter synaptic conductance with no change in neuronal or network activity. The response is similar to the computational model response to chloride current injection, providing evidence that synaptic conductance for the LP-to-PD synapse is regulated by post-synaptic chloride concentration homeostasis.

CHAPTER 2 :

EVIDENCE FOR REGULATION OF INHIBITORY SYNAPTIC CONDUCTANCE BY POST-SYNAPTIC CHLORIDE CONCENTRATION HOMEOSTASIS

INTRODUCTION

The regulation of synaptic strength is an important topic in neuroscience. Neuronal networks often respond to activity perturbations by altering the strength of their synapses. For example, many studies have found network activity blockade can trigger the strengthening of excitatory synapses and/or weakening of inhibitory synapses (Turrigiano, Leslie et al. 1998, Kilman, van Rossum et al. 2002, Gonzalez-Islas and Wenner 2006, Hartman, Pal et al. 2006, Stellwagen and Malenka 2006), a phenomenon known as homeostatic synaptic plasticity (HSP). HSP of inhibitory synapses has been shown to be mediated by changes in post-synaptic receptor number (Kilman, van Rossum et al. 2002) as well as pre-synaptic vesicle filling (Hartman, Pal et al. 2006). The general understanding is that these responses exist to compensate for the activity block and recover network activity (Turrigiano 2012), although how the need for such changes is sensed in the network and exactly how synaptic strength dynamics affect ongoing network activity are ongoing questions.

Much of what is known about HSP has been found in dissociated culture or slice preparations using network-wide perturbations, such as chronic activity deprivation via globally-applied drug treatment in the culture dish. These cultured networks bear challenges though, that make it difficult or not feasible to identify and track the strength of an individual connection throughout a targeted perturbation of a single neuron. Overcoming these challenges could expand our understanding of

the dynamics of HSP, its effect on network activity, and how such regulatory mechanisms might be mediated.

Thus there is substantial benefit to investigate synaptic regulation in a more accessible small neural network where one can continuously observe how an identified connection between two neurons affects network performance over several hours as changes occur and precisely study the dynamic effect of synaptic plasticity. For this work, I focus on the central pattern generating pyloric network in the crab *Cancer borealis* stomatogastric ganglion (STG) because the component neurons and synaptic connections are identified and well-characterized (Marder and Bucher 2007) and because the network output is stereotyped, quantifiable, and shows little variation throughout life. Therefore, I could readily measure network activity changes by quantifying the characteristic attributes of the circuit output before, during, and after perturbation (see Figure 2.1 for examples of pyloric activity attributes).

The *Cancer borealis* pyloric network consists of three neuronal nodes: the intrinsically oscillating pacemaker complex [one anterior burster (AB) neuron electrically connected through gap junctions to two pyloric dilator (PD) neurons], the lateral pyloric (LP) neuron, and the 3-5 electrically connected pyloric (PY) neurons. The three nodes are connected through inhibitory synapses (Figure 1.4). Each node successively fires a burst of spikes in a stable triphasic pattern with a network cycle period that ranges from 0.53–1.44 s (Goaillard, Taylor et al. 2009),

which can be recorded extracellularly from the lateral ventricular nerve (lvn) (Figure 2.1).

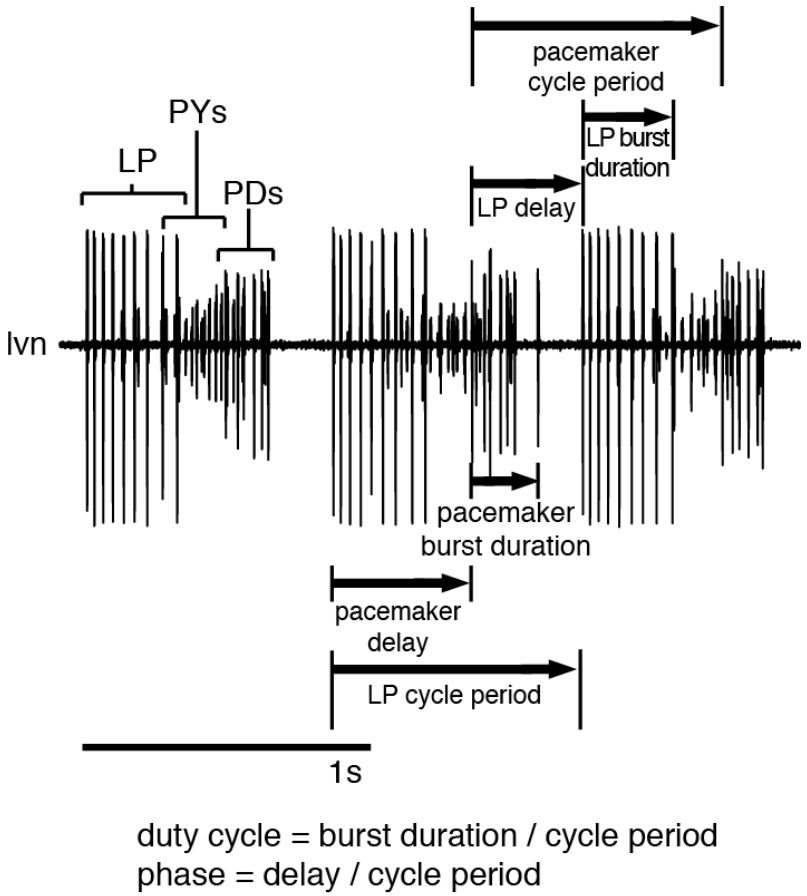

Figure 2.1 Pyloric network activity attributes.

A recording from the lvn shows the characteristic triphasic bursting pattern of the pyloric network with each neuronal node labeled at left. Attributes of network activity are labeled in the subsequent two cycles with pacemaker-cycle-period-referenced attributes labeled above and LP-cycle-period-referenced attributes labeled below.

Here, I focus on the connection from LP to one of the PD neurons, a primarily-chloride-mediated glutamatergic inhibitory synapse (Marder and Paupardin-Tritsch 1978, Eisen and Marder 1982, Cleland and Selverston 1995, Cleland 1996, Cleland and Selverston 1998) that provides the sole chemical synaptic feedback to the pacemaker complex. To determine how this synapse is expected to affect the multiple attributes of the characteristic pyloric network activity (Figure 2.1), the effect of increasing LP-to-PD synaptic conductance was systematically examined in an established database of computational pyloric network models (Prinz, Bucher et al. 2004). After establishing how the synapse is expected to respond if it were to homeostatically influence network activity, it was important to determine whether this synapse changed strength in response to an activity perturbation in the living system. Previous theoretical work in a pyloric network model of activity-dependent synaptic plasticity has predicted that depolarizing or hyperpolarizing a postsynaptic STG neuron should induce a respective increase or decrease in inhibitory synaptic strength (Soto-Trevino, Thoroughman et al. 2001). I examined experimentally whether this synapse was activity-dependent and whether it behaved as this theoretical study predicted by perturbing the post-synaptic PD voltage and measuring the synaptic strength over the course of six-hour-long voltage clamp experiments.

I show that the synapse changed strength following voltage manipulation, but surprisingly in the opposite direction than expected. To establish whether this change in synaptic conductance (g_{syn}) constituted a homeostatic response for

network activity, I quantified its effect on the quantifiable attributes of pyloric activity (Figure 2.1). Using the results from the computational network model database and a series of novel metrics designed to quantify homeostatic behavior, I show that the synapse not only responded in the opposite direction than expected, but in a manner unlikely to represent homeostatic synaptic regulation of network activity. Instead, the response seemed consistent with a homeostatic target of peak synaptic current (peak I_{syn}) levels or synaptic reversal potential (E_{syn}).

Because both potentially-regulated attributes peak I_{syn} and E_{syn} were dependent on internal chloride, I hypothesized that a change in post-synaptic internal chloride concentration ($[Cl^-]_{in}$) could be the underlying trigger of the observed synaptic plasticity. To test this hypothesis, I explore a different potential target of HSP: post-synaptic $[Cl^-]_{in}$. First, I built a single-compartment computational model neuron that incorporates a rule to homeostatically regulate synaptic conductance depending on the neuron's $[Cl^-]_{in}$. I show that the model qualitatively matches the voltage perturbation study's g_{syn}, E_{syn}, and peak I_{syn} traces. I then test a prediction from the model experimentally by iontophoretically injecting chloride into the post-synaptic PD neuron under voltage clamp, and find that the synapse changes strength in response to chloride-loading in a manner that again matches the computational model. This result shows that disrupting $[Cl^-]_{in}$ alone, independently from network activity, can trigger a change in synaptic conductance and provides compelling evidence that the strength of the LP-to-PD synapse is not

regulated to establish a target level of network activity, but rather to achieve a target post-synaptic $[Cl^-]_{in}$.

RESULTS

Using model pyloric networks to investigate the network activity effects of changes to LP-to-PD synaptic strength

In the crustacean pyloric network, it is not entirely clear what role the LP-to-PD synapse – the only feedback synapse to the pacemaker complex – has, if any, to regulate the various attributes that define the characteristic pyloric network activity, such as pre- and post-synaptic burst durations, duty cycles, delays, and phases (Figure 2.1). Thus, in this first study, I use a database of computational model pyloric networks to systematically examine how changes in the LP-to-PD synaptic strength are expected to influence these well-established quantifiable attributes of pyloric circuit activity.

The particular activity attributes shown in Figure 2.1 were selected because together they provide a comprehensive quantifiable description of a stereotyped activity pattern. The cycle period quantifies how frequent the bursts of action potentials occur in each neuron, while the burst duration is a measure of how long each cell bursts. In the live animal, these neuronal activity measures translate to

how frequently the stomach muscle contracts (cycle period) and how long it contracts during each contraction event (burst duration). A normalized measure taken from these attributes describes how long each cell bursts normalized by the cycle period (duty cycle). Of course, different motor neurons innervate different muscles; so another quantifiable measure of activity is the difference in timing between one neuron's burst in the network and another's burst (delay). This measure can also be normalized by the cycle period to describe when in the oscillatory cycle the next cell bursts (phase). Of these attributes, some show more animal-to-animal variability than others, e.g. cycle periods, burst durations, and delays vary across animals (~threefold range) despite showing little variation within one animal on a cycle-to-cycle basis. Notably, burst durations and delays, although variable across animals, scale with cycle period. Therefore, measures that are normalized by cycle period (duty cycle and phase) are relatively invariant across animals. This has been demonstrated in *Cancer borealis* (Goaillard, Taylor et al. 2009) as well as in the American lobster, *Homarus americanus* (Bucher, Prinz et al. 2005).

To investigate the expected effects of an increase in LP-to-PD synaptic conductance (g_{syn}) on these pre- and post-synaptic activity attributes, I used a database of model pyloric networks that has been described previously (Prinz, Bucher et al. 2004). The database contains network activity descriptions of >20 million models of the pyloric network constructed by using different combinations of synaptic conductances that connected five or six different versions of each of the

neuronal nodes in the pyloric circuit (see methods chapter for more details). This method established a large set of network parameter combinations. Each network was simulated long enough to sufficiently determine its characteristic activity, which was measured and stored in the database. Because the PD neurons and the AB neuron were lumped together and modeled as a single AB/PD intrinsic burster in this study, I refer to it as the pacemaker, or PM, for this analysis but continue to refer to the synapse of interest as the LP-to-PD synapse.

For this study, I focused on the ~20% of the database (4,047,375 networks) that displayed "pyloric-like" rhythmic activity. "Pyloric-like" networks were networks that produced a repetitive firing pattern with bursts of action potentials in the correct pyloric order: PD-LP-PY. Narrowing the analysis to this functional subset of the entire database, two approaches were used.

For the first approach, I identified families of functional model networks that differed only in the strength of the LP-to-PD synapse, but were identical in all other cellular and synaptic parameters. Networks that belong to the same family are referred to as sibling networks. The database contained LP-to-PD synaptic strength values of either 0 nS, 3 nS, 10 nS, 30 nS, or 100 nS. I further narrowed the analysis within each family to sibling networks that were adjacent on the scale of possible LP-to-PD synaptic strength values (see methods chapter for more details).

In this way, the pyloric activity effect of a stepwise increase in synaptic

strength from adjacent sibling networks could be evaluated within each network family. I used this approach to establish whether only increasing the LP-to-PD g_{syn} – and holding all other cellular and synaptic conductances constant – produced a consistent average increase or decrease in any attribute of pyloric activity (those shown in Figure 2.1). Because the conductance magnitudes of the stepwise increases in g_{syn} differed (from 0 nS to 3 nS is only a 3 nS increase, whereas from 30 nS to 100 nS is a 70 nS increase), each change in attribute output was normalized by the magnitude of g_{syn} increase to establish an attribute change per nS that was more readily comparable across different pairs of sibling networks (see methods for further clarification).

Using this approach over 1.1 million families of pyloric-like networks were isolated, with a total of 3,647,930 networks analyzed. Qualitatively, there was a positive effect of the synapse on pacemaker cycle period and phase as well as the burst duration and delay of both the pacemaker and LP. This is demonstrated by observing that for each of these network activity attributes, each step-wise increase in synaptic conductance shown on the x-axis is associated with a positive (>0) change in the attribute on the y-axis (Figure 2.2). Therefore, an increase in g_{syn} within a family typically led to an increase in these activity attributes.

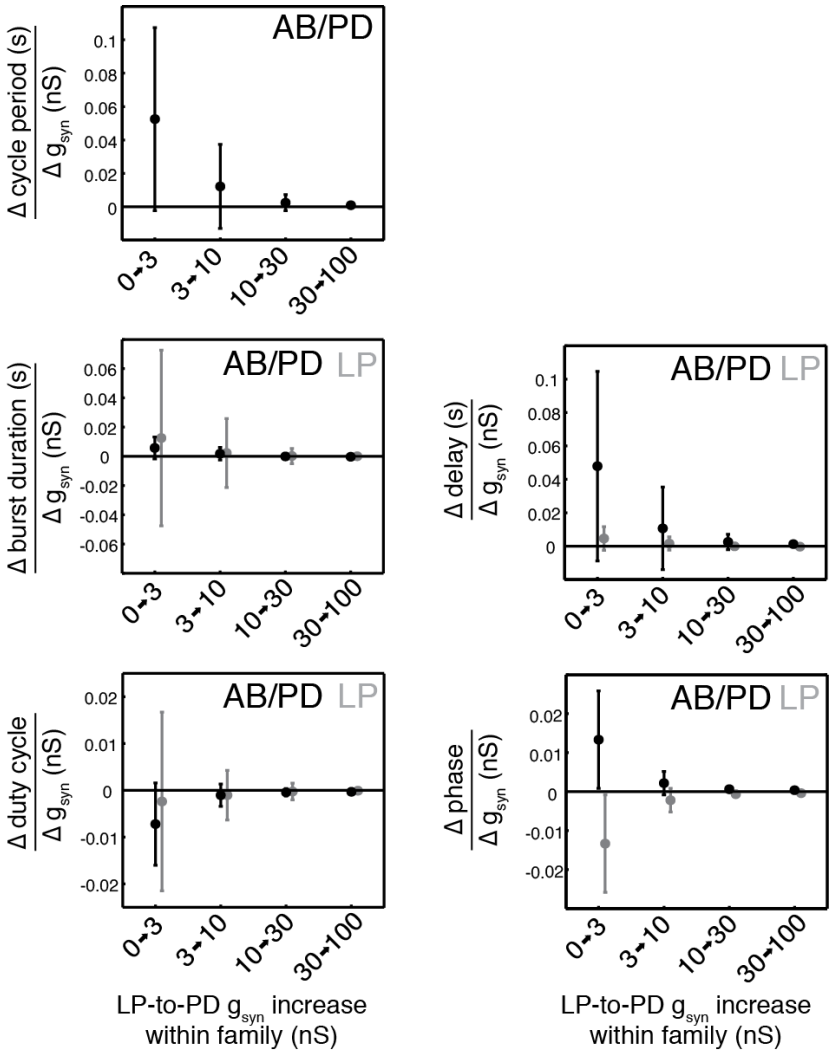

Figure 2.2 The effect of an increase in LP-to-PD g_{syn} on attributes of network activity within a family of similar model networks.

X-axis shows the g_{syn} increases among neighboring values within a family of model networks. Y-axis shows the effect on the activity attribute of an increase in g_{syn} normalized by the magnitude of g_{syn} increase. Attributes are shown for pacemaker complex (AB/PD) activity in black and LP activity attributes in grey. See Figure 2.1 *for attribute examples. Plots are shown using descriptive statistics (mean ± SD). Number of families analyzed: 0⟶3 nS, n=722,000; 3⟶10 nS, n=653,635; 10⟶30 nS, n=548,115; 30⟶100 nS, n=452,102.*

The increase in g_{syn} at smaller initial ranges (e.g. 0→3 nS) had a larger average impact on the activity attribute outputs than an additional g_{syn} increase when the synapse was already strong. Despite the waning influence as the synapse got stronger, the directionality was consistent: increasing the synaptic strength had a positive effect on these attributes on average. Conversely, an increase in g_{syn} had a negative effect on both pacemaker and LP duty cycles as well as the LP phase; a g_{syn} increase within a family led to an average decrease (activity attribute <0 on the y-axis) in these activity attributes. Notably, the way these attributes are defined in the database, LP phase + AB/PD phase = 1. This explains why the AB/PD phase and LP phase plots are mirror images of each other around the zero line, because a change in AB/PD phase translates to an equal and opposite change in LP phase.

For the second approach, I constructed histograms of the activity attribute outputs for each of the LP-to-PD five different synaptic strength values explored in the database regardless of the other cellular or synaptic parameters in the network (in contrast to holding them fixed as in the first approach). In this way, the overall effect of increasing g_{syn} can be assessed for that attribute, without assuming that the other cellular and synaptic parameters need to remain fixed.

Using the second method, the effect of increasing g_{syn} on pacemaker activity can be seen by looking at the histograms of the underlying activity distributions and identifying directional shifts in activity output for increasing values of g_{syn} (Figure

2.3). For example, focusing on the pacemaker cycle period histograms, by isolating and plotting the cycle period distribution for only “pyloric-like” networks that have an LP-to-PD g_{syn} equal to 0 nS (orange histogram), one observes five sharp peaks. These peaks correspond to the intrinsic oscillation frequencies of the five different

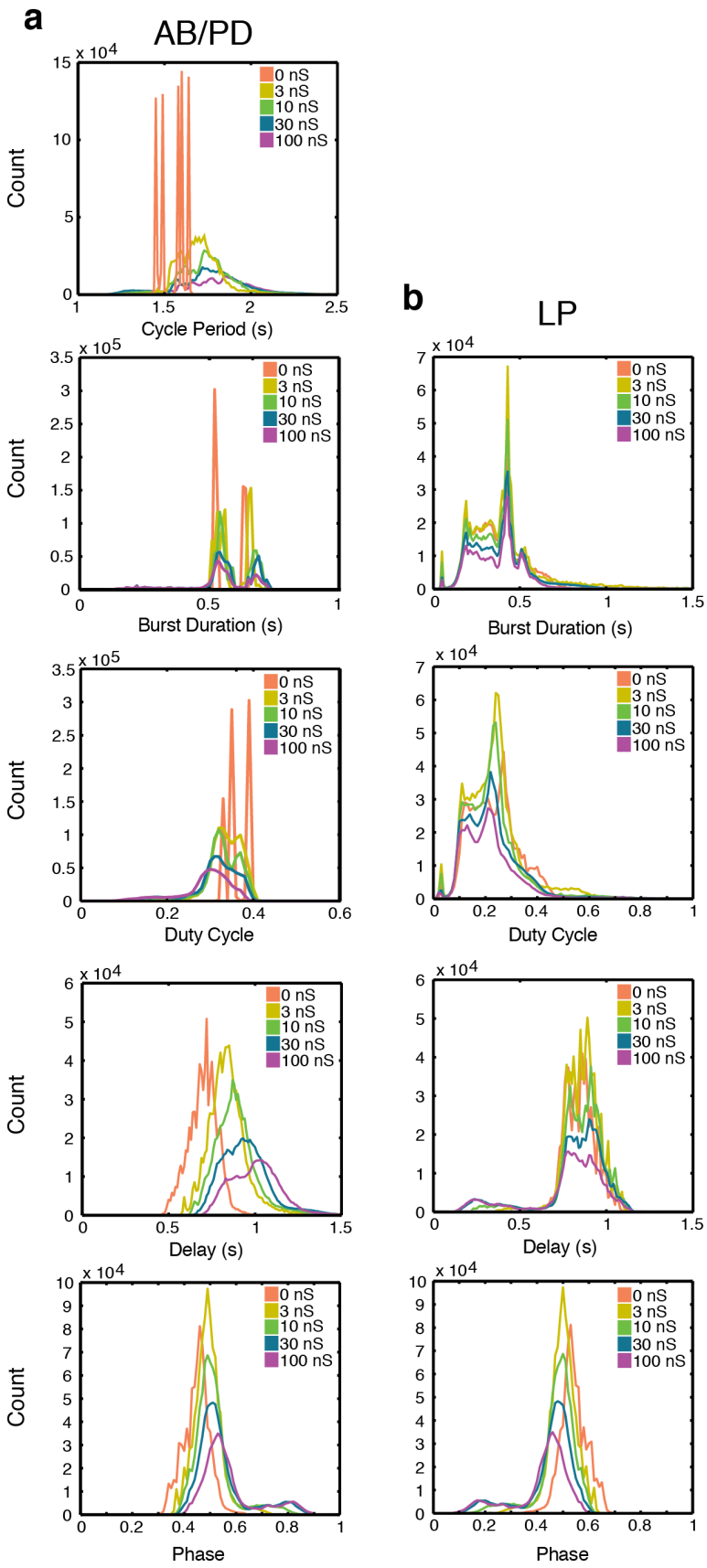
a
AB/PD
b
LP
Count
Cycle Period (s)
Burst Duration (s)
Duty Cycle
Delay (s)
Phase
0 nS
3 nS
10 nS
30 nS
100 nS
x 10^4
x 10^5

Figure 2.3 The effect of an increase in LP-to-PD g_{syn} on attributes of network activity among all model networks.

Networks from the model network database were isolated according to the strength of the LP-to-PD synapse (regardless of the other membrane or synaptic conductances). Histograms were then produced for each activity attribute of the AB/PD pacemaker complex (a) and the LP (b) neuron, at each synaptic strength level. The overall effect of LP-to-PD g_{syn} can be witnessed by observing either a leftward or rightward shift in the distributions as the synaptic conductance increases. Bin widths were 0.01 seconds for cycle period, burst duration, and delay histograms and 0.01 for duty cycle and phase histograms.

pacemaker neuron models that were used in the network database. Looking at the histogram of networks with an increased value of g_{syn}, e.g. 3 nS (yellow), one can see that the distribution is shifted rightward with a higher average cycle period value. The trend continues at higher g_{syn} histograms, so it appears that overall the LP-to-PD synapse is expected to have a positive effect on pacemaker cycle period. This is the same effect found earlier by looking within network families.

For most network attributes, the histogram analysis confirmed the effects seen using the first method, although for some network attributes the effect of increasing g_{syn} is slight. For example, increasing g_{syn} onto PD does not noticeably shift the histograms of the LP attributes such as burst duration, duty cycle, and delay (Figure 2.3b). The pacemaker burst duration histograms are also not appreciably

shifted by changing g_{syn}.

In summary, using both methods of network database analysis, the expectation is for the LP-to-PD synapse to have a positive effect on pacemaker cycle period, delay, and phase. Using this analysis, one would also expect for the synapse to have a negative effect on pacemaker duty cycle and LP phase. Furthermore, one would expect the synapse to have a negligible effect on pacemaker burst duration and LP burst duration, duty cycle, and delay.

These results establish a predicted synaptic response to perturbation if the synapse were to homeostatically regulate any of these network activity attributes. For example, if a perturbation were to reduce the pacemaker delay, this synapse should strengthen if it were homeostatically regulating this attribute to a constrained range. This is because the network model database analysis suggests that an increase in g_{syn} should lead to an increase in pacemaker delay, a response that would homeostatically oppose the perturbation.

Post-synaptic voltage perturbation triggers change in LP-to-PD synaptic strength

Next, I experimentally tested whether this synapse changes in strength in the living system in response to a strong perturbation of network activity over the course of several hours. Computational work has predicted that activity-dependent

HSP rules implemented at each pyloric synapse could lead to normal activity from random initial synaptic strengths (Soto-Trevino, Thoroughman et al. 2001), but it has not been clear how pyloric synapses respond dynamically to activity perturbations in the living system over several hours. One study found that several synapses in the lobster pyloric network, including the LP-to-PD synapse, decrease in strength following loss of extrinsic neuromodulators (Thoby-Brisson and Simmers 2002), a perturbation that typically leads to a loss of coordinated activity, but the dynamics of the change in synaptic strength, how it affected network activity, and how the reduction was triggered was not clear. Because the LP-to-PD synapse is the only chemical connection the pacemaker complex receives, it is poised to provide critical feedback about the rest of the network activity, though previous studies have questioned whether changes in strength of this synapse can appreciably affect ongoing network activity (Prinz, Thirumalai et al. 2003, Mamiya and Nadim 2004, Thirumalai, Prinz et al. 2006, Johnson, Brown et al. 2011, Nadim, Zhao et al. 2011). Therefore, I aimed to examine whether activity-dependent HSP existed at this inhibitory synaptic connection.

In order to determine what, if any, homeostatic regulation exists at this synapse, I introduced a voltage perturbation into one of the PD neurons in the pacemaker complex to disrupt network activity using two-electrode voltage clamp (TEVC) (Figure 2.4a). Synaptic currents from LP were measured continuously throughout each six-hour-long experiment. The experimental protocol included a baseline-voltage epoch (epoch 1), a perturbation-voltage epoch (epoch 2), and a

return-to-baseline-voltage epoch (epoch 3), each lasting two hours (Figure 2.4b).

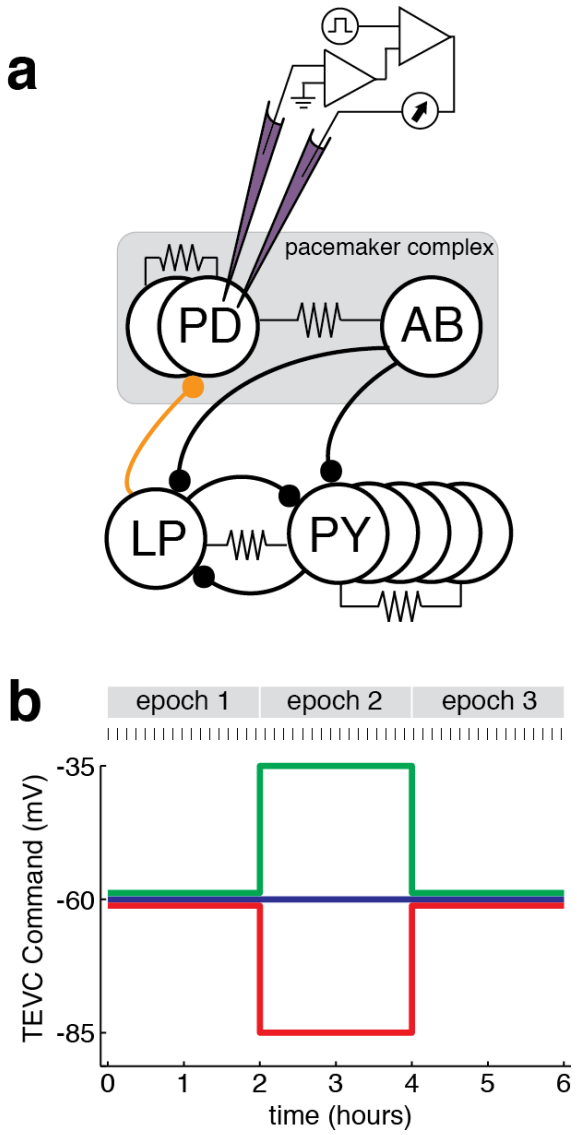

Figure 2.4 Voltage perturbation study experimental method.

(a) Two sharp microelectrodes were used to impale one of the PD neurons in the pacemaker complex. Two-electrode voltage clamp (TEVC) was used throughout the experiment. All synapses are inhibitory. Resistor symbols represent electrical connections. (b) TEVC holding potential values for the three cases tested. Red/green/blue color scheme is used throughout. Tick marks above represent applications of the 40-second voltage step protocol described in methods and shown in Figure 2.6.

During each experiment, PD was either held at a baseline membrane potential (-60 mV) or perturbed by ± 25 mV during epoch 2 (Figure 2.4b; see methods for further details). The color scheme used in Figure 2.4b is used throughout. Because the two PDs are large and share an electrical connection with each other and AB, the entire pacemaker complex could not be fully clamped. Oscillatory activity remained in the other PD and, at times, blunted spikes escaped from the impaled PD (Figure 2.5). Therefore, I refer to the activity attributes from the rest of the pacemaker complex as "pacemaker attributes" and the perturbations are referred to as "hyperpolarizing" or "depolarizing" to more accurately reflect the nature of this manipulation.

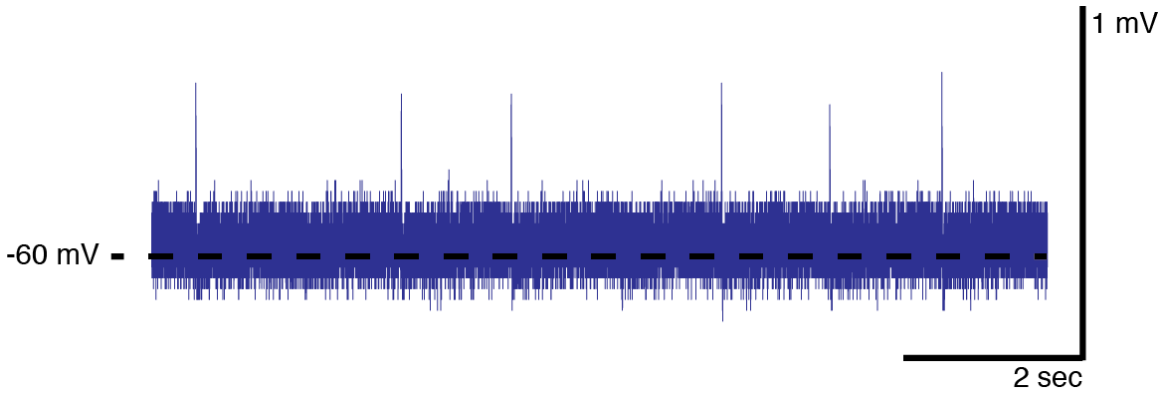

Figure 2.5 Blunted spikes present in intracellular voltage clamp recording.

Due to a distant spike-initiation zone, soma voltage-clamp was not able to fully clamp the PD neuron from spiking. Therefore, blunted remnants of spikes were seen in the intracellular PD recording electrode as in the example shown above where six <1 mV spikes are seen. Because of this, we refer to the voltage perturbations as "hyperpolarizing" or "depolarizing".

To quantify synaptic strength through the six-hour-long experiment, a forty-second-long voltage step protocol was applied every six minutes (instances signified by tick marks in Figure 2.4b). An example of one application of the voltage step protocol is shown in Figure 2.6.

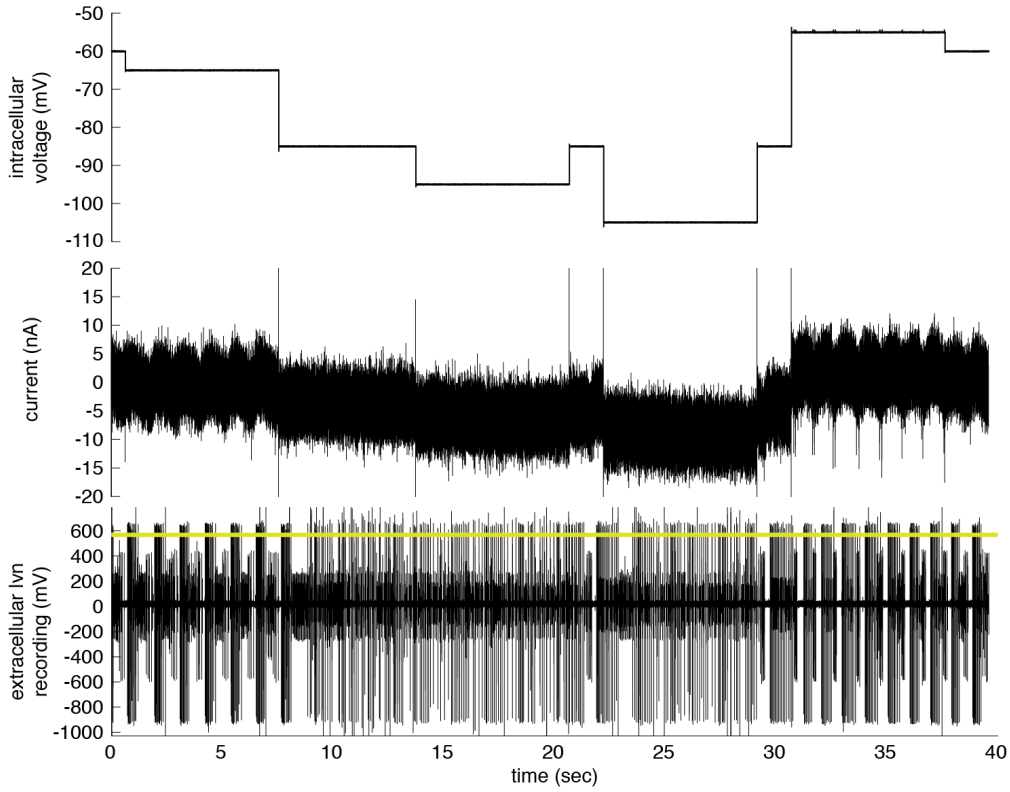

Figure 2.6 Voltage step protocol.

One instance of the 40-second voltage step protocol is shown as an example. The PD intracellular recording from the voltage-recording electrode of the TEVC is shown above. The injected current into PD from the current-injection electrode is shown in the center. The extracellular lvn recording showing network spikes is shown at bottom. Largest amplitude spikes in extracellular recording (those above the yellow threshold line) are from LP and were used for spike-triggered averages to calculate LP-to-PD E_{syn} *and* g_{syn} *(see* Figure 2.7*). Note more examples of blunted spikes that escaped the voltage clamp are visible in the intracellular recordings at ~35 sec.*

During each voltage step protocol, PD voltage was briefly held at the five potentials labeled on the x-axis of Figure 2.7 where average currents triggered from extracellular LP spikes were collected. A synaptic reversal potential (E_{syn}) and a synaptic conductance (g_{syn}) for the LP input were determined for each instance of the voltage step protocol using the line-of-best-fit to the peak synaptic currents (I_{syn}) (Figure 2.7).

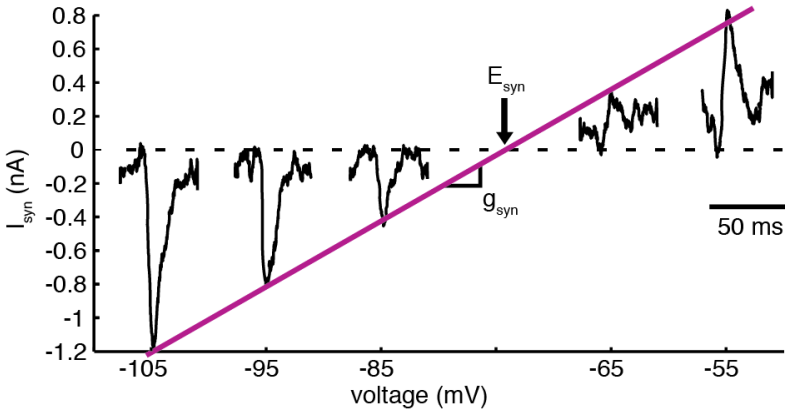

Figure 2.7 Calculating synaptic reversal potential and conductance from spike-triggered averaged current traces.

*LP-spike-triggered synaptic currents were collected and averaged according to the PD holding voltage (x-axis) during the voltage step protocol (*Figure 2.6*). The average current traces were used to calculate a synaptic reversal potential (E_{syn}), and a synaptic conductance (g_{syn}) value using the line-of-best-fit (magenta line) to the peak synaptic currents (I_{syn}). This was done for each instance of the voltage step protocol.*

When looking at the underlying synaptic strength profiles, it is evident that although the initial values of g_{syn} varied between preparations, the synapse did respond to the perturbations in a repeatable way (Figure 2.8a-c). The primary response during epoch 2 appeared to be a change in the slope of g_{syn} – particularly in the depolarized preparations (Figure 2.8a) – where the inhibition from LP weakened in response to a depolarization of PD.

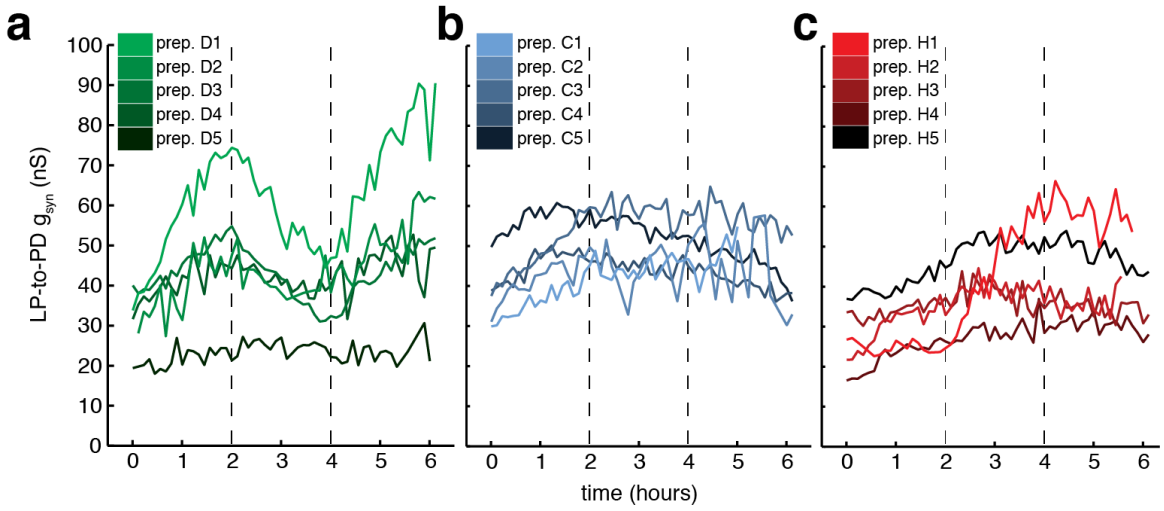

Figure 2.8 Post-synaptic voltage perturbation alters LP-to-PD synaptic strength.

Underlying LP-to-PD synaptic conductance (g_{syn}) is shown for every experimental preparation. Colors correspond to experimental groups from Figure 2.4*b. Briefly, (a) green: depolarized during epoch 2; (b) blue: control voltage (-60 mV) during epoch 2; (c) red: hyperpolarized during epoch 2. Dashed lines denote epoch boundaries.*

To quantify the g_{syn} slope, a least-squares regression line was fit to each epoch in each preparation (Figure 2.9).

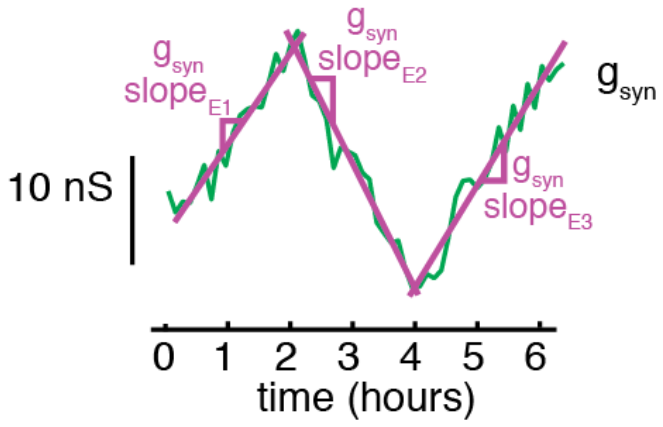

Figure 2.9 Schematic showing g_{syn} slopes by epoch

The method of quantifying g_{syn} slopes is shown for a representative example g_{syn} trace (green trace - prep. D3). The slopes were calculated using a least-squares regression line for each of the data points in an epoch. Magenta lines represent lines of best fit for each epoch (E1, Epoch 1; E2, Epoch 2; E3, Epoch 3). For more detail, see methods chapter.

On average, all preparations showed increasing synaptic conductance (i.e. g_{syn} slope>0) during epoch 1 (Figure 2.10a). During epoch 2, g_{syn} continued to increase slightly in hyperpolarized preparations, plateaued in controls, and decreased in depolarized preparations. Controls and hyperpolarized preparations were indistinct during epoch 3, while depolarized preparations showed a significant increase in $g_{syn.}$ To control for inter-animal variability of g_{syn} slope magnitude, the change (Δ) in g_{syn} slope from one epoch to the next was calculated for each preparation. Depolarized preparations underwent the largest significant changes in mean slope of g_{syn} (Figure 2.10b).

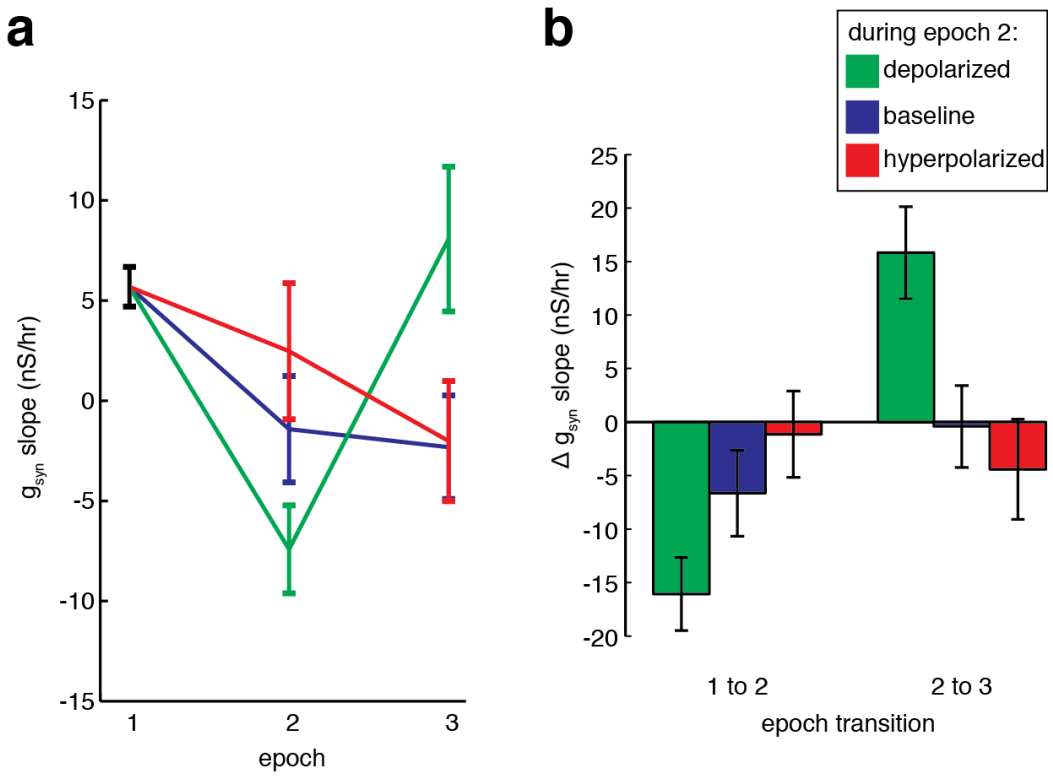

Figure 2.10 The effect of post-synaptic voltage perturbation on synaptic conductance.

LP-to-PD g_{syn} slopes were calculated as shown in Figure 2.9 *for each epoch in a preparation. (a) Average g_{syn} slope was determined for epoch 1 by calculating a weighted mean g_{syn} slope for all preparations (n=15). The mean was weighted according to the error in each slope's fit (see methods chapter for more details). For the subsequent epochs, the weighted means shown were calculated using only the preparations from each condition (n=5 for each condition). (b) The change in g_{syn} slope from one epoch to the next within each preparation was calculated and a weighted mean for each condition is shown. (a,b) Error shown as weighted mean ± 95% C.I. Non-overlapping C.I.s are considered significant.*

Taken together, Figure 2.8 and Figure 2.10 show that the voltage perturbation was able to elicit a change in the slope of the synaptic strength trace. The direction of that change, though, was unexpected because it was the opposite of theoretical predictions about how synaptic homeostasis could be implemented in the pyloric network and how these synapses might respond to post-synaptic voltage perturbation (Soto-Trevino, Thoroughman et al. 2001). For example, rather than change to more strongly inhibit the depolarized post-synaptic neuron, inhibition was markedly reduced in depolarized (green) preparations.

Post-synaptic voltage perturbation affects pyloric network activity

One anticipated secondary effect of depolarizing or hyperpolarizing a pacemaker neuron in the interconnected pyloric network is that the perturbation propagates to the other neurons and alters attributes of the characteristic network activity, such as those highlighted in Figure 2.1. In general at the beginning of epoch 2, PD depolarization instantaneously shortened the cycle period – speeding up the rhythmic oscillations – while hyperpolarization acutely slowed the triphasic rhythm. In lvn traces taken from representative preparations (prep. D3, prep. C3, and prep. H5), it is noticeable that while the three preparations have comparable cycle periods shortly before the initial voltage perturbation, the depolarized preparation has a shorter cycle period and the hyperpolarized preparation has a longer cycle period

shortly after the perturbation is applied, while controls continue unchanged (Figure 2.11).

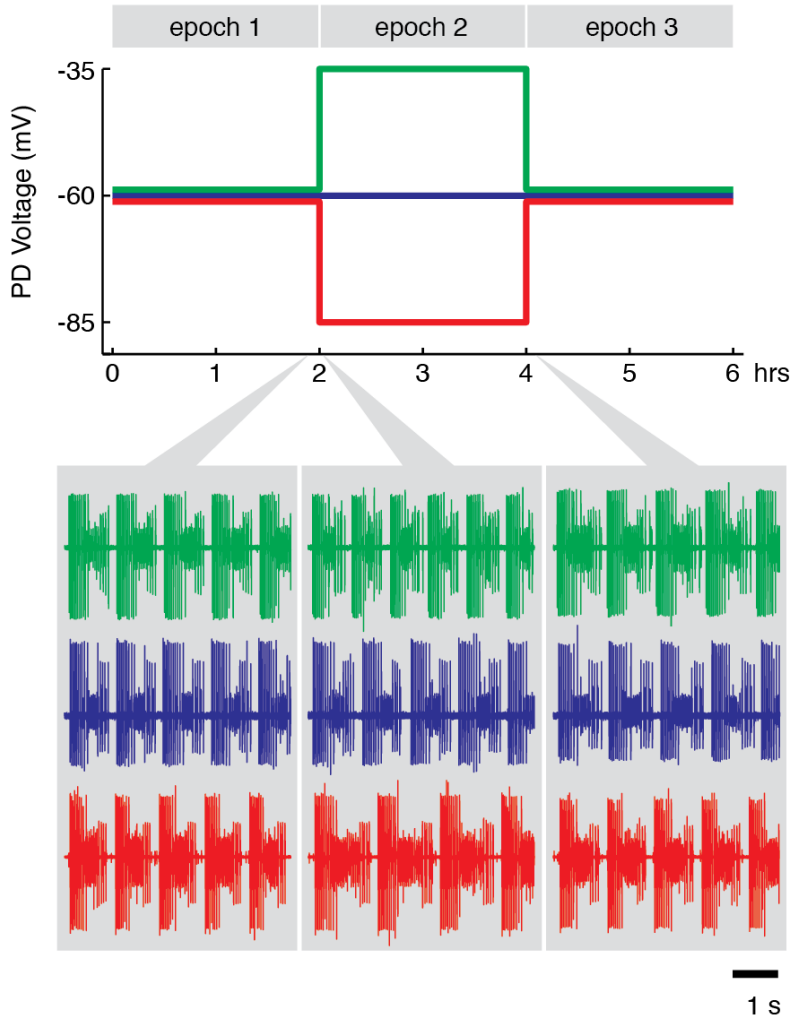

Figure 2.11 Effect of acute voltage perturbation on pyloric network activity.

Each colored extracellular trace is a 5 sec long snapshot of pyloric activity from the lvn taken at the times indicated by the grey arrows from representative preparations (prep. D3, prep. C3, and prep. H5). The depolarizing perturbation typically acutely shortened the network cycle period during epoch 2 (middle panel) when compared to shortly before depolarization (left panel) and altered activity attributes from Figure 2.1. *The hyperpolarizing perturbation typically lengthened the network cycle period during epoch 2.*

Post-synaptic voltage perturbation affects synaptic reversal potential and synaptic currents

As I have shown, depolarizing or hyperpolarizing the PD neuron under TEVC for hours is a strong perturbation that can affect pyloric network activity. In addition, altering the voltage level of any neuron for hours affects neuronal properties that are voltage-dependent, such as voltage-gated activations and driving forces for currents. The voltage perturbation also affected the LP-to-PD synaptic reversal potential, E_{syn}; in general, depolarized preparations exhibited an acute depolarization in E_{syn} at the beginning of epoch 2, hyperpolarized preparations saw a slight hyperpolarization of E_{syn}, and control preparations did not change substantially after hour 2 (Figure 2.12a).

Due to these changes in E_{syn}, along with the acute jump in membrane potential, the voltage perturbation affected the driving force for I_{syn} as well. The sudden large increase in driving force (by the depolarization up to -35 mV) caused synaptic currents in depolarized preparations to acutely strengthen at the beginning of epoch 2 (Figure 2.12b-c, green; current traces shown in Figure 2.12b correspond in time to the orange arrows in Figure 2.12a).

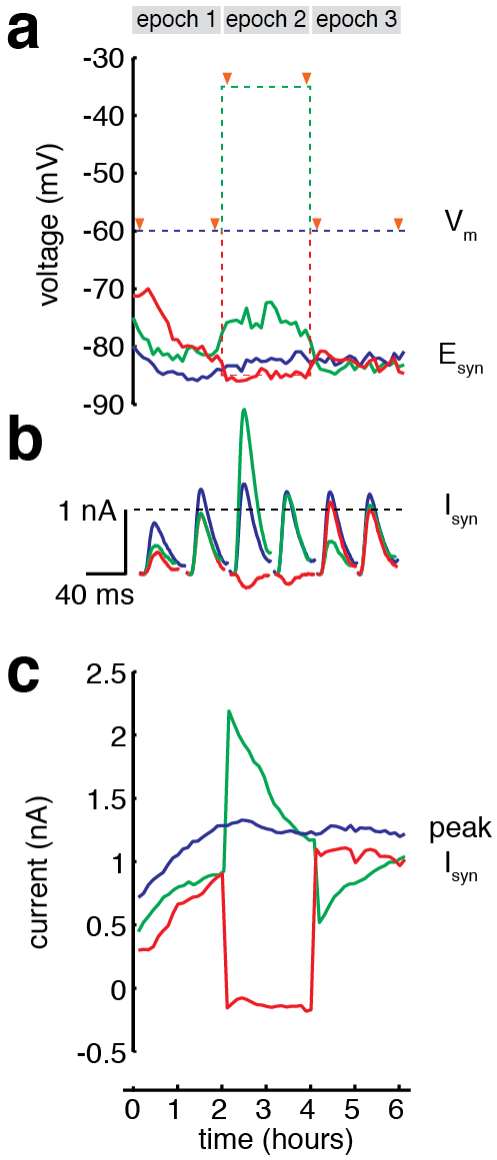

Figure 2.12 Effect of voltage perturbation on synaptic reversal potential and synaptic current.

(a) Time course of E_{syn} for representative preparations (prep. D3, prep. C3, and prep. H5). Colored dashed lines show PD membrane voltage for each experimental condition. Orange arrows in (a) denote times where spike-triggered I_{syn}s in (b) were measured. (c) Time course of peak I_{syn} for representative preparations.

Interestingly, in depolarized preparations, this sudden increase in peak I_{syn} was followed by a gradual decrease back to near-baseline current by the end of epoch 2 due to the reduced conductance in depolarized preparations during epoch 2. The voltage step back to -60 mV at the end of epoch 2 led to a sudden I_{syn} decrease, which was followed by a steady increase toward baseline current during epoch 3. Control experiments typically showed a small increase in current during epoch 1 that eventually plateaued (Figure 2.12b-c, blue) while hyperpolarized preparations exhibited a decrease in peak I_{syn} at the start of epoch 2 but did not recover toward baseline current during epoch 2 (Figure 2.12b-c, red).

In summary, by instantaneously altering current driving force via acute voltage perturbation, E_{syn} and peak I_{syn} were simultaneously perturbed with the change in voltage. Interestingly, though the synaptic response from Figure 2.8 seemed inconsistent with our expectation of HSP, it was entirely consistent as a homeostatic response to the perturbations in both E_{syn} and peak I_{syn}. For example, in depolarized preparations, E_{syn} is depolarized during epoch 2 (Figure 2.12a, green). Because chloride is the predominant permeant ion through these synaptic channels, this depolarization of E_{syn} is presumably due to chloride accumulation from the suddenly increased I_{syn} and increased driving force for chloride leak. In this case, the reduction in synaptic strength in depolarized preparations should slow this accumulation, opposing the perturbation. That the neuron could adjust and change conductance in the right direction to restore peak I_{syn} and E_{syn} to baseline levels following a change in voltage suggested that these elements might be under

homeostatic control.

Analyzing the extent of homeostatic synaptic regulation among network attributes

Although the synaptic conductance change was not what was anticipated as a response to post-synaptic voltage perturbation, it is possible that it was instead triggered by a change in a specific attribute of network activity (e.g. the cycle period or the phase of the pacemaker burst) or by the change in E_{syn} or peak I_{syn} and that the response was in the right direction to homeostatically oppose the change in one of those particular attributes. Indeed, the pyloric circuit contains network activity attributes that are stereotyped and change very little throughout life and even across different animals (Bucher, Prinz et al. 2005), characteristics that may signal that they are under homeostatic control.

To assess whether any specific network attribute is homeostatically regulated through a compensatory adjustment in synaptic conductance, four novel homeostasis metrics were established. These four metrics were conceived to study different aspects of a presumptive negative feedback system. The first metric assesses if there is a relationship between the acute perturbation magnitude and the subsequent response (Δg_{syn} slope) magnitude to determine a potential trigger attribute. The second and third metrics ignore the Δg_{syn} slope and focus only on the attributes themselves in an attempt to find evidence for well-regulated behavior. Do

these recover homeostatically after perturbation (Metric 2)? Is there a difference in their values before perturbation and after perturbation (Metric 3)? Closing the feedback loop, the fourth metric examines the general relationship between g_{syn} and each attribute. Do large changes in g_{syn} translate to large changes in the attribute? Is there any consistent effect of changes in g_{syn} on the attribute?

To illustrate how the metrics were calculated and what time periods were used for calculations, the peak I_{syn} trace from a representative depolarized preparation (prep. D3) is used as an example attribute (Figure 2.13).

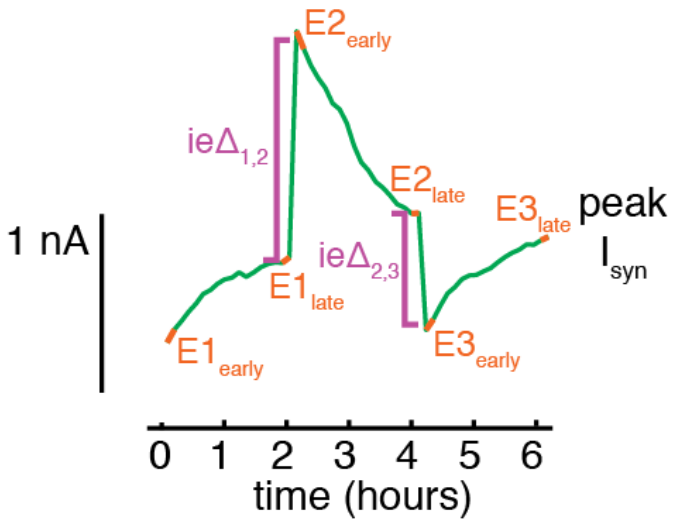

Figure 2.13 Schematic showing measurements and time periods used for homeostasis metrics.

Labeled time periods (orange) and measured values (magenta) used for homeostasis metrics are shown overlaid over the peak I_{syn} trace of a representative depolarized preparation (prep. D3).

As highlighted previously, the predominant synaptic response was that of a change in the slope of the g_{syn} trace; some preparations exhibited a large change in g_{syn} slope while others showed a more modest response. Therefore, for the first metric I argue that if a particular attribute were responsible for triggering a homeostatic synaptic response, one would expect there to be a relationship between the magnitudes of the acute changes in that attribute and the resulting changes in g_{syn} slope, i.e. a gradation between the perturbation and the response magnitudes.

Therefore to examine this relationship for each network attribute, I measured how much the attribute changed when the voltage stepped between epochs, which from now on will be referred to as the inter-epoch difference (ieΔ). Because there are two sudden changes in voltage for each perturbed experiment, there are two ieΔs per preparation (Figure 2.13). In Figure 2.14a, open circles are ieΔs gathered from the initial voltage step (epoch 1 to epoch 2) and filled circles are from the return-to-baseline-voltage step (epoch 2 to epoch 3). Focusing on where these points fall on the x-axis of Figure 2.14a, one can see the effect of the voltage step on one particular attribute, the peak I_{syn}. As with Figure 2.13, it is evident that in depolarized preparations the initial depolarization (Figure 2.14a, green open circles) gave positive peak I_{syn} ieΔ values – i.e. depolarization led to a sudden increase in peak I_{syn} – while the subsequent return to baseline voltage (Figure 2.14a, green filled circles) reduced peak I_{syn}. Conversely, the initial hyperpolarization reduced peak I_{syn} (Figure 2.14a, red open circles) and the return to baseline voltage increased peak Isyn (Figure 2.14a, red filled circles).

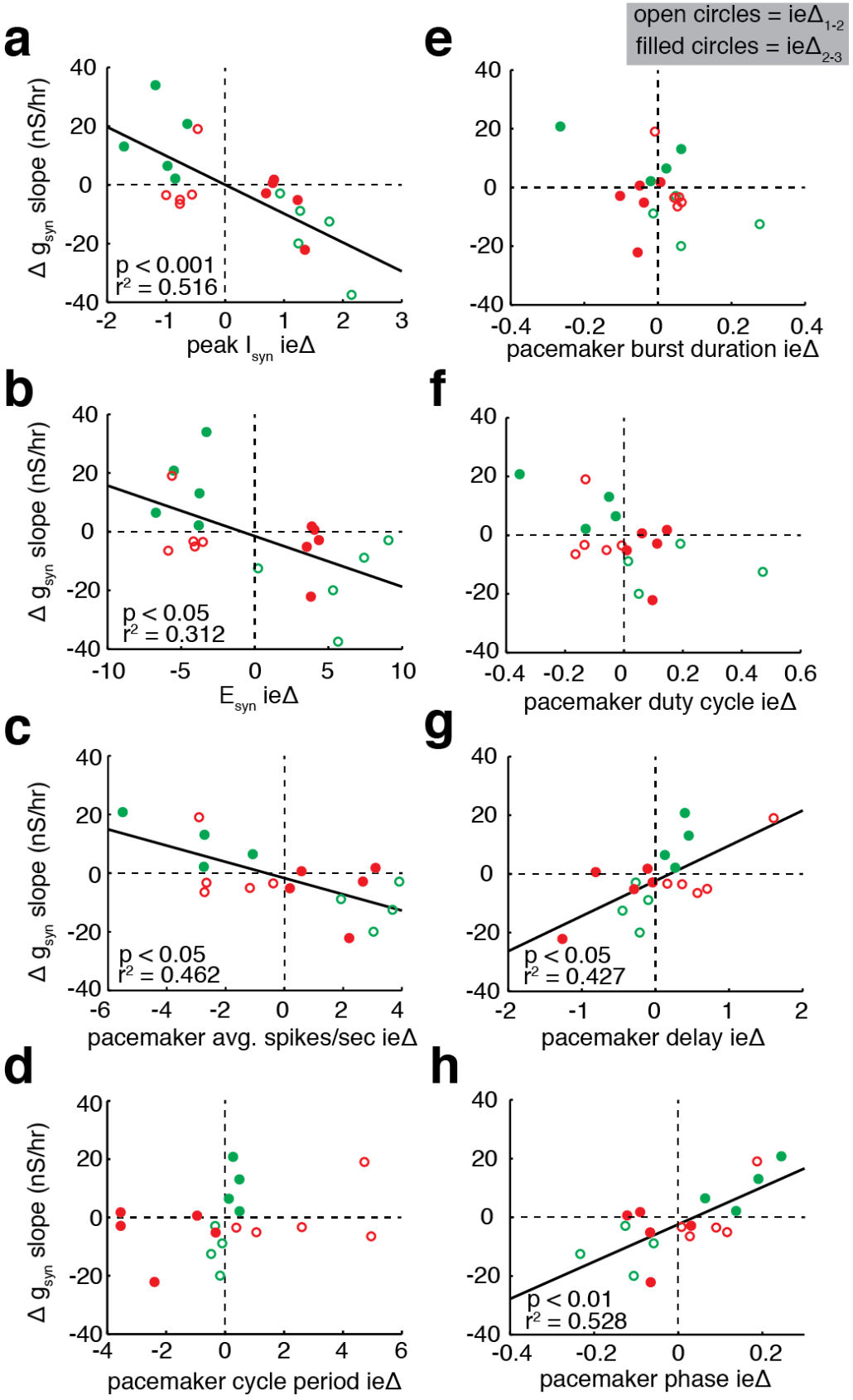
a
b
c
d
e
f
g
h
open circles = ieΔ1-2
filled circles = ieΔ2-3
Δ gsyn slope (nS/hr)
peak Isyn ieΔ
p < 0.001
r2 = 0.516
Esyn ieΔ
p < 0.05
r2 = 0.312
pacemaker avg. spikes/sec ieΔ
p < 0.05
r2 = 0.462
pacemaker cycle period ieΔ
pacemaker burst duration ieΔ
pacemaker duty cycle ieΔ
pacemaker delay ieΔ
p < 0.05
r2 = 0.427
pacemaker phase ieΔ
p < 0.01
r2 = 0.528

Figure 2.14 Correlations between network attribute perturbations and change in g_{syn} slope.

Analysis is shown for the relationship between the acute perturbation in attribute (x-axis) and the subsequent change in g_{syn} slope (y-axis). The change in g_{syn} slope is significantly correlated with the magnitude of peak I_{syn} and E_{syn} ieΔs, as well as pacemaker average spikes/second, delay, and phase ieΔs. Points gathered between epoch 1 and 2 are shown as open circles and transitions between epoch 2 and 3 are shown as filled circles. Black fitted lines represent significant correlation of p<0.05, Spearman's rho.

In this way, the effect of the voltage manipulation can be seen for all the examined attributes (Figure 2.14a-h). This analysis confirms that, as in Figure 2.12a, depolarized preparations see an initial acute depolarization of E_{syn}, followed by a hyperpolarization of E_{syn} when the voltage is brought back to -60 mV; the opposite is true for hyperpolarized preparations (Figure 2.14b).

How the voltage perturbation acutely affects the quantifiable network activity attributes can also be systematically examined (Figure 2.14c-h). Note that in one of the depolarized preparations, I was not able to record from the pdn to gather reliable activity attribute measurements of the pacemaker activity. Therefore, in the ensuing analyses of the pacemaker activity attributes (Figure 2.14c-h; Figure 2.15; Figure 2.16), there is an N of 4 for the initial depolarization (open circles) and the return to baseline voltage (filled circles) of depolarized preparations. Nevertheless, upon analyzing how voltage perturbation affects

network activity, the acute effect seen in Figure 2.11 is confirmed and extended: depolarization acutely increases average pacemaker spikes per second, reduces cycle period, increases burst duration and duty cycle, and reduces delay and phase (Figure 2.14c-h, green open circles) and the converse tends to be true for the return to baseline voltage (Figure 2.14c-h, green filled circles). Again, the opposite can be seen for initial hyperpolarization (Figure 2.14c-h, red open and filled circles).

By plotting these points with the subsequent change in g_{syn} slope on the y-axis, I examined whether the acute ieΔs correlated with the ensuing change in conductance slope. There were significant relationships involving changes in peak I_{syn}, E_{syn}, as well as the pacemaker average spikes per second, delay, and phase (Figure 2.14a-c,g,h, fitted lines represent significant correlation of $p<0.05$, Spearman's rho).

Again, the relationships for the pacemaker activity attributes were opposite to expectation if those attributes were homeostatically regulated by this synapse. Using the depolarized preparations as an example, the initial depolarization increases average spikes per second in the pacemaker complex, but the synapse responded by reducing inhibition (negative Δg_{syn} slope) onto an already overly spiking neuron (Figure 2.14c, green open circles). Additionally, the synapse reduced inhibition following a shortened pacemaker delay and phase (Figure 2.14g,h, green open circles). Recalling the network model database analysis, the strength of the LP-to-PD synapse was expected to have a positive effect on both pacemaker delay

and phase (Figure 2.2 and Figure 2.3a). Therefore, the expectation was that, in response to a reduction in these attributes, the synapse should instead strengthen to increase them, providing negative feedback to homeostatically oppose the change.

There was still the possibility that, even though the change in g_{syn} slope was opposite to the expected response for the activity attributes of the pacemaker, the expectation could have been incorrect, and the activity attributes might have actually recovered from the acute ieΔs. Indeed, the hallmark of homeostasis is the tendency to compensate and recover from perturbation. Were these attributes able to recover from the ieΔs during the epoch that followed?

For the second metric of homeostatic regulation, I aimed to answer this question by quantifying the percent recovery of each attribute during epochs 2 and 3 (epochs that followed an ieΔ). Using Figure 2.13, in this example one can qualitatively see a recovery of peak I_{syn} during epoch 2 toward the value immediately before $ie\Delta_{1,2}$ ($E1_{late}$) and during epoch 3 toward the value immediately before $ie\Delta_{2,3}$ ($E2_{late}$). To quantify this, I used $100*[(ie\Delta_{1,2} - (E2_{late} - E1_{late})) / ie\Delta_{1,2}]$ as the percent recovery during epoch 2 and $100*[(ie\Delta_{2,3} - (E3_{late} - E2_{late})) / ie\Delta_{2,3}]$ as the percent recovery during epoch 3. 100% represents ideal homeostatic recovery; positive percentages indicate instances where the attribute changed in the right direction for recovery (although >100% represents an overshoot); and any negative percentage signifies a change in a non-homeostatic direction.

By applying this metric, it can be determined which attributes exhibit the best ability to homeostatically recover from perturbation (presented graphically in Figure 2.15, tabulated descriptive statistics are presented in Table 2.1). Open circles indicate recovery when perturbed by the initial voltage step (during epoch 2) and filled circles are from the return-to-baseline-voltage step (during epoch 3).

When both depolarization and hyperpolarization preparations were considered, only peak I_{syn} exhibited a mean percent recovery significantly different from zero ($p<0.05$, one-sample t-test). Peak I_{syn} and E_{syn} achieved significance when only depolarized preparations were considered. Thus, following an ieΔ, none of the attributes that quantified the characteristic pyloric electrical activity displayed a consistent ability to recover. The attributes that did show a tendency to recover, peak I_{syn} and E_{syn}, did so preferentially in depolarized preparations. This could be explained by the significant change in synaptic conductance preferentially seen in depolarized preparations (Figure 2.10b). Indeed, in peak I_{syn} recovery, there was a significant difference in the percent recovery of depolarized preparations and hyperpolarized preparations means (paired sample t-test, $p<0.05$).

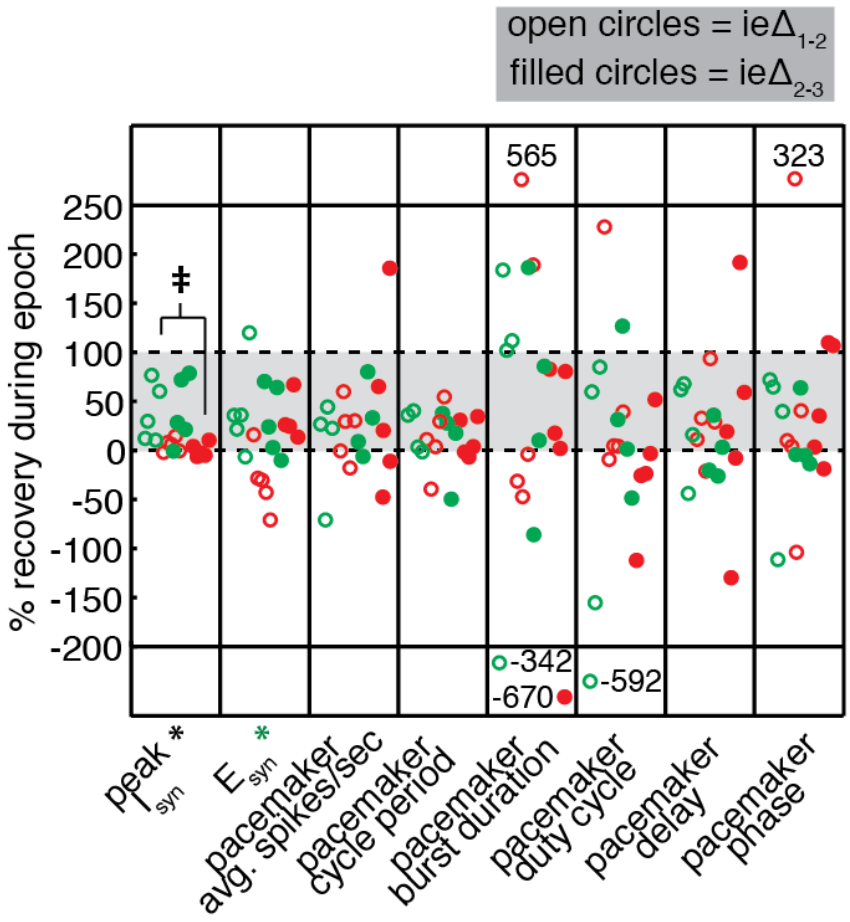

Figure 2.15 Percent recovery of each network attribute following an ieΔ.

A measure of how well attributes were able to recover from perturbation is shown. Positive values indicate recovery in a homeostatic direction, although >100% is an overshoot. Points outside the y-axis bounds are shown in the outside boxes with their values adjacent. Black asterisk by label signifies mean from all perturbed preparations significantly different from zero, while green asterisk signifies only depolarized means significantly different from zero ($p<0.05$, one-sample t-test). Double dagger symbol (‡) indicates a significant difference in means when comparing depolarized values to hyperpolarized values (paired sample t-test, $p<0.05$).

Table 2.1 Percent recovery following an ieΔ.

attribute	perturbations considered	n	mean	s.d.
peak I_{syn}				
	Depol. * ‡	5	38.87	30.13
	Hyperpol. ‡	5	2.63	6.99
	All *	10	20.75	28.26
E_{syn}				
	Depol. *	5	35.79	40.03
	Hyperpol.	5	-2.82	42.93
	All	10	17.50	44.86
pacemaker avg. spikes/sec				
	Depol.	4	17.31	43.84
	Hyperpol.	5	31.35	64.49
	All	9	25.11	55.18
pacemaker cycle period				
	Depol.	4	13.97	30.13
	Hyperpol.	5	12.00	26.45
	All	9	12.88	27.30
pacemaker burst duration				
	Depol.	4	31.52	175.45
	Hyperpol.	5	18.37	301.40
	All	9	24.22	246.60
pacemaker duty cycle				
	Depol.	4	-61.44	231.28
	Hyperpol.	5	15.41	86.77
	All	9	-18.75	166.00
pacemaker delay				
	Depol.	4	11.85	41.26
	Hyperpol.	5	27.74	82.39
	All	9	20.68	66.03
pacemaker phase				
	Depol.	4	13.22	61.24
	Hyperpol.	5	51.02	113.54
	All	9	34.22	93.50

n = number of preparations analyzed. There were two calculations per preparation (one for each ieΔ). As with Figure 2.15*, asterisk (*) signifies mean significantly different from zero (Student's t-test, p<0.05) and double dagger symbol (‡) indicates a significant difference in means (paired sample t-test, p<0.05) when comparing depolarized values versus hyperpolarized values.*

It is possible that for some of the attributes, the voltage perturbation was disruptive enough to not allow for recovery while it was being applied. As with studies that use bath-applied drugs to silence network activity, often the effects of the homeostatic regulation (such as increased spiking activity) are not seen until the perturbation is removed or washed away and the network is returned to its pre-perturbation state. Thus, for the third metric I investigated how each attribute's value changed following the perturbation in epoch 2 compared to its pre-perturbation value. Again using the labels in Figure 2.13, I quantified this metric as ($100*[(E3_{early} - E1_{late}) / E1_{late}]$). In Figure 2.13, the peak I_{syn} immediately following epoch 2 ($E3_{early}$) is less than immediately preceding epoch 2 ($E1_{late}$); the decrease represents a negative percent change in this depolarized case. This occurs because of the conductance decrease during epoch 2 in depolarized preparations. If peak I_{syn} were under homeostatic control, one would expect all other depolarized preparations should see a similar result (negative percent change), while all hyperpolarized preparations should see the opposite (positive percent change). Similarly, one would expect a cultured network with HSP regulating spiking activity to exhibit a consistent increase in spiking after being relieved from activity block and a consistent decrease following an induced network hyperactivity when compared to pre-perturbation spiking levels. Therefore, the expectation was that there should be a clear positive/negative separation for this metric depending on which voltage perturbation was applied.

When this metric was applied to all attributes, only peak I_{syn} showed such a separation, again providing the result most consistent with an attribute that is under homeostatic regulation (Figure 2.16). Depolarized preparations had peak I_{syn} values that were smaller after epoch 2 compared to before, while hyperpolarized preparations displayed the opposite.

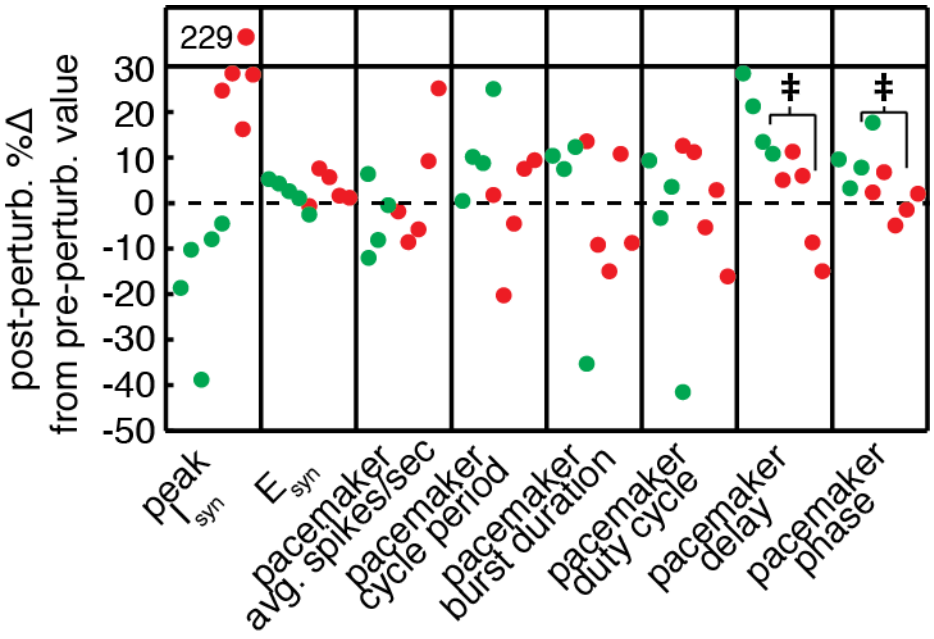

Figure 2.16 The post-perturbation change of each network attribute as a percentage of its pre-perturbation value.

A measure of how different post-perturbation values are from pre-perturbation values is shown. The expectation was that, qualitatively, depolarized and hyperpolarized preparations would be segregated on either side of zero. Only peak I_{syn} satisfied this condition. Points outside the y-axis bounds are shown in the outside box with their values adjacent. Double dagger symbol (‡) indicates a significant difference in means when comparing depolarized values to hyperpolarized values (paired sample t-test, $p<0.05$).

Table 2.2 Post-perturbation change of each network attribute as a percentage of its pre-perturbation value

attribute	perturbations considered	n	mean	s.d.
peak I_{syn}				
	Depol.	5	-16.03	13.75
	Hyperpol.	5	65.34	91.70
E_{syn}				
	Depol.	5	2.13	3.05
	Hyperpol.	5	3.07	3.43
pacemaker avg. spikes/sec				
	Depol.	4	-3.56	8.19
	Hyperpol.	5	3.63	13.81
pacemaker cycle period				
	Depol.	4	11.09	10.23
	Hyperpol.	5	-1.22	11.96
pacemaker burst duration				
	Depol.	4	-1.29	22.76
	Hyperpol.	5	-1.72	12.95
pacemaker duty cycle				
	Depol.	4	-7.98	22.94
	Hyperpol.	5	1.03	11.98
pacemaker delay				
	Depol. ‡	4	18.49	7.99
	Hyperpol. ‡	5	-0.27	11.03
pacemaker phase				
	Depol. ‡	4	9.56	6.01
	Hyperpol. ‡	5	0.96	4.40

n = number of preparations analyzed. Double dagger symbol (‡) indicates a significant difference in means (paired sample t-test, $p<0.05$) when comparing depolarized values versus hyperpolarized values.

Interestingly, when statistical analyses were applied to these data comparing means of hyperpolarized and depolarized preparations, peak I_{syn} means were not statistically distinct due to the one large outlier hyperpolarized preparation, which led to a very large calculated standard deviation for the hyperpolarized preparations (Table 2.2). The depolarized means were significantly different for the hyperpolarized means of pacemaker delay and phase, though they were not strictly separated on either side of zero as expected and as demonstrated by the peak I_{syn} values.

Lastly, if the synapse were involved in a regulatory feedback loop, when the g_{syn} changes, so should the attribute. If changes in g_{syn} do not translate to changes in the attribute, one would not consider the synapse to be very effective in regulating that attribute. Therefore, for the fourth metric, I looked for correlations between g_{syn} slope during an epoch and any change in network attribute output within that same epoch for all preparations to assess whether changes in g_{syn} affect the attribute in a consistent way. Only peak I_{syn} was significantly correlated ($p<0.001$, Table 2.3), an unsurprising finding considering g_{syn} was calculated using measurements of peak I_{syn}.

Table 2.3 p values of correlation analysis between changes in g_{syn} and changes in attribute within the same epoch

attribute	p
peak I_{syn} *	<0.001
E_{syn}	0.18
pacemaker avg. spikes/sec	0.07
pacemaker cycle period	0.23
pacemaker burst duration	0.41
pacemaker duty cycle	0.29
pacemaker delay	0.24
pacemaker phase	0.52

Correlations between changes in g_{syn} and changes in attribute were assessed for every epoch in every preparation. Asterisk (*) indicates a significant correlation ($p<0.05$, Spearman's Rho).

To summarize, the four metrics of homeostatic regulation provide evidence that this synapse does not regulate or actively act to recover any attribute of network spiking/bursting activity or the timing of those bursts in the time scale considered. Therefore, these results leave two attributes as the most plausible triggers for the changes in g_{syn}: E_{syn} (which showed recovery in depolarized preparations) and especially peak I_{syn}, which most closely resembled an attribute regulated by homeostatic synaptic plasticity according to all metrics.

Computational model of $[Cl^-]$-dependent homeostatic synaptic regulation

The analyses from the voltage perturbation study suggested that peak I_{syn} was most well-suited as the target of synaptic regulation. Because chloride is the

primary permeant ion through these inhibitory channels, one way this could be implemented functionally in the cell is through a chloride sensor that feeds back onto and affects synaptic strength. To test whether this hypothesis could reproduce the observed I_{syn}, E_{syn}, and g_{syn} responses, I created a proof-of-concept computational model.

This single-compartmental computational model of a post-synaptic neuron used the $[Cl^-]_{in}$ as feedback to homeostatically regulate its synaptic currents to achieve a target $[Cl^-]_{in}$ of 25 mM (see methods for model details). Chloride enters the cell through synaptic channels and leak channels and exits the cell through the activity of chloride pumps to establish an equilibrium level of $[Cl^-]_{in}$ when these processes balance (Figure 2.17). Information about the $[Cl^-]_{in}$ is then used as negative feedback to regulate g_{syn}.

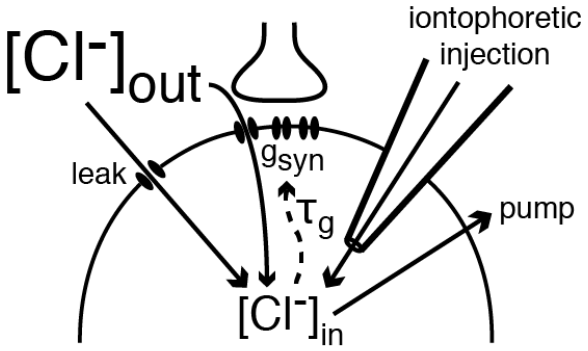

Figure 2.17 Schematic diagram of computational model of synaptic regulation of post-synaptic $[Cl^-]_{in}$.

In the computational model, chloride enters the cell either through leak channels, synaptic channels, or via iontophoretic injection and exits the cell through the action of pumps. Information about the internal chloride concentration is fed back to the synaptic channels to

regulate conductance with a time constant τ_g.

When the same protocol is applied as in the voltage perturbation experiments, the model qualitatively replicates the effect on E_{syn}, peak I_{syn}, and g_{syn} (Figure 2.18).

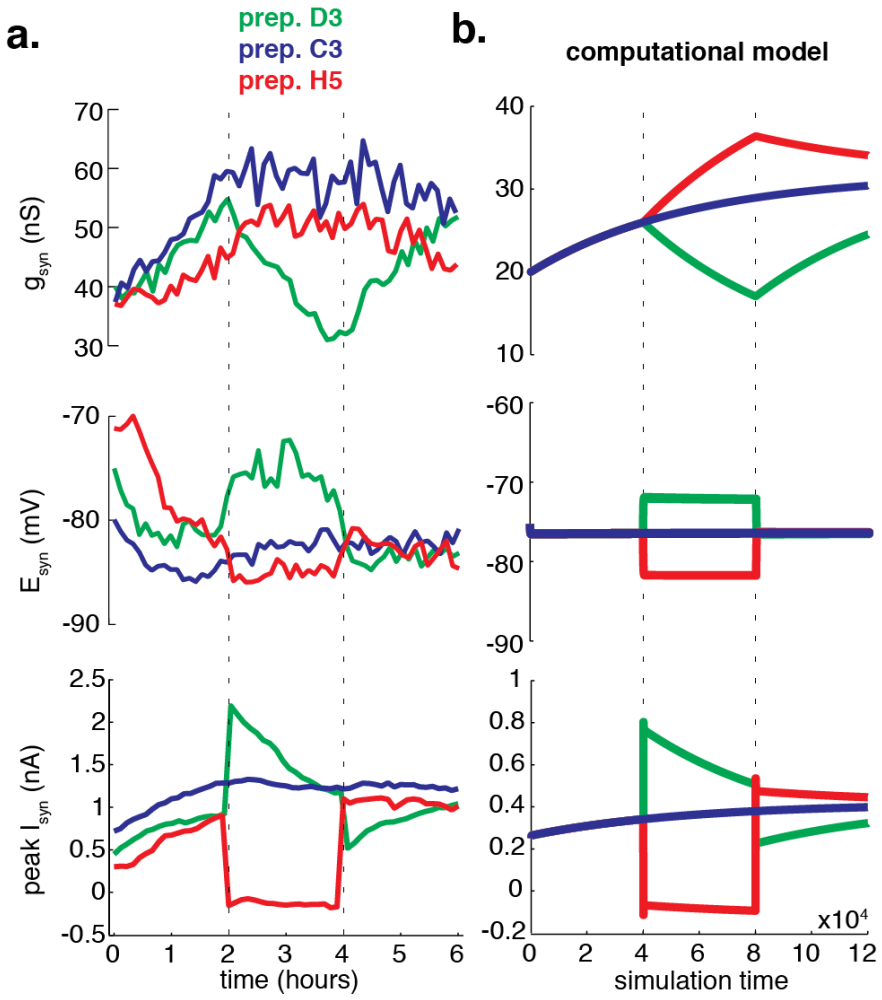

Figure 2.18 Comparison between example traces from living system and output from computational model of synaptic regulation of $[Cl^-]_{in}$.

Simulations run matching experimental conditions from voltage perturbation study qualitatively replicate experimental data. (a) Trajectory of g_{syn}, E_{syn}, and peak I_{syn} from representative experimental preparations. (b) Trajectory of g_{syn}, E_{syn}, and peak I_{syn} from

computational model of synaptic regulation of $[Cl^-]_{in}$.

Focusing on the green traces in Figure 2.18b, depolarizing the neuron to -35 mV caused a sudden increase in driving force for chloride during epoch 2. This led to more chloride entry through synaptic and leak channels, so the E_{syn} remained depolarized during epoch 2 due to chloride accumulation. The accumulation was registered by the $[Cl^-]_{in}$ sensor and fed back to reduce g_{syn}. The reduction in g_{syn} in turn reduced peak I_{syn} homeostatically but did not have as strong an effect on E_{syn}, presumably due to the larger conductance of leak channels (g_{leak} = 52 nS) that were still open.

Looking at the red traces in Figure 2.18b, the model explains why peak I_{syn} and E_{syn} seemed to recover more reliably for depolarized preparations than hyperpolarized preparations (as found in the voltage perturbation study): hyperpolarized preparations have very little driving force during epoch 2. When the hyperpolarizing perturbation is applied, the membrane potential is suddenly brought to -85 mV – which is very near E_{syn} – cutting the driving force sharply. Despite the $[Cl^-]_{in}$ feedback onto the synapses providing a continued drive to increase conductance during epoch 2, the driving force is so small that even large changes in conductance would have very little effect on peak I_{syn} and E_{syn}, giving the appearance of a unidirectional homeostatic rule.

With aid from the computational model, it is now evident why E_{syn} may not have performed as well as peak I_{syn} in the homeostasis metrics: a large leak current

prevented a fast E_{syn} recovery in both voltage perturbations and a small driving force hindered recovery in hyperpolarized preparations.

Though peak I_{syn} performed best according to the metrics, the model incorporates a homeostatic rule regulating $[Cl^-]_{in}$ and not peak I_{syn} directly. Therefore, I could tease apart these homeostatic targets by modeling iontophoretic injection of chloride, which – like the depolarized perturbation – would increase chloride accumulation, but would not do so due to increased synaptic current.

Simulating 3 nA of chloride injection into the model during epoch 2, the model predicts that a direct perturbation of $[Cl^-]_{in}$ – while maintaining membrane voltage unchanged at -60 mV – will lead to a change in peak I_{syn} in a non-homeostatic direction (Figure 2.19). At the beginning of epoch 2, the simulated chloride injection depolarizes E_{syn}, which reduces synaptic driving force (see reduction in the difference between V_m and E_{syn}), quickly reducing peak I_{syn}. If peak I_{syn} were the homeostatic target, one would expect g_{syn} to increase to counteract the reduction in current. Instead, g_{syn} decreases, reducing peak I_{syn} further during epoch 2. This occurs because the model was built to respond to the increase in $[Cl^-]_{in}$, not the decrease in peak I_{syn}.

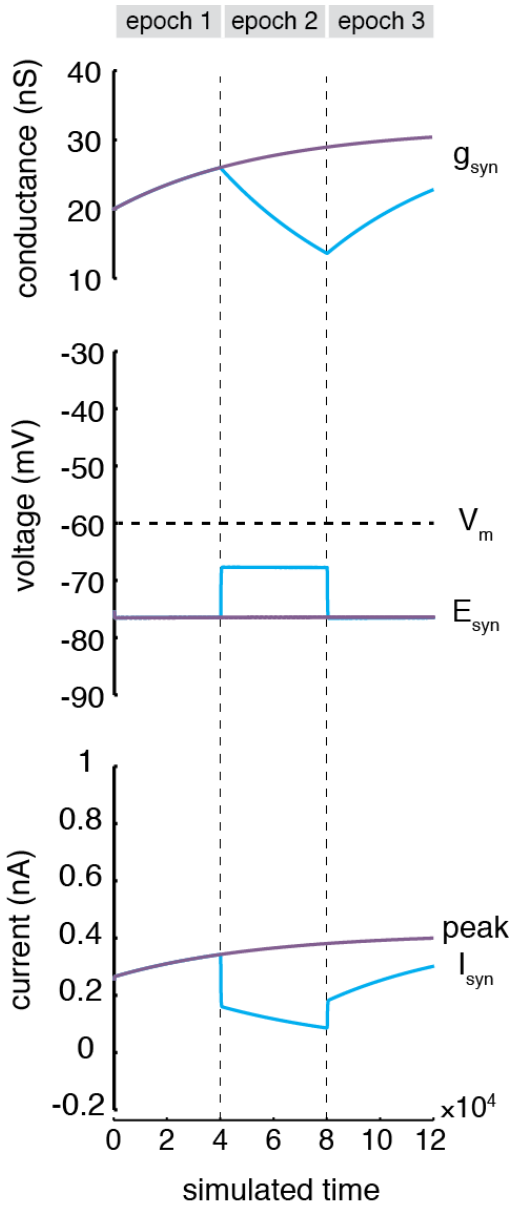

Figure 2.19 Prediction from model of synaptic regulation of $[Cl^-]_{in}$.

Simulation of 3 nA iontophoretic Cl^- injection during epoch 2 is shown in cyan. Purple traces simulate no Cl^- injection. The model predicts that Cl^- injection will depolarize E_{syn}, reducing driving force, and the regulation will act in a non-homeostatic direction for peak I_{syn}. The initial reduction in peak I_{syn} from the reduction in driving force is followed by a further reduction in current from the reduction in synaptic conductance because the model adjusts g_{syn} in a negative feedback loop in response to the change in $[Cl^-]_{in}$, not peak I_{syn}.

In summary, the computational model of $[Cl^-]$-dependent homeostatic synaptic regulation qualitatively matches the experimental results, and predicts that – if post-synaptic $[Cl^-]_{in}$ were indeed the regulatory target in the living system – iontophoretic injection of chloride into PD should lead to a decrease in LP-to-PD synaptic conductance.

Post-synaptic chloride injection triggers reduction in LP-to-PD synaptic strength

To test whether the LP-to-PD synapse in the living system behaves in a manner similar to the computational model of $[Cl^-]_{in}$ regulation and to eliminate any voltage-dependent or network-activity-sensitive effects, I used two-electrode voltage clamp (TEVC) to hold PD at -60 mV while a third electrode performed iontophoretic injection into PD (Figure 2.20a). Similar to the voltage perturbation study, the experimental protocol was split into three time epochs (Figure 2.20b). In this study, each epoch lasted for one hour. The same short voltage step protocol as in the previous study was applied every six minutes to calculate E_{syn} and g_{syn}. Iontophoretic injection was performed during the middle hour (epoch 2) using either a KCl electrode hereafter referred to as a "chloride electrode" (cyan in subsequent figures) or from an electrode with the same fill solution as the TEVC electrodes, hereafter referred to as a "sulfate electrode" (purple in subsequent figures).

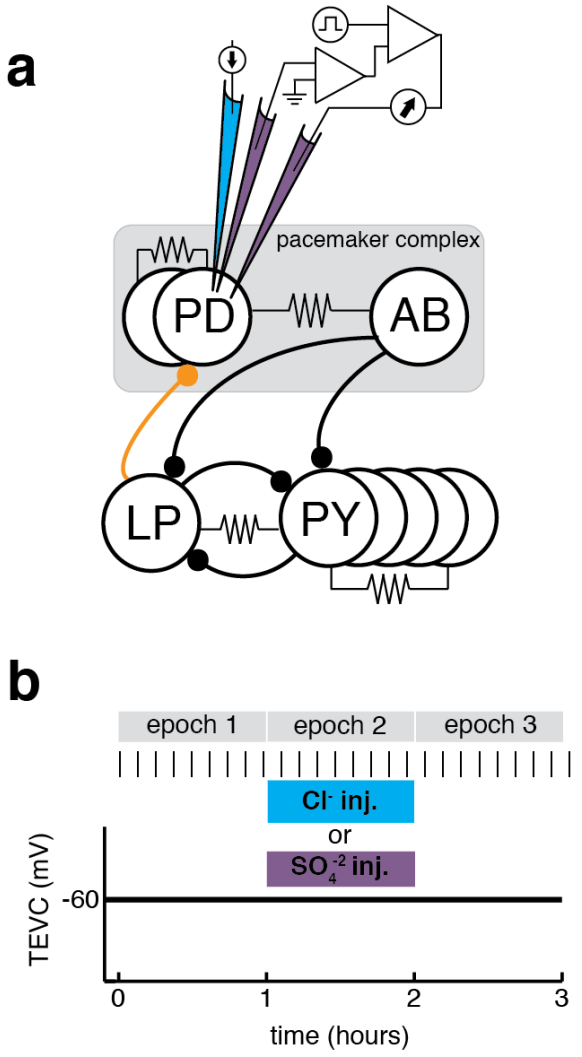

Figure 2.20 Iontophoretic injection study experimental method

(a) One of the PD neurons in the pacemaker complex was impaled with three sharp microelectrodes. Two-electrode voltage clamp (TEVC) was used to hold the PD membrane potential to -60 mV throughout the experiment (b). Cyan/purple color scheme is used throughout where cyan represents iontophoretic injection with chloride electrode and purple represents injection with sulfate electrode. Tick marks above indicate applications of voltage step protocol described in methods and shown in Figure 2.6.

Because the membrane voltage was maintained at -60 mV throughout, ongoing network activity was not disrupted, so these experiments divorced the effect in response to $[Cl^-]_{in}$ perturbation from any potential voltage-dependent effect or any response triggered by a change in network activity.

As with the voltage perturbation study, absolute values of g_{syn} varied between preparations, but much like the previous depolarized preparations, the synapse weakened during epoch 2 in response to the $[Cl^-]_{in}$ perturbation (Figure 2.21a). This was in contrast to the preparations that underwent iontophoretic injection using the sulfate electrode, which on average continued to increase in conductance (Figure 2.21b).

The preparations again began with a modest average increasing g_{syn} (g_{syn} slope>0) (Figure 2.22a). During epoch 2, Cl^--loaded preparations had an average negative g_{syn} slope, while sulfate preparations saw a slight rise in g_{syn} slope; both had a slight positive slope during the last hour. In terms of how g_{syn} changes between epochs within each preparation, the Cl^--loaded preparations were very similar to the depolarized preparations in the voltage perturbation study, where there was a large decrease in g_{syn} slope from epochs 1 to 2 and a subsequent increase from epochs 2 to 3 (Figure 2.22b, compare to Figure 2.10b).

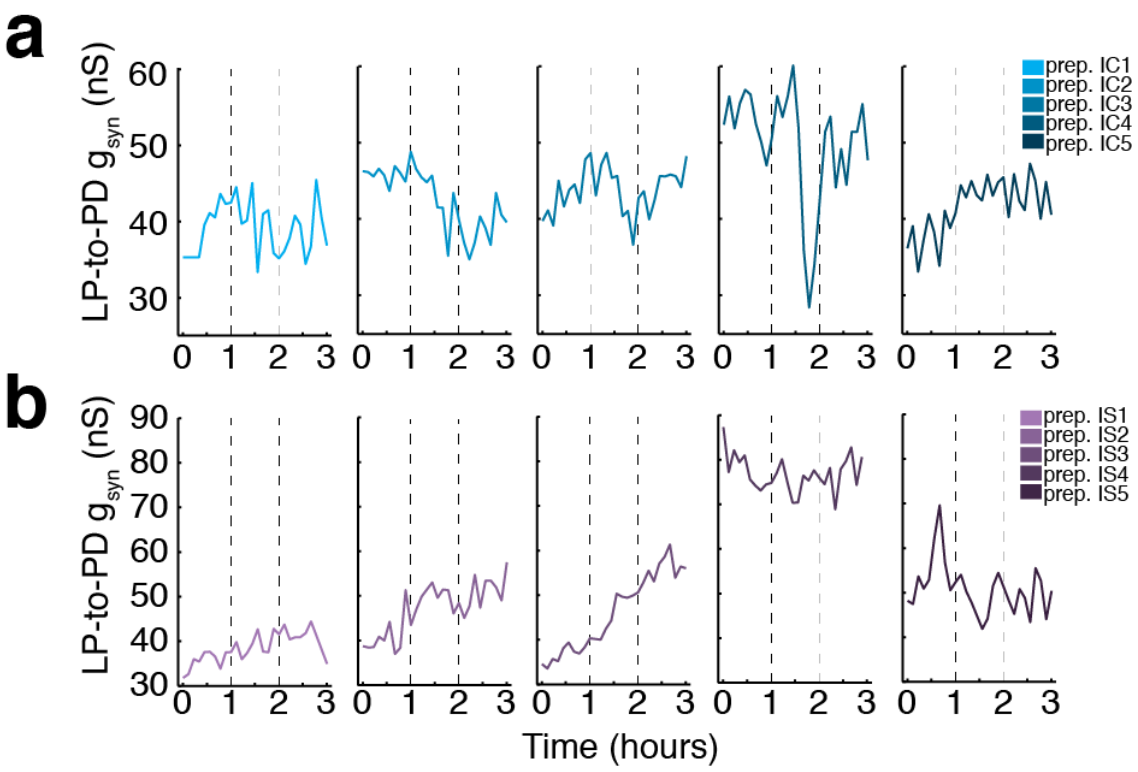

Figure 2.21 Changes in LP-to-PD synaptic strength following post-synaptic iontophoretic injection.

Underlying LP-to-PD synaptic conductance (g_{syn}) is shown for every experimental preparation. Colors correspond to experimental groups from Figure 2.20*b. Briefly, (a) cyan: 3 nA hyperpolarizing iontophoretic injection with chloride electrode (0.5 or 1 M KCl) during epoch 2; (b) purple: 3 nA hyperpolarizing iontophoretic injection with sulfate electrode (0.6 M K_2SO_4 + 20 mM KCl) during epoch 2; Dashed lines denote epoch boundaries.*

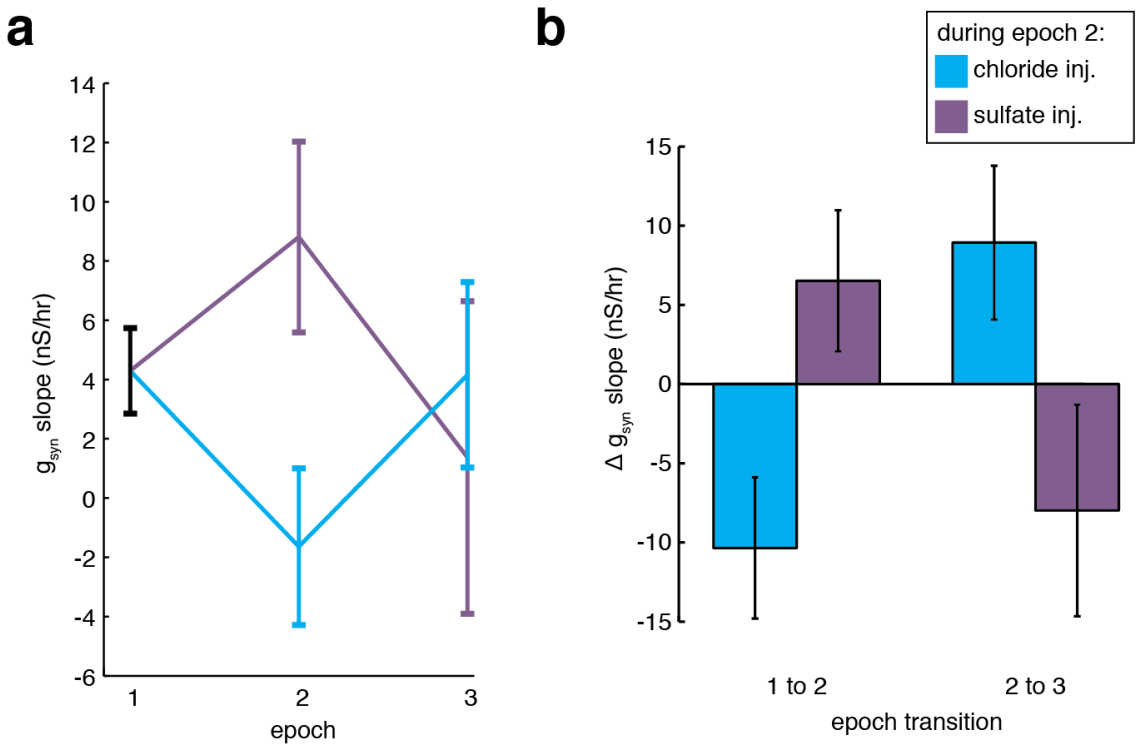

Figure 2.22 The effect of iontophoretic chloride injection on synaptic conductance.

LP-to-PD g_{syn} slopes were calculated as shown in Figure 2.9 *for each epoch in a preparation. (a) Average g_{syn} slope was determined for epoch 1 by calculating a weighted mean g_{syn} slope for all preparations (n=10). The mean was weighted according to the error in each slope's fit (see methods chapter for more details). For the subsequent epochs, the weighted means shown were calculated using only the preparations from each condition (n=5 for each condition). (b) The change in g_{syn} slope from one epoch to the next within each preparation was calculated and a weighted mean for each condition is shown. (a,b) Error shown as weighted mean ± 95% C.I. Non-overlapping C.I.s are considered significant.*

The iontophoretic injection study matched the prediction from the computational model of $[Cl^-]_{in}$ regulation. By incorporating a hypothesized $[Cl^-]_{in}$ regulation rule in the model, I simulated a situation where the system decreased conductance following a reduction in peak I_{syn}. The synapse in the living system behaved as qualitatively predicted by the model following chloride loading (Figure 2.23, cyan). The preparation that received current injection through the sulfate electrode did not change strongly in either E_{syn} or peak I_{syn} during epoch 2 (Figure 2.23a, purple).

In the voltage perturbation study, I analyzed whether the magnitude change that peak I_{syn} and E_{syn} experienced in between epochs (the inter-epoch change, or ieΔ) correlated with the subsequent change in g_{syn} slope and found that there was a significant relationship with both attributes (Figure 2.14a,b). Therefore, I examined whether a significant graded relationship also existed in the iontophoretic experiments between the ieΔ of E_{syn} or peak I_{syn} and the subsequent change in g_{syn} slope. Again, both E_{syn} and peak I_{syn} exhibited a significant correlation (Figure 2.24). Because the synapse was now responding in the opposite direction for a decrease in peak I_{syn}, the relationship with peak I_{syn} ieΔ was different than in the voltage perturbation study (Figure 2.24, peak I_{syn} grey line shows correlation line from Figure 2.14a). The correlation with E_{syn} ieΔ was nearly identical to that in the voltage perturbation study (Figure 2.24, E_{syn} grey line shows correlation line from Figure 2.14b), suggesting that the synapse responded to a disruption of $[Cl^-]_{in}$ with

the same graded change in g_{syn} slope regardless of how the perturbation occurred – either through a change in voltage or a direct iontophoretic injection of chloride.

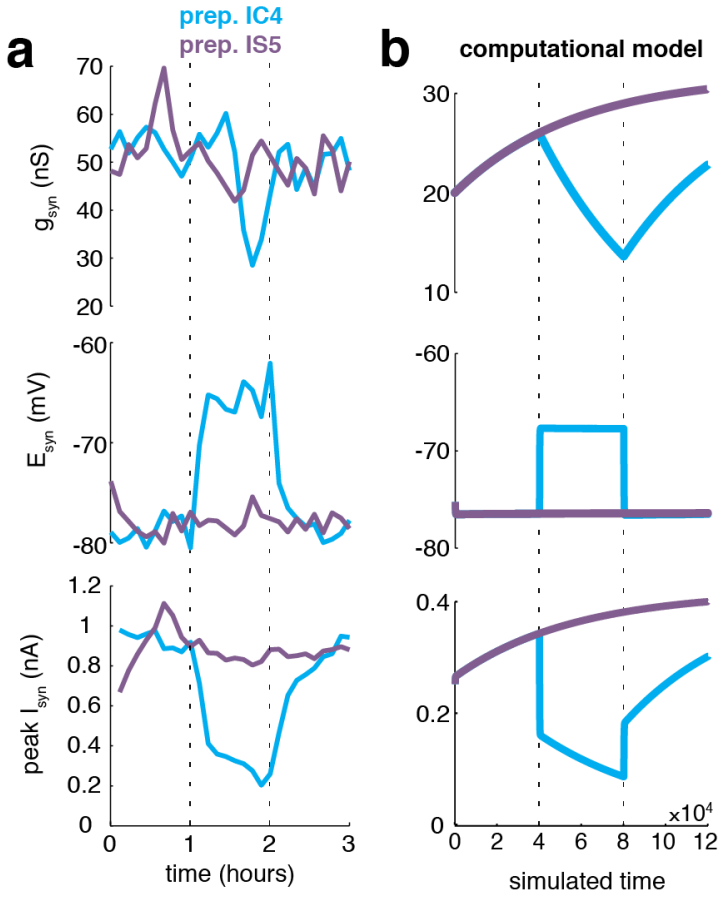

Figure 2.23 Comparison between example traces from living system and computational model of synaptic regulation of $[Cl^-]_{in}$.

Experimental results from living system qualitatively match predictions made by the computational model of synaptic regulation of $[Cl^-]_{in}$. (a) Trajectory of g_{syn}, E_{syn}, and peak I_{syn} from two representative experimental preparations from the n=5 pool for each condition. (b) Trajectory of g_{syn}, E_{syn}, and peak I_{syn} from computational model of synaptic regulation of $[Cl^-]_{in}$.

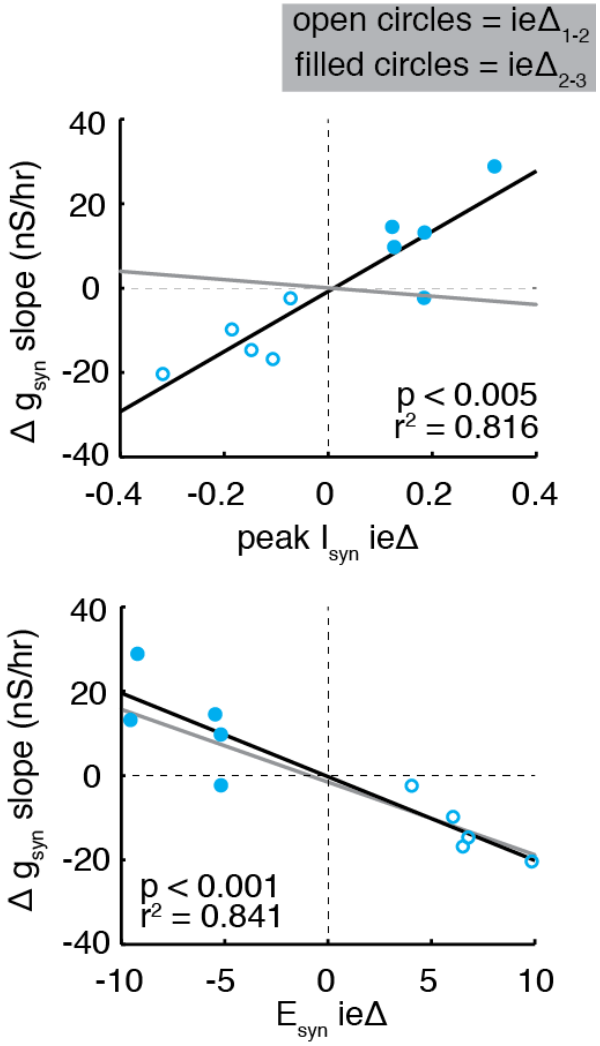

Figure 2.24 Analysis of graded correlation between peak I_{syn} ieΔ or E_{syn} ieΔ and the subsequent Δg_{syn} slope.

As in Figure 2.14*, analysis is shown for the relationship between the acute perturbation in peak I_{syn} (top) or E_{syn} (bottom plot) and the subsequent change in g_{syn} slope. Black line shows correlation determined from iontophoretic injection study. Grey line shows previous correlation from voltage perturbation study. Points gathered between epoch 1 and 2 are shown as open circles and transitions between epoch 2 and 3 are shown as filled circles.*

DISCUSSION

Owing to its stereotyped activity and accessibility, the neurons of the crusteacean STG have been key for studies of activity homeostasis. Many previous homeostasis studies in the crustacean STG have focused on changes in cell-intrinsic membrane currents (Turrigiano, Abbott et al. 1994, Turrigiano, LeMasson et al. 1995, Golowasch, Abbott et al. 1999, Golowasch, Casey et al. 1999, Haedo and Golowasch 2006), presence or absence of neuromodulators (Thoby-Brisson and Simmers 1998, Golowasch, Casey et al. 1999, Thoby-Brisson and Simmers 2000, Thoby-Brisson and Simmers 2002, Luther, Robie et al. 2003, Khorkova and Golowasch 2007), and/or the coordinated relationships between currents (MacLean, Zhang et al. 2003, Schulz, Goaillard et al. 2006, Khorkova and Golowasch 2007, Schulz, Goaillard et al. 2007, Goaillard, Taylor et al. 2009) in long-term regulation of pyloric output. As in other systems, pyloric activity was predicted to be under homeostatic synaptic control as well (Soto-Trevino, Thoroughman et al. 2001), but such activity-dependent regulation had never been described experimentally.

In the voltage perturbation study, by perturbing the membrane potential of the post-synaptic PD neuron for two hours, I show that the LP-to-PD synapse does display activity-dependence and respond with a change in the slope of its synaptic conductance trace. Surprisingly though, the change in g_{syn} is in the opposite direction than expected for homeostasis of network activity (Figure 2.8). In

addition, the results from the four homeostasis metrics provide little evidence that the changes in LP-to-PD synaptic strength influence any attribute of pyloric circuit output at the time-scale studied (Figure 2.14; Figure 2.15; Table 2.1; Figure 2.16). LP-to-PD synaptic influence on pre-synaptic LP activity attributes were also analyzed and showed similar results (data not shown).

One possibility to explain these unexpected findings is that the perturbation of network activity was not applied for a sufficient amount of time to trigger HSP. Despite it being possible to induce the synaptic scaling form of HSP on the time-scale of a few hours (Ibata, Sun et al. 2008), most other studies of HSP have found that it is typically expressed on a longer time scale, often taking days of disrupted activity to see homeostatic changes in synaptic currents (Turrigiano and Nelson 2004). Therefore, this synapse might change strength in the expected direction to regulate network activity at longer time scales or in a loss-of-neuromodulator dependent manner. This may explain the fact that lobster pyloric neurons see reduced inhibition several days after removal of the descending neuromodulatory input to the STG, a perturbation that typically silences network-wide pyloric activity for days (Thoby-Brisson and Simmers 2002). However, the finding that the magnitude of LP-to-PD g_{syn} slope does not have a reliable predictive effect on changes in network activity raises doubts about how effective such synaptic regulation would be in recovering activity.

Another possibility is that this regulation of g_{syn} does not operate with a target

of network activity because changes to this synapse's conductance do not substantially or consistently influence pre- or post-synaptic activity. Independent of synaptic influence, adjustments to intrinsic cellular conductances alone can allow STG neurons to recover their characteristic bursting activity when isolated from their network partners in culture (Turrigiano, Abbott et al. 1994, Turrigiano, LeMasson et al. 1995, Haedo and Golowasch 2006). Perhaps each STG neuron primarily adjusts intrinsic properties to recover its own individual spiking activity and/or excitability, relying on synapses to promote network stability through the timing, not necessarily strength, of their activation. This idea is consistent with previous studies in the crustacean pyloric network that have concluded that the LP-to-PD synapse may serve to stabilize the network in the face of perturbation primarily through its phase and duration of activation in the ongoing rhythm (Prinz, Thirumalai et al. 2003, Mamiya and Nadim 2004, Thirumalai, Prinz et al. 2006, Johnson, Brown et al. 2011, Nadim, Zhao et al. 2011).

Variability in parameters that underlie stable activity is also a much-studied phenomenon in the STG (Bucher, Prinz et al. 2005, Marder and Goaillard 2006, Goaillard, Taylor et al. 2009). As has been observed in other central pattern generating networks such as the leech heartbeat system (Tobin and Calabrese 2005, Roffman, Norris et al. 2012) and has been predicted theoretically in the STG (Prinz, Bucher et al. 2004) and shown in other synapses of the pyloric network (Goaillard, Taylor et al. 2009), the present study showed that at time 0, the pyloric circuit produced functional output with variable strengths of LP-to-PD g_{syn} (Figure 2.8a-c).

This provides further evidence that the pyloric network need not achieve a constrained conductance level at the LP-to-PD synapse for the network to produce functional activity. Indeed, functional pyloric activity is seen here across animals with g_{syn} values that vary almost three-fold.

If the strength of the LP-to-PD synapse does not significantly influence pyloric activity and the network can produce functional behavior with a large variability of underlying synaptic strengths, why then did the slope of synaptic conductance change at all? According to the homeostasis metrics, both peak I_{syn} and E_{syn} displayed behavior that appeared consistent with homeostatic control – especially peak I_{syn}. Changes to both attributes were correlated with the ensuing change in g_{syn} slope, suggesting a potentially graded response (Figure 2.14a,b). Taking all perturbed preparations into account, peak I_{syn} showed a significant non-zero percent recovery following an ieΔ, which was in the right direction for homeostasis; E_{syn} achieved significant non-zero percent recovery when only depolarized preparations were considered (Figure 2.15). Depolarized preparations displayed a consistently decreased level of peak I_{syn} after perturbation while hyperpolarized preparations showed an increased level, a finding that suggests that the change in g_{syn} slope had a consistent effect during the perturbation epoch 2 (Figure 2.16). Lastly, the magnitude of g_{syn} slope only showed a significant correlation with changes in peak I_{syn} during an epoch, again highlighting that synaptic conductance is particularly effective at consistently influencing synaptic current above all other attributes.

Therefore, it is possible that the true target of the homeostatic synaptic response is not network activity, but peak I_{syn} or E_{syn}. Because chloride is the predominant ion that flows through glutamatergic inhibitory channels in decapod crustacean STGs (Marder and Paupardin-Tritsch 1978, Eisen and Marder 1982, Cleland and Selverston 1995, Cleland 1996, Cleland and Selverston 1998), both peak I_{syn} and E_{syn} depend on $[Cl^-]_{in}$. The present hypothesis – that postsynaptic $[Cl^-]_{in}$ is under homeostatic control and a change in $[Cl^-]_{in}$ triggers a compensatory synaptic response – is supported by a computational model of synaptic regulation by intracellular chloride homeostasis, which qualitatively matched the results of the voltage perturbation study (Figure 2.18).

To bypass activity perturbations and voltage-dependent post-synaptic effects and to elucidate how this synaptic plasticity might be mediated in the STG, I perturbed the post-synaptic concentration of intracellular chloride with no disruption of ongoing network activity and was able to trigger a change in inhibitory synaptic conductance slope. The change in g_{syn} slope was correlated with the change in peak I_{syn} and E_{syn} after chloride injection, consistent with a graded response.

Although the experimental and computational results are consistent with a target of post-synaptic $[Cl^-]_{in}$, it is currently not clear where it is intended for this target concentration to be established in the cell and where it is assessed how well

the actual $[Cl^-]_{in}$ is conforming to the target. The LP-to-PD synapse, though a single functional connection, is believed to be distributed throughout multiple synaptic contact sites in the dense STG neuropil (Harris-Warrick, Marder et al. 1992).

One possibility is that there is a global cell-wide target level of $[Cl^-]_{in}$ that the combined synaptic sites attempt to influence through their conductance level. This would be akin to a homeostatic target of a global synaptic reversal potential as measured at the cell body (as I have measured E_{syn}). There is evidence from this work supporting this possibility, such as the fact that the synapse exhibits the same graded response following a disruption of E_{syn}, either by voltage perturbation or chloride injection (Figure 2.24, E_{syn}), or that depolarized preparations see significant recovery of E_{syn} following perturbation (Figure 2.15, E_{syn}).

On the other hand, there is evidence suggesting that synaptic conductance would not be a very effective regulator of a global E_{syn} target. For example, there was not a significant correlation between changes in g_{syn} over the course of an epoch and the simultaneous change in E_{syn} during the same epoch. Also, an increase in synaptic conductance should enable more chloride entry through synaptic channels, increased chloride accumulation, and a depolarization of E_{syn} when the cell is clamped at -60 mV. Despite this, almost every preparation began with an increasing g_{syn} during epoch one, but instead displayed a steadily hyperpolarizing E_{syn} during that same epoch (see Figure 2.18a, epoch one). Lastly, by incorporating a chloride component to the leak current that exists in STG neurons (Golowasch 1990) into the

computational model, changes to g_{syn} end up having a very small effect on E_{syn} (Figure 2.18b). Thus, it is difficult to grasp why this g_{syn} regulation mechanism would exist to constrain a global cell-wide E_{syn} if g_{syn} is not very effective or consistent at influencing the target parameter.

In contrast, synaptic current is a parameter that is undoubtedly influenced by g_{syn}. Therefore, another possibility is that, instead of a global cell-wide $[Cl^-]_{in}$ target, there exists a target level of inhibitory synaptic transmission and the cell assesses performance by using local or quasi-local post-synaptic $[Cl^-]_{in}$ as a proxy. According to this hypothesis, there would be a $[Cl^-]_{in}$ sensor near each synaptic site that the synapse would influence. The cell could use this near-synapse $[Cl^-]_{in}$ information and, by dynamically tuning synaptic conductances, could achieve a target level of inhibitory synaptic current. Many examples of local synapse-specific regulation of synaptic efficacy exist for excitatory currents (Sutton, Ito et al. 2006, Sutton and Schuman 2006, Hou, Zhang et al. 2008, Kim and Tsien 2008, Jakawich, Nasser et al. 2010, Soden and Chen 2010, Beique, Na et al. 2011, Deeg and Aizenman 2011, Henry, McCartney et al. 2012), therefore it is tempting to hypothesize that a similar synapse-specific mechanism may be at play here. From the experimental and computational results, this appears to be the most likely possibility.

Peak I_{syn} consistently outperformed every other attribute in the metrics of homeostatic synaptic control in the previous voltage perturbation study (Figure 2.14; Figure 2.15; Figure 2.16). The computational model provided further evidence

that a $[Cl^-]_{in}$–dependent synaptic regulation rule could achieve homeostatic recovery of peak I_{syn} toward a target level; simulations tended to converge toward a peak I_{syn} level of ~0.4 nA after deflection (Figure 2.18b, peak I_{syn}). However, in the model I simulated a situation where g_{syn} decreased rather than increased following a reduction in peak I_{syn}, a phenomenon that was replicated experimentally (Figure 2.23). Though at first glance, this seems to argue against a target level of synaptic current, our hypothesis argues that the cell uses $[Cl^-]_{in}$ as a proxy for synaptic current levels, putting $[Cl^-]_{in}$ downstream of the hypothesized target. Thus, it is conceivable that by injecting 3 nA of chloride current into PD continuously for 1 hour, the increased $[Cl^-]_{in}$ reached areas in the cell near synaptic sites and was registered as if it were caused by an increase in synaptic current. Thus, the cell responded exactly as expected if current levels were above target: with a decrease in g_{syn}.

The hypothesis that chloride levels are sensed and regulated near synapses is also supported by previous experimental work that found that cultured lobster STG neurons plated with a short neurite stump display a significantly depolarized reversal potential for inhibitory glutamate channels, possibly due to a diminished ability of the plated neurons to regulate $[Cl-]_{in}$ levels near receptor sites (Cleland and Selverston 1995).

Though the possibility of homeostatic synaptic regulation mediated by local $[Cl-]_{in}$ as a means of establishing a target level of inhibitory current matches the

experimental data very well, there was one caveat to this mechanism's effectiveness. Using the computational model, I determined why it was effective at recovering peak I_{syn} following depolarization, but not particularly effective at recovering peak I_{syn} levels when the cell was hyperpolarized: the driving force for synaptic current was almost non-existent during strong hyperpolarization.

To illustrate this point, assume there is a PD neuron with a membrane potential of -60 mV and a synaptic reversal potential of -80 mV. If one were to weakly hyperpolarize the neuron, e.g. by 5 mV to -65 mV, the I_{syn} would be reduced due to the decrease in driving force for synaptic current. But because E_{syn} is still more hyperpolarized than the membrane voltage, one would still see net chloride entry into the cell (positive or "outward" current) when synaptic channels open. Thus, increasing synaptic conductance should lead to more chloride entry (larger positive outward current) in a homeostatic increase toward recovery of the previously larger current.

Conversely, when a stronger voltage perturbation is applied that hyperpolarizes the neuron to a level very near E_{syn}, such as the one employed in the voltage perturbation study, driving force for synaptic current becomes negligible; when synaptic channels open, there is no net current flow into or out of the cell (Figure 2.18, red peak I_{syn} during epoch two). In this situation, changes to g_{syn} have no effect on I_{syn}, so it becomes impossible to homeostatically recover the previous level of peak I_{syn} through changes in g_{syn} alone.

This synaptic regulation rule is especially ineffective if the cell were ever more hyperpolarized than E_{syn}. In this situation, the very negative membrane potential would actually cause the cell to extrude chloride during each synaptic event. Again, it would be impossible to homeostatically recover the appropriate level of positive outward I_{syn} by changing g_{syn} alone. In fact, the normal response to a weak hyperpolarization or a slight decrease in current – an increase in g_{syn} – would actually lead in a non-homeostatic direction, allowing more chloride to be extruded leading to a larger negative or inward current.

This difference in effectiveness can be observed in the results from the voltage perturbation analysis (Figure 2.15, peak I_{syn}), where depolarized preparations on average showed a higher positive percent recovery of I_{syn} than hyperpolarized preparations. Though this regulation seems not to be effective when the cell's membrane is more hyperpolarized than E_{syn}, such a situation is unlikely to occur naturally during the life of the animal unless chloride were allowed to accumulate unimpeded or the post-synaptic neuron's membrane potential becomes abnormally hyperpolarized.

Interestingly, in the voltage perturbation study only one preparation showed a strong increase in g_{syn} upon acute hyperpolarization, so there was no significant difference in Δg_{syn} slope between hyperpolarized preparations and controls (Figure 2.8 and Figure 2.10). One possible way this preferentially unidirectional response

could occur is if there is a baseline level of chloride concentration that is necessary to trigger changes in g_{syn} slope. For instance, if local near-synapse chloride interacts with some factor or acts directly on channels to reduce synaptic conductance, it is possible that in the hyperpolarized experiments – when little to no net chloride current was entering the cell from synaptic channels during epoch two (Figure 2.18a, red peak Isyn) – too few chloride ions were available to interact with the factor or act on synaptic channels, so no change in g_{syn} slope was initiated. Thus, it is possible that there is a dynamic range of $[Cl^-]_{in}$ for which this regulation acts, and I might have gone below the minimum $[Cl^-]_{in}$ upon strong hyperpolarization of PD.

Considering that one way chloride may affect g_{syn} is by directly acting on or initializing a chloride-dependent pathway that acts on post-synaptic channels through post-translational modifications, another possibility to explain the preferential unidirectionality of the change in g_{syn} slope is that there is a finite number of channels that can be modified to increase conductance at any given time. This would establish a "ceiling" level of synaptic conductance before new protein synthesis and channel insertion would be necessary to increase conductance any further, a change that might occur at longer time scales than could have been observed in this study.

CHAPTER 3 :

DETAILED METHODS

Network model database study

The database of computational pyloric network models used has been described previously (Prinz, Bucher et al. 2004). The architecture of the network models used to create the database is summarized below.

Each neuronal node in the network was modeled as a single model neuron: one model neuron to jointly represent the AB/PD, one model neuron to represent LP, and one model neuron to represent the PY neurons. Each model neuron was a single compartment model with eight Hodgkin-Huxley type membrane currents and an intracellular calcium buffer (Prinz, Billimoria et al. 2003, Prinz, Thirumalai et al. 2003). The eight membrane currents were: a Na^+ current, I_{Na}; a fast and a slow transient Ca^{2+} current, I_{CaT} and I_{CaS}; a transient K^+ current, I_A; a Ca^{2+}-dependent K^+ current, $I_{K(Ca)}$; a delayed rectifier K^+ current, I_{Kd}; a hyperpolarization-activated inward current, I_H; and a leak current, I_{leak}. The different model neurons used for each of the three nodes differed only in the maximal conductance densities for these eight membrane currents; voltage dependencies and dynamics of the currents did not differ between the model neurons.

The model neurons present in the database were: 1 of 5 different versions of the AB/PD pacemaker complex, 1 of 5 versions of LP, and 1 of 6 versions of PY. The different versions of each of the neuronal nodes were defined by different

combinations of underlying maximal conductance densities of the membrane currents incorporated (Table 3.1).

Table 3.1 Maximal conductance densities of model neurons used in network model database

Model neuron	Maximal membrane conductance density in mS/cm^2							
	$g(I_{Na})$	$g(I_{CaT})$	$g(I_{CaS})$	$g(I_A)$	$g(I_{K(Ca)})$	$g(I_{Kd})$	$g(I_H)$	$g(I_{leak})$
AB/PD 1	400	2.5	6	50	10	100	0.01	0.00
AB/PD 2	100	2.5	6	50	5	100	0.01	0.00
AB/PD 3	200	2.5	4	50	5	50	0.01	0.00
AB/PD 4	200	5.0	4	40	5	125	0.01	0.00
AB/PD 5	300	2.5	2	10	5	125	0.01	0.00
LP 1	100	0.0	8	40	5	75	0.05	0.02
LP 2	100	0.0	6	30	5	50	0.05	0.02
LP 3	100	0.0	10	50	5	100	0.00	0.03
LP 4	100	0.0	4	20	0	25	0.05	0.03
LP 5	100	0.0	6	30	0	50	0.03	0.02
PY 1	100	2.5	2	50	0	125	0.05	0.01
PY 2	200	7.5	0	50	0	75	0.05	0.00
PY 3	200	10.0	0	50	0	100	0.03	0.00
PY 4	400	2.5	2	50	0	75	0.05	0.00
PY 5	500	2.5	2	40	0	125	0.01	0.03
PY 6	500	2.5	2	40	0	125	0.00	0.02

Values gathered from (Prinz, Bucher et al. 2004).

The combinations of maximal conductances that were selected for each neuron type were considered good candidates for the respective neuron type based on two criteria.

First, the isolated activity of the model neuron needed to mimic the activity of the living neuron when synaptically isolated. For example, AB/PD model neurons were selected based on their ability to produce oscillatory bursts of action potentials within physiological ranges in isolation, just as the AB/PD circuit pacemaker does in the crustacean STG, e.g. isolated AB/PD model neuron cycle periods were kept within physiological ranges: AB/PD #1: 1.46 s; AB/PD #2: 1.49 s; AB/PD # 3: 1.58 s; AB/PD # 4: 1.61 s; AB/PD # 5: 1.64 s. LP and PY model neurons do not show oscillatory bursting behavior when synaptically isolated in the STG, so models that were silent or slowly (<11.5 Hz) spiking when isolated – but that exhibit a burst of action potentials when rebounding from inhibition – were selected as good candidate LPs or PYs.

The second criterion for determining which model neurons to use as the AB/PD, LP, and PY nodes was that the models cover as wide a range of maximal conductance densities as possible.

To combine these different versions of AB/PD, LP, and PY into connected networks, synaptic connections were modeled by 5 or 6 possible conductance values for each synapse (0 nS, 3 nS, 10 nS, 30 nS, and 100 nS – and for synapses onto

PY, 1 nS). The different possible combinations of different model neurons combined with the possible combinations in synaptic strengths in the network resulted in over 20 million total combinations of pyloric model networks. Of those, ~20% were considered "pyloric-like" (4,047,375 networks). Networks were classified as "pyloric-like" if, when simulated, they produced a triphasic bursting pattern similar to that in the living STG and did so in the same bursting sequence as in the animal (PD-LP-PY). As described in the original paper: "in every cycle (defined as the period between one AB/PD burst start and the next), the LP burst began before the start of the PY burst and finished before the end of the PY burst; and the AB/PD burst finished before the start of the LP burst, creating a gap in firing activity" (Prinz, Bucher et al. 2004).

In this work, I used a database that included the output of only those "pyloric-like" networks so that I could measure functional activity attributes such as those highlighted in Figure 2.1. Analysis of database content was performed in MATLAB (r2009a, The MathWorks).

Families of network models

Here, I define a family as a group of network models that share every cellular and synaptic parameter, except for the LP-to-PD synaptic conductance. Sibling networks are those that belong to the same network family. Because I limited the analysis to neighboring g_{syn} values on the scale of possible synaptic strengths (0 nS,

3 nS, 10 nS, 30 nS, and 100 nS for this particular synapse), families whose sibling networks were not neighbors on the scale were excluded. For instance, if the only "pyloric-like" sibling networks had LP-to-PD g_{syn} values of 10 nS and 100 nS, the family would be excluded. Conversely the family would be included if the 30 nS sibling were present so that I could assess the expected effect of a 1 nS g_{syn} increase from 10 nS to 30 nS and 30 nS to 100 nS.

The expected normalized effect of an increase in LP-to-PD g_{syn} within a family was calculated by finding the mean effect of each increase in g_{syn} between neighbors on the scale of synaptic strength values and dividing by the difference in the neighboring conductance values. For example within a family, the change in cycle period when we examine the 0 nS to 3 nS sibling networks is divided by 3 nS, whereas the change from 30 nS to 100 nS is divided by 70 nS.

Dissection

Adult *Cancer borealis* crabs (n=15) were purchased from commercial suppliers and stored in artificial seawater at ~12°C. Crab saline (11 mM KCl, 440 mM NaCl, 13 mM $CaCl_2 \bullet 2H_2O$, 26 mM $MgCl_2 \bullet 6H_2O$, 11.2 mM Trizma base, 5.1 mM maleic acid, pH 7.45 ± 0.03) was refrigerated until used.

Animals were cold-anesthetized for 20-30 minutes on ice prior to dissection. The stomach, which includes the stomatogastric nervous system, was removed from

the animal, pinned into a Sylgard-lined dish, and submerged in chilled (10-14°C) saline (Figure 3.1a). The stomatogastric nervous system, including the STG and the nerves that innervate the stomach muscles, was dissected from the stomach and pinned in a Sylgard-lined Petri dish (Figure 3.1b).

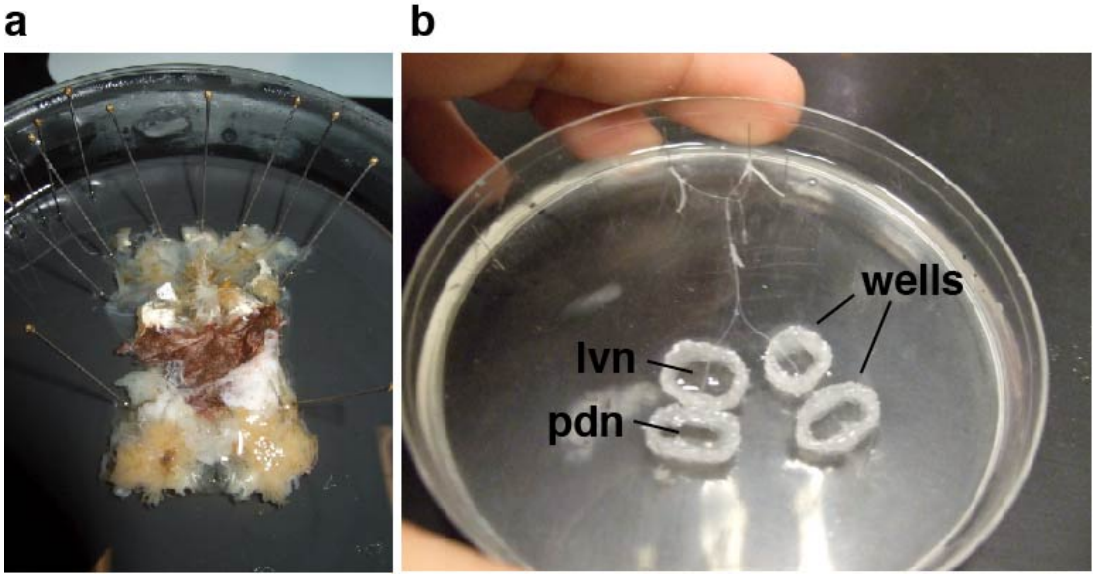

Figure 3.1 *Cancer borealis* stomach and stomatogastric nervous system.

(a) The dissected stomach is shown pinned in a glass dish in chilled saline. After removal of tissue surrounding the nerves, the stomatogastric nervous system was transferred and pinned to a Sylgard-lined Petri dish (b) where petroleum jelly wells were constructed around nerves. In (b), nerves are labeled at left, but are also present in the wells labeled at right.

Fresh, chilled saline was applied to the preparation every ~15-20 min during dissection. The glial sheath covering the STG was opened and the preparation was transferred to an electrophysiology rig where fresh saline was chilled with a Peltier thermoelectric cooler (Warner Instruments SC-20 connected to a Warner Instruments CL-100 temperature controller) and superfused over the nervous system.

Experimental design

Voltage step protocol

Every 360 seconds throughout every experiment in both experimental studies, the cell underwent a 40-second "voltage step protocol" in which its somatic voltage was brought to five potentials (in order: -65 mV, -85 mV, -95 mV, -105 mV, -55 mV; see Figure 2.6). Average injected currents during these five short voltage steps were used to construct an IV curve and resting membrane potential and input resistance were calculated according to a least-squares fit regression line and Ohm's law. Only experimental attempts free from sudden and prolonged large shifts in input resistance or resting membrane potential (experiments free from >10 MΩ changes in input resistance or >20 mV changes in resting membrane potential that last longer than 1 hour) were considered successful and were included. Spike-triggered averages from the large amplitude LP spikes in the extracellular lvn trace were used to determine LP-to-PD inhibitory post-synaptic currents (IPSCs) at the

five potentials. Spike-triggered IPSCs (peak - base) at each potential were used to construct a peak I_{syn}-V curve where synaptic reversal potential (E_{syn}) and synaptic conductance (g_{syn}) were determined according to a least-squares fit regression line and Ohm's law (Figure 2.7). Data points where the peak I_{syn}-V regression line had a fit of insufficient linearity ($r^2<0.90$) were excluded.

Voltage perturbation study

The voltage perturbation study was broken up into three epochs: epoch 1 (hour 0 – hour 2), epoch 2 (hour 2 - hour 4), and the epoch 3 (hour 4 - hour 6). At the time of designing these experiments, it was unknown what the time course of changes to synaptic strength would be. Therefore, experiments were chosen to be 6 hours long because we imagined 6 hours represented an acceptable balance between being long enough to begin to see changes in synaptic strength if they existed, but also not so long as to be unfeasible. Aside from the voltage step protocol run every 360 seconds, the PD neuron's membrane potential was held throughout each experiment at either the set baseline potential (-60 mV) or stepped to a new potential by either hyperpolarizing or depolarizing PD by 25 mV during epoch 2 (Figure 2.4b).

Iontophoretic injection study

The iontophoretic injection study was also broken up into three epochs, but because I had a better understanding of the time course of synaptic strength changes when designing these experiments, the total duration of the each experiment was halved: epoch 1 (hour 0 – hour 1), epoch 2 (hour 1 - hour 2), and the epoch 3 (hour 2 - hour 3). Preparations were held in TEVC at -60 mV for 3 hours in this study. The experimental protocol was broken up into three epochs: epoch 1 (0-1 hrs), epoch 2 (1-2 hrs), and epoch 3 (2-3 hrs). I had two experimental conditions: preparations that were iontophoretically loaded via the third electrode with a 3 nA injection of negative current from either a KCl electrode or an electrode with the same fill solution as the TEVC electrodes (Figure 2.20). During the voltage step protocol, the iontophoretic injection current from the third electrode was turned off.

Data acquisition and electrophysiology

Petroleum jelly wells (which can be seen in Figure 3.1b) were built around the lvn – which contains axons from PD, LP, and PY neurons – and the pyloric dilator nerve (pdn), which contains axons from PD. A stainless steel wire electrode was placed in each well for extracellular nerve recordings of pyloric network activity and activity attributes (e.g. cycle frequency, burst durations, phases, etc.). An A-M Systems Model 1700 Differential AC Amplifier (Figure 3.2, extracellular amplifier)

amplified the extracellular signal from the stainless steel wire. Because the lvn recording contained spikes from each of the pyloric neurons, it provided a convenient measure of network activity. Another benefit for this study was that the largest amplitude spikes present in the lvn recording belong to LP. Thus, LP spike times could be collected using a simple threshold on the lvn trace (as is demonstrated by the yellow threshold line in Figure 2.6).

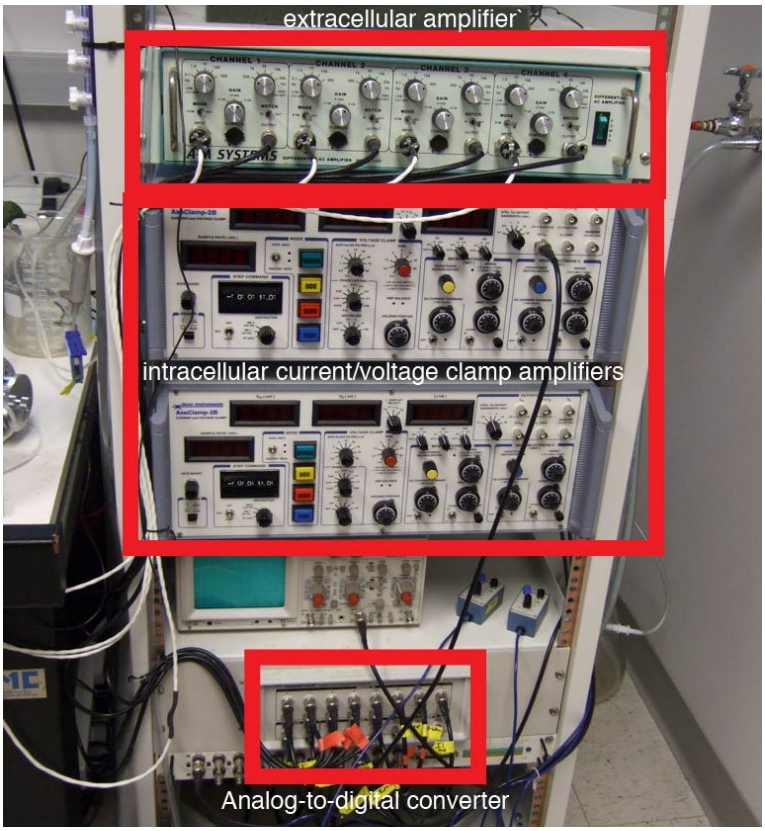

Figure 3.2 Electrophysiology rig.

The electrophysiology equipment used to record from and interface with the stomatogastric nervous system is shown. Recordings from the extracellular and intracellular amplifiers are digitized by the analog-to-digital converter and sent to a PC. The PC also sends an output signal that can adjust the voltage clamp holding potential and current injection level of the intracellular amplifiers.

For intracellular recordings, sharp glass microelectrodes (15-25 MΩ) were pulled using a P-97 Flaming/Brown Micropipette Puller (Sutter Instruments, Novato, CA) to an electrode resistance of 15-25 MΩ (Figure 3.3).

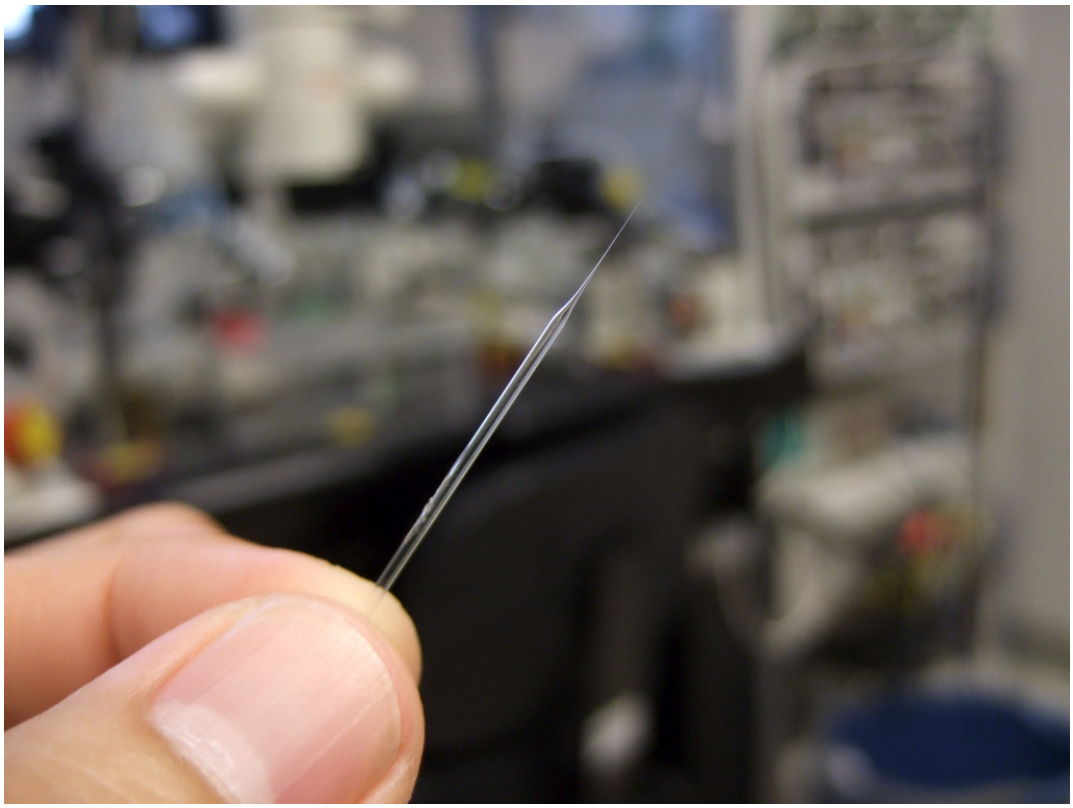

Figure 3.3 Sharp glass microelectrodes

Fine-tipped glass microelectrodes (15-25 MΩ electrode resistance) such as the example displayed above were pulled using a Sutter Instruments P-97 Flaming/Brown Micropipette Puller and used to impale the PD neuron for intracellular recording/voltage manipulation/current injection.

Sharp microelectrodes were placed into amplifier headstages, which were secured on Leitz mechanical micromanipulators. Using the micromanipulators, the position of the fine tip of the microelectrode could be precisely guided to impale the PD neuron in the STG and record its membrane potential as well as inject current to manipulate the voltage across the PD membrane. For these studies, it was particularly helpful to use sturdy mechanical micromanipulators because they do not display the slow drift in position that hydraulic micromanipulators often display. Initially, hydraulic micromanipulator use was attempted but many experimental attempts were unsuccessful due to this slow drift in position, which becomes significant and problematic over the course of 6+ hour-long intracellular recording experiments.

Biological experiments were performed by impaling one of the PD neurons with either two (for the voltage perturbation study) or three (or the iontophoretic injection study) sharp glass microelectrodes. Intracellular recordings were identified as being from one of the PD neurons based on the characteristic oscillatory voltage profile and based on the timing of its spikes compared to extracellular recordings of the lvn and pdn (Figure 3.4).

To amplify the intracellular signal and manipulate PD voltage, an Axoclamp 2B (Molecular Devices, Union City, CA) current/voltage clamp amplifier was used (Figure 3.2) with the left and right microelectrodes connected to Axoclamp 2B inputs ME1 and ME2, respectively.

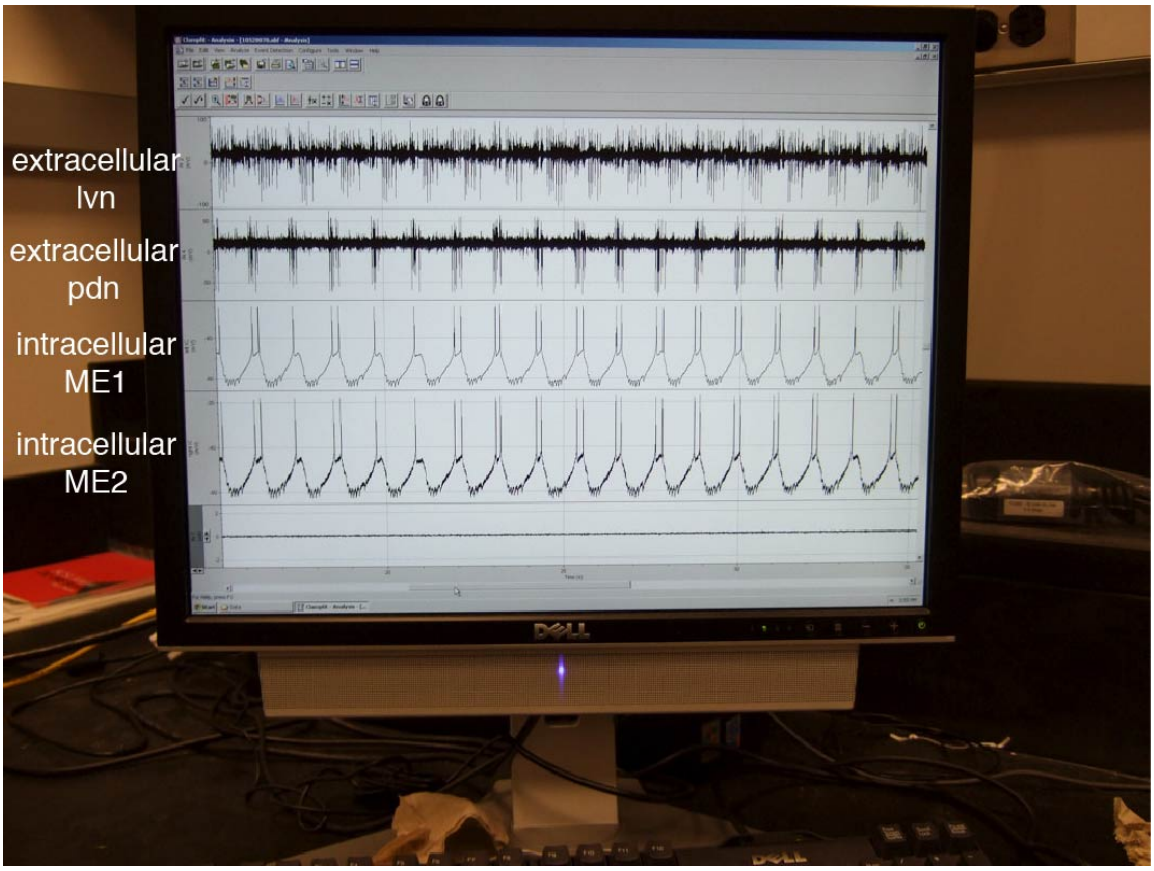

Figure 3.4 PC running Clampex software acquiring electrophysiological data

A PC was used to acquire extra- and intracellular recordings. In this example, the cell impaled with intracellular microelectrodes ME1 and ME2 was identified as PD due to its characteristic oscillatory activity and the fact that its spikes occur in time with extracellular pdn spikes.

TEVC electrodes were filled with 0.6 M potassium sulfate (K_2SO_4) and 20 mM potassium chloride (KCl). In the iontophoretic injection study, a third electrode was used to impale PD and was amplified by a separate Axoclamp 2B amplifier as input ME1 (notice the two Axoclamp 2B intracellular amplifiers in Figure 3.2). Chloride injections were performed by injecting 3 nA of negative current into PD with either a 0.5 M or 1.0 M KCl filled microelectrode. The control or vehicle iontophoretic injection electrode contained the same fill solution as the TEVC electrodes.

After impalement, the cell was allowed to recover for ~10-20 minutes while free-running intracellular and extracellular activity was monitored. After recovery, the TEVC was engaged and the cell's somatic potential was clamped to -60 mV. From then on, the cell remained in TEVC until the end of the experiment.

The Axoclamp-2B hardware low-pass filter was set with a cutoff frequency of 10 kHz. Extracellular and intracellular data was acquired and digitized with an Axon Instruments Digidata 1322A analog-to-digital converter sampled at 10 kHz (Figure 3.2). The digital signals were sent to a PC running Clampex software from the pClamp 9.2 software suite (Molecular Devices) (Figure 3.4).

Amplifier settings and Clampex protocols

After impaling one of the PD neurons with both electrodes, the hand-tuned knobs on the STEP COMMAND section of the front face of the Axoclamp 2B voltage-

clamp amplifier were set to -60 mV with the DESTINATION knob below set to "VC (mV)" and the voltage clamp was switched on by depressing the blue TEVC button in the MODE section and turning the GAIN in the VOLTAGE CLAMP section up to approximately 800 V/V (as shown in Figure 3.5). The PC interfaced with the amplifier and sent voltage clamp commands using a cable connected into the EXT. VC COMMAND input on the back of the amplifier.

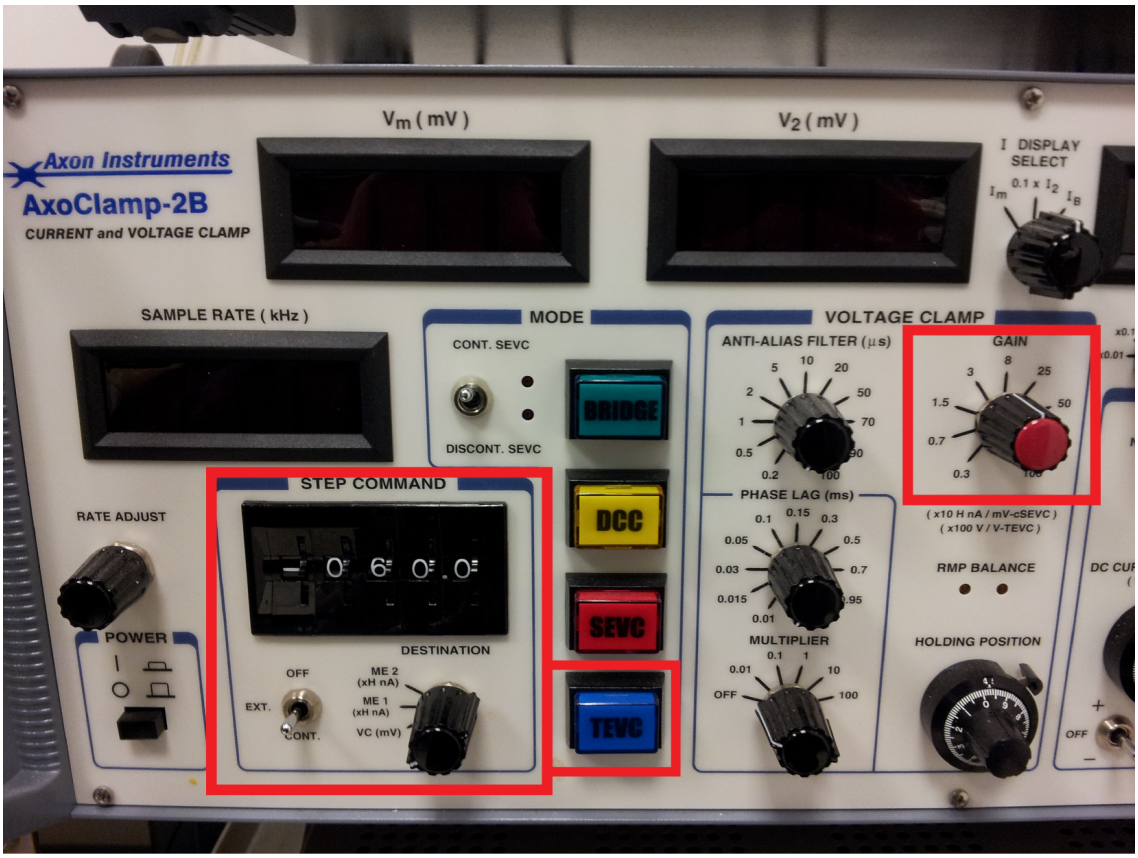

Figure 3.5 Settings on the AxoClamp-2B amplifier.

The AxoClamp-2B current and voltage clamp amplifier is shown with the sections referred to in the text highlighted in red. The voltage perturbation values shown in Figure 2.4*b are manually adjusted using the STEP COMMAND dials. The voltage step protocol was executed by a Clampex protocol on the PC (*Figure 3.6*).*

In general, the Clampex protocols used to control the amplifier alternated between a free-running recording protocol (six minutes) that only recorded activity and did not alter the command voltage and the voltage step protocol that added to the hand-tuned voltage clamp STEP COMMAND voltage shown on the front of the amplifier via the EXT. VC COMMAND input (approximately forty seconds). An example of one of the voltage step Clampex command protocols is shown in Figure 3.6. Notice that the voltage levels in the Waveform Preview window ultimately add to the set -60 mV level on the amplifier front panel to achieve the desired voltage step protocol levels of -65 mV, -85 mV, -95 mV, -105 mV, and -55 mV. Depolarizations or hyperpolarizations during epoch two of each experiment were done by manually changing the dials on the STEP COMMAND on the front face of the amplifier at the appropriate time to either -35 mV or -85 mV, respectively. During epoch two, the six-minute free-running recording Clampex protocol was the same (because the amplifier itself was used to set the voltage clamp level), but because of the additive nature of the EXT. VC COMMAND, different Clampex protocol files were needed to add to the -35 mV or -85 mV STEP COMMAND level and achieve the desired voltage step protocol levels.

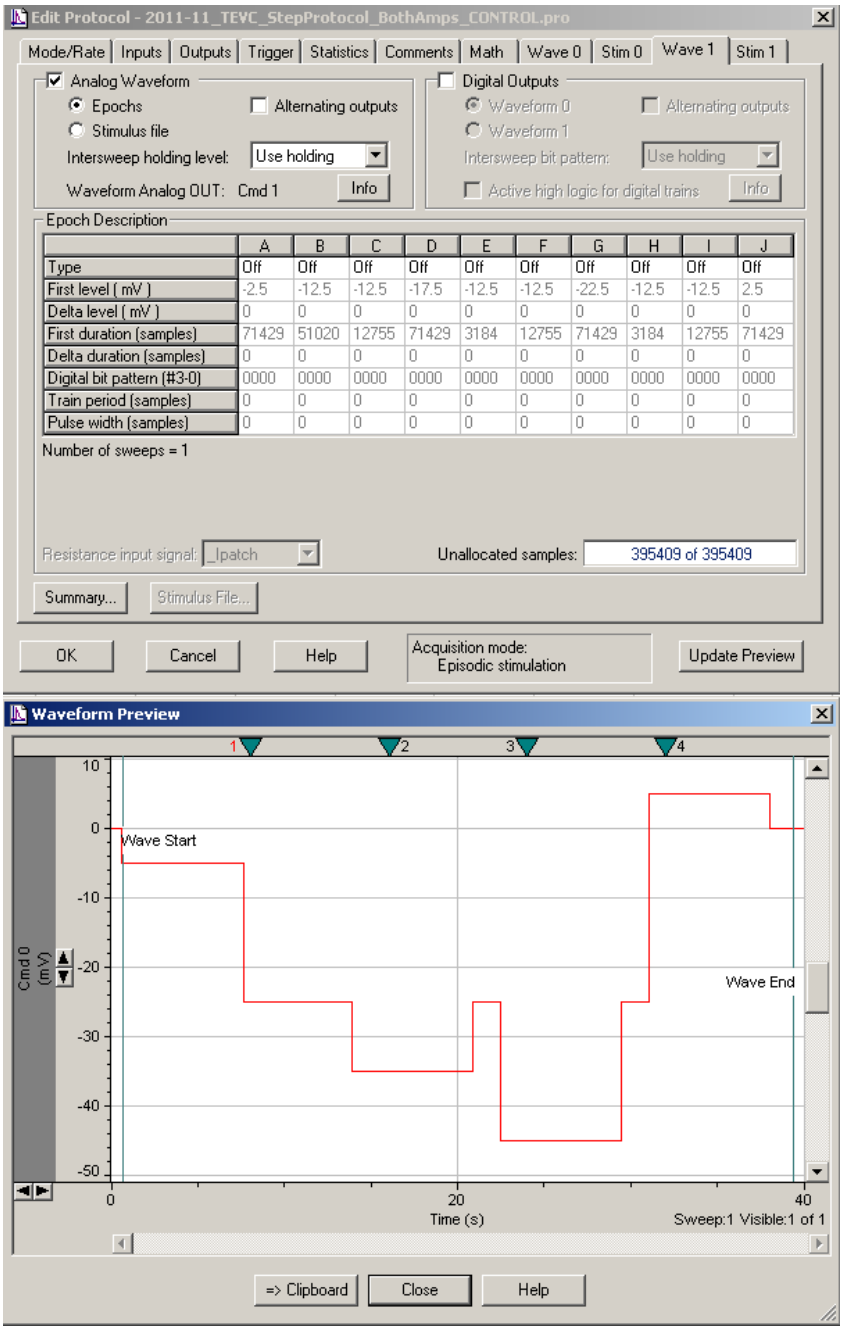

Figure 3.6 Clampex voltage step command protocol.

The voltage levels used to command the amplifier to initiate the voltage step protocol is shown (top) for a PD neuron held at -60 mV. The Waveform Preview window (bottom) shows that the voltage level output from the Clampex command adds to the hand-tuned voltage to achieve the desired voltage step protocol levels.

Data analysis

All data analysis and statistical analyses were performed using MATLAB (either r2009a for Windows or r2007a for Mac OSX , The MathWorks).

g_{syn} slopes and Δg_{syn} slopes

LP-to-PD g_{syn} traces were analyzed by fitting a simple least-squares-fit regression line to each epoch as shown in Figure 3.7.

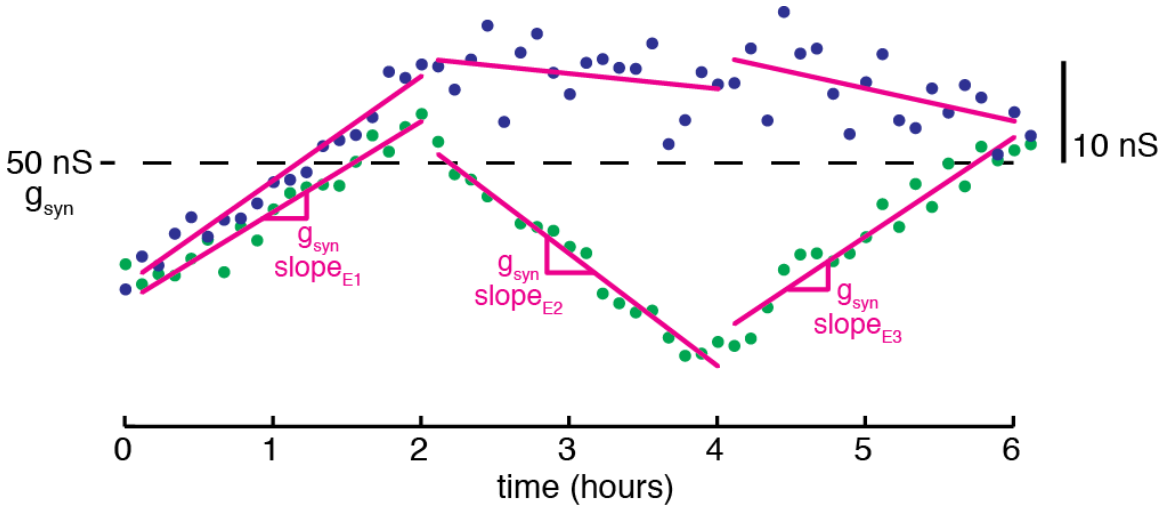

Figure 3.7 Demonstration of the quantification of g_{syn} slopes by epoch.

Two g_{syn} traces are shown from the voltage perturbation study (green is prep. D3; blue is prep. C3.; Figure 2.8*). Each individual data point is acquired from an instance of the voltage step protocol. Magenta lines (shown with labels on the green trace) represent the g_{syn} slope at each of the three epochs. Notice the differences in how well the data points fit the slope lines; e.g. blue points in epochs 2 and 3 show more spread than in epoch 1.*

Figure 3.7 demonstrates that there was also error in the linear slope fits; the green points are very well described by the line in each of the three epochs while the blue points in epochs 2 and 3 show more spread about the line-of-best-fit than in epoch 1. Because of this, the "standard error of the estimate", an error term that describes the spread about the regression line, was calculated according to the equation below.

$$s_{slope} = \sqrt{\frac{\sum\left(y_i - y_i^{fit}\right)^2}{n-2}}$$

where $(y_i - y_i^{fit})$ is each data point's y-distance from the line-of-best-fit and n is the number of data points used in the regression.

In this way, each preparation was described by three g_{syn} slope values (one for each epoch) and three "standard error of the estimate" values (one to describe the spread in each slope fit). To combine slope values for different preparations into a grand mean g_{syn} slope for each epoch (Figure 2.10a and Figure 2.22a), a mean that was weighted according to the standard error of each slope fit was calculated (equation below).

$$\text{weighted mean slope} = \frac{\sum\left(\frac{slope_i}{s_i^2}\right)}{\sum\left(\frac{1}{s_i^2}\right)}$$

where s_i is the "standard error of the estimate" value for each $slope_i$ used in the calculation. The error of the weighted g_{syn} slope mean was calculated using the weighted mean error equation below.

$$s_{\substack{weighted\ mean \\ slope}} = \sqrt{\frac{1}{\sum\left(\frac{1}{s_i^2}\right)}}$$

I was not only interested in the slope of the g_{syn} trace by epoch, but how that slope changed when a perturbation was applied within each preparation. Therefore, the change in gsyn slope (Δg_{syn} slope) was calculated (Figure 2.10b and Figure 2.22b by taking the difference in the slopes from adjacent epochs (g_{syn} $slope_{E2}$ – g_{syn} $slope_{E1}$ and g_{syn} $slope_{E3}$ – g_{syn} $slope_{E2}$. See Figure 3.7). Again, to incorporate the error associated with each measured slope, the error in the Δg_{syn} slopes was computed using error propagation methods where the propagated error for a difference of two values equals the square root of the squared sum of the individual errors.

$$s_{a-b} = \sqrt{s_a^2 + s_b^2}$$

95% confidence intervals were computed for weighted g_{syn} slope means and Δg_{syn} slopes using the inverse of Student's T cumulative distribution function. In

Figure 2.10 and Figure 2.22 non-overlapping confidence intervals were considered significant. Confidence intervals were used because they simplified the process of assessing significant differences between weighted means with propagated standard error terms.

Homeostasis metrics

Homeostasis metrics for every attribute except E_{syn} were calculated by measuring the activity during the six-minute intervals in between applications of the voltage step protocol. For E_{syn}, measurements could only be taken during the voltage step protocol.

Peak I_{syn} traces (as demonstrated in Figure 2.12c) were determined by breaking each six-minute interval into six one-minute-long sections. For each minute-long section, all of the LP-spike-triggered synaptic currents were averaged together to get an average IPSC trace. The peak values for each of the six minute-long sections were recorded and the median peak I_{syn} value was used as the single peak I_{syn} value for that six-minute time period (for instance, for the $E1_{late}$ time period shown in Figure 2.13).

Network activity attributes such as the pacemaker cycle period, burst duration, duty cycle, delay and phase, were tabulated for each burst using a threshold to determine spike times in the lvn and pdn (if the pdn was available).

Each attribute's tabulated measurements were passed through a median filter of thirty samples. The overall median value for each activity attribute over the six-minute intervals was then used to get a single attribute value for each time period. These values from the time periods shown in Figure 2.13 were used for the homeostasis metrics for each attribute.

Because I was most concerned with determining whether there was a relationship between ranks, correlations between depolarization- or hyperpolarization-induced changes in network attribute (ieΔ) and Δg_{syn} slopes were determined using Spearman's rho ($p<0.05$). In the percent recovery metric (Figure 2.15), a one-sample t-test was used to determine if means were significantly different from zero ($p<0.05$) and paired sample t-tests were used to determine whether depolarized and hyperpolarized means of the same attribute were significantly different from each other ($p<0.05$).

Computational model of Cl^--dependent homeostatic synaptic regulation

All simulations were done in XPP version 6.10 for Mac OSX (Bard Ermentrout, http://www.math.pitt.edu/~bard/xpp/xpp.html). To construct the model, I used a simple pool model of calcium concentration (Koch and Segev 1998) as a template, replacing the calcium terms with chloride and using terms for a chloride injection current, chloride leak, and the entry of chloride from synaptic channels. The first equation describes how the chloride concentration in the

internal volume of the cell changes depending on how much chloride enters the cell through injection or synaptic and leak channels and how quickly it is transported out of the intracellular pool (by pumping and buffering of Cl^- ions).

$$(1) \qquad \frac{d\,[Cl^-]_{in}}{dt} = \frac{I_{syn} + I_{leak} + I_{inj}}{Fv} - \beta\,([Cl^-]_{in} - [Cl^-]_{min})$$

where F is Faraday's constant (96,485.3365 C/mol), v is the volume of the intracellular compartment (v=0.26808 nL for a spherical cell with an 80 μm diameter), and β=0.0095 is a buffering term which allows the internal chloride concentration $[Cl^-]_{in}$ to relax exponentially toward the minimum chloride concentration, $[Cl^-]_{min}$ = 20 mM, with a time constant 1/ β. The injected current, I_{inj}, was only used in the results shown in Figure 2.19, otherwise it was zero. The leak current was determined using the current equation, ($I = g(V_m - E)$), and g_{leak} was fixed at 52 nS. The synaptic current was also calculated using the current equation but gsyn was not fixed ($g_{syn} = s*\bar{g}_{syn}$) and the maximal synaptic conductance, $\bar{g}_{syn}$, changed dynamically. The pre-synaptic input was a Morris-Lecar oscillator that provided rhythmic activation (from 0 to 1) of the synaptic variable, *s*, approximately every 50 simulation time-steps. The feedback effect of the chloride concentration on the dynamic maximal synaptic conductance is modeled by the second equation, which is an adapted form of an equation modeling activity-dependent regulation of channel densities (LeMasson, Marder et al. 1993):

$$\tau_g \frac{d\bar{g}_{syn}}{dt} = \frac{G_{max}}{1+e^{\gamma([Cl^-]_{in}-[Cl^-]_T)}} - \bar{g}_{syn} \quad (2)$$

In equation 2, the maximal synaptic conductance $\bar{g}_{syn}$ changes dynamically with a time constant τ_g = 60000 simulation time steps (equivalent to ~3 hours experimentally) and a grand maximal conductance value G_{max} = 50 nS depending on how far $[Cl^-]_{in}$ is from the target level of internal chloride concentration, C_T = 25 mM. γ = 500 is a term that determines the slope of the sigmoidal function. I determined the synaptic reversal potential by the Nernst equation using $[Cl^-]_{in}$ and a constant extracellular chloride concentration of 529 mM (the same chloride concentration of the saline that was superfused over the experimental preparations). The XPP code used is shown on the subsequent page.

```
# PRESYNAPTIC
dv/dt=(i+gl*(vl-v)+gk*w*(vk-v)+gca*minf(v)*(vca-v))/c
dw/dt=lamw(v)*(winf(v)-w)
ds/dt=alpha*k(v)*(1-s)-beta*s
minf(v)=.5*(1+tanh((v-v1)/v2))
winf(v)=.5*(1+tanh((v-v3)/v4))
lamw(v)=phi*cosh((v-v3)/(2*v4))
k(v)=1/(1+exp(-(v-vt)/vs))
param vk=-84,vl=-60,vca=120
param i=80,gk=8,gl=2, gca=4, c=20
param v1=-1.2,v2=18,v3=12,v4=17.4,phi=.066666667
param vsyn=120,vt=20,vs=2,alpha=1,beta=.25
# for type II dynamics, use v3=2,v4=30,phi=.04
# for type I dynamics, use v3=12,v4=17.4,phi=.06666667
v(0)=-24.22
w(0)=.305
s(0)=.056

#POSTSYNAPTIC

#CONSTANTS
number z=-1, F=96485.3365, R=8.3145, temp=286.15
parameter Clout=529e-3, taugsyn=60000,Clt=25e-3, Clmin=20e-3, Vpost=-60e-3, Vcell=0.26808,
· buffCell=0.0095, gmax=50, gamma=500, gleak=52, iinj=0

esyn = (R*temp/(z*F))*ln(Clout/ClinCell)
isyn = gsyn*s*(Vpost-esyn)
ileak = gleak*(Vpost-esyn)
gsyn' = ((sigm(ClinCell)*gmax)-gsyn)/taugsyn
sigm(ClinCell) = 1/(1+exp((ClinCell-Clt)*gamma))
ClinCell' = -iinj/(z*F*Vcell)-ileak/(z*F*Vcell)-isyn/(z*F*Vcell)-buffCell*(ClinCell-Clmin)

aux isyn = isyn
aux esyn = esyn
aux ileak = ileak

init gsyn=20, ClinCell=25e-3

# Change value of post-synaptic voltage below.
# Voltage perturbation study
global 1 t-40000 {Vpost=-0.035}
global 1 t-80000 {Vpost=-0.060}

# Change value of post-synaptic chloride injection below
# Iontophoretic injection study
#global 1 t-40000 {iinj=3}
#global 1 t-80000 {iinj=0}

@ total=120000,dt=0.01,method=euler,maxstor=10000000,nout=100,bound=100000000
done
```

CHAPTER 4 :

GENERAL DISCUSSION

Overall summary

In this dissertation, I used a well-studied small neural network, the pyloric network of the crab *Cancer borealis*, as a model neural network with a quantifiable, well-defined pattern of activity. I systematically studied how changes in the strength of a single, identified inhibitory connection in this network – the LP-to-PD synapse – affected various attributes that define the patterned output of the network to determine whether any attributes were likely to be under homeostatic control.

I first investigated the matter in an established pyloric model network database in order to make predictions about how this synapse is expected to affect various quantifiable attributes of network activity. Using two methods of network database analysis, I found that increasing the conductance of the LP-to-PD synapse was expected to have a positive relationship with the network cycle period as well as the delay and phase of the pacemaker burst, but was expected to have a negative relationship with the pacemaker duty cycle. I then tested these predictions in the living system by perturbing post-synaptic voltage levels – and in turn, perturbing these network activity attributes – and measuring the ensuing change in synaptic conductance. I find that the primary response to this network activity perturbation was for the synaptic conductance to decrease following post-synaptic depolarization and subsequently increase in conductance when the depolarized preparations were brought back to baseline voltage. Contrary to expectation, this observed change in

synaptic conductance was not associated with a recovery toward pre-perturbation baseline in any of the perturbed network activity attributes. Upon scrutiny, the properties that seemed most likely to be under homeostatic control were the peak synaptic current level and the synaptic reversal potential.

This led to the hypothesis that a change in an underlying factor of these two synaptic attributes – specifically the intracellular chloride concentration – was the true trigger of the synaptic conductance change we observed and perhaps the true target of the synaptic regulation machinery. I tested this hypothesis by building a single-compartment model post-synaptic neuron that incorporated a chloride-concentration-dependent regulation of synaptic conductance. I showed that the model was able to qualitatively match the experimentally observed trajectories of synaptic conductance, reversal potential, and current, suggesting that the hypothesis could explain the experimental results. Next, I used the computational model to establish a prediction of how the synapse would respond to a targeted perturbation of the post-synaptic neuron's intracellular chloride concentration. I find that, if intracellular chloride were indeed a regulating factor providing negative feedback onto synapses as in the model, the LP-to-PD synaptic conductance should decrease in response to post-synaptic chloride-loading in the living system.

Lastly, I test the prediction in the living system, and show that the synapse reduces in conductance in response to intracellular iontophoretic chloride injection into the post-synaptic neuron, again matching the computational model.

Most previous studies of homeostatic synaptic plasticity have concluded that compensatory changes in synaptic currents following activity perturbations exist to recover target levels of network spiking activity (Turrigiano 2012). Taken together, in this dissertation I provide experimental and computational evidence that this change in inhibitory synaptic conductance appears not to operate with a homeostatic target of network activity, but rather with a homeostatic target of post-synaptic chloride concentration.

Chloride in STG neurons

Several early electrophysiological studies in the crustacean STG focused on characterizing the types of ionic currents present in stomatogastric neurons and the ions that flow through synaptic channels. Interestingly, the descriptions of the response of stomatogastric neurons to perturbations of extra- and intra-cellular chloride concentrations in these studies further supports the hypothesis that the internal chloride concentration is a tightly-regulated cellular property in these neurons.

For example, in a study in a related species *Cancer pagurus*, L-glutamate was iontophoretically applied to an STG neuron before, during, and after intracellular chloride-loading to determine ion permeability (Marder and Paupardin-Tritsch 1978). As in the work presented here, the chloride injection led to an acute depolarization of the inhibitory glutamate receptor reversal potential but was re-

polarized back to baseline within 15 min. A similar finding was reported later for the LP-to-PD synaptic reversal potential after acute chloride-loading into PD in the spiny lobster *Panulirus interruptus* (Eisen and Marder 1982). In *Cancer pagurus*, experiments were also performed in which they manipulated the extracellular saline by replacing 50% of the Cl^- with either isethionate or sulphate and found that the inhibitory glutamate receptor reversal potential again depolarized (Marder and Paupardin-Tritsch 1978). Notably, the authors report that upon acute wash with normal saline, the reversal potential was hyperpolarized beyond control, an effect that lasted from 15-30 min before returning to control levels.

Similar findings were demonstrated in the *Cancer borealis* LP neuron in a later study that showed that reducing extracellular chloride produced a small transient cell depolarization (as predicted by Nernst equation), but quickly changed to a membrane potential hyperpolarization (Golowasch 1990). Thus, Golowasch concluded that one possibility was that "there are active mechanisms that can rapidly modify E_{Cl} and that may be dependent on Cl^- itself", a hypothesis that is consistent with the results presented here.

One compelling consideration is that, though not found in the detailed studies done on spiny lobster inhibitory glutamatergic receptors, which demonstrated "inseparable permeabilities" to chloride and potassium (Eisen and Marder 1982, Cleland 1996), evidence was found in *Cancer pagurus* for a separate potassium-dependent or chloride-dependent inhibitory response upon application

of L-glutamate (Marder and Paupardin-Tritsch 1978). Both potassium- and chloride-dependent responses were activated by L-glutamate and blocked by PTX, suggesting that these may represent very similar, but distinct, receptors with different permeabilities. Thus it is possible that *Cancer pagurus*, and in turn possibly *Cancer borealis*, might actually express different inhibitory glutamatergic receptors for the flux of chloride and for potassium and might do so at varying ratios to effectively vary synaptic strength (due to the different reversal potentials and thus, driving forces of the separate ions) (Cleland 1996).

This thought could explain the differences in synaptic conductance changes I observe for the hyperpolarized preparations, where one particular preparation displayed a very large acute increase in conductance following hyperpolarization (prep. H1), while the other hyperpolarized preparations did not. It is possible that the presumptive chloride-dependent mechanism only targets its negative feedback regulation to one population of inhibitory channels (for instance, the intracellular chloride targets chloride-permeable receptor conductance) and that preparation H1 may happened to have had a high ratio of that particular receptor; thus it displayed a more robust response.

Chloride in other neurons

One can appreciate why it would be important for this (and any) neuron to constrain its levels of intracellular chloride. In the central nervous system and

invertebrate nervous systems, chloride is the primary permeant ion through inhibitory GABA, glycine, and glutamate channels, making it critical for any neuron receiving inhibition to tightly regulate internal chloride levels. For this reason, much recent work has gone into understanding neuronal chloride homeostasis (Blaesse, Airaksinen et al. 2009).

Post-synaptic chloride concentration greatly affects the efficacy of synaptic inhibition (Fiumelli and Woodin 2007, Gonzalez-Islas, Chub et al. 2010, Jedlicka, Deller et al. 2011). Changes in the efficacy of network inhibition, in turn, can have profound effects on mammalian brain function. For example, some drugs such as benzodiazepines – which can be sleep-inducing or can be used to treat anxiety, panic disorders and epilepsy – act though GABA-A receptor binding that increases the receptor's affinity for GABA, thereby increasing chloride-mediated inhibition (Belelli and Lambert 2005, Rudolph and Mohler 2006). There is also evidence that the effects of alcohol on brain function are caused by increases in GABAergic neurotransmission (Lobo and Harris 2008), possibly mediated by a stimulation of neurosteroid production that facilitates synaptic inhibition (Belelli and Lambert 2005).

Another example of the importance of internal chloride homeostasis occurs during development. In the developing central nervous system, there is a shift in the chloride reversal potential from depolarizing to hyperpolarizing that is mediated by differential expression of chloride co-transporters. Immature neurons

express higher levels of the NKCC1 Na-K-Cl co-transporter, which accumulates chloride intracellularly and actually leads to an excitatory chloride reversal potential. Mature neurons preferentially express the KCC2 K-Cl co-transporter, which extrudes chloride and establishes a hyperpolarized inhibitory reversal potential (Ben-Ari 2002, Blaesse, Airaksinen et al. 2009). The depolarizing effect of high levels of internal chloride is generally thought to underlie the large bursts of spontaneous network activity that are often seen in the immature nervous system (Marchetti, Tabak et al. 2005).

The co-transporters that establish these differential chloride concentrations are also targets of regulation themselves. For example, members of the With No K = lysine (WNK) family of protein kinases promote accumulation of chloride in neurons by reciprocally activating NKCC1 and inhibiting KCC2 (Rinehart, Vazquez et al. 2011). Other studies have found regulation of KCC2 by brain-derived neurotrophic factor (Rivera, Li et al. 2002, Wardle and Poo 2003), an effect that is activity-dependent (Chamma, Chevy et al. 2012). The fact that there are several cellular regulatory mechanisms to ensure a stable intracellular chloride concentration underscores its importance for proper neuronal function.

In general, mammalian pathological conditions such as neuropathic pain (Coull, Beggs et al. 2005) and epilepsy (Rivera, Li et al. 2002, Huberfeld, Wittner et al. 2007) have been associated with intracellular chloride dysregulation or GABA channel dysfunction (Kullmann 2010), making the regulation of internal chloride

concentration by synaptic conductance a topic of importance as a possible therapeutic avenue as well (De Koninck 2007).

Transduction of intracellular chloride signal

Although it is unclear what factors transduce the change in $[Cl^-]_{in}$ to a change in synaptic conductance in the PD neuron, potential mechanisms exist in other systems. Several chloride-dependent neuronal factors exist that may represent possible effectors in a chloride-dependent pathway (Duran, Thompson et al. 2010) such as the aforementioned WNK family of kinases, which have putative chloride-sensing potential and have been shown to participate in pathways of chloride homeostasis (Verissimo and Jordan 2001, de Los Heros, Kahle et al. 2006, Kahle, Rinehart et al. 2006, Garzon-Muvdi, Pacheco-Alvarez et al. 2007, Pacheco-Alvarez and Gamba 2011, Rinehart, Vazquez et al. 2011). Other work finds that chloride can act as an intracellular messenger with effects on the timing of GABA and glycine receptor deactivation through direct channel action (Houston, Bright et al. 2009, Moroni, Biro et al. 2011). Additionally, a recent study shows that chloride can influence the expression of $GABA_A$ receptor subunits (Succol, Fiumelli et al. 2012), which can affect transmission levels. Taken together, there is accumulating evidence to suggest that chloride can be considered an important intracellular signaling molecule, which can initialize an intracellular cascade and, in this work, I show that one target of such a potential chloride-dependent pathway may be the particular inhibitory synaptic conductance through which chloride itself flows.

As it is unclear whether chloride acts through direct channel action or through a chloride-dependent pathway in the PD neuron, future work is needed to determine the mechanism of transduction.

Is electrical activity the true target of homeostatic synaptic plasticity? (revisited)

As with any negative-feedback control system, it is important to know the target set-point of the system to understand and appreciate its function. As I discussed in the introduction, there is growing evidence that in some systems, the homeostatic form of synaptic plasticity is not induced by exclusive changes in post-synaptic electrical activity. In fact, work from the developing chick embryo shows that blocking GABAergic neurotransmission, and in turn affecting $[Cl^-]_{in}$, while maintaining relatively normal network activity can trigger scaling of GABAergic and AMPAergic post-synaptic currents (Wilhelm and Wenner 2008, Gonzalez-Islas, Chub et al. 2010). Teasing apart these homeostatic targets (either electrical activity or neurotransmission levels) is complicated by the fact that in many prior studies where activity deprivation induced synaptic scaling, spike-mediated neurotransmission was eliminated as well due to the blocking of network spikes – such as in (Lissin, Gomperts et al. 1998, O'Brien, Kamboj et al. 1998, Turrigiano, Leslie et al. 1998, Kilman, van Rossum et al. 2002, Gonzalez-Islas and Wenner 2006, Hartman, Pal et al. 2006, Stellwagen and Malenka 2006).

The work I present here appears consistent with a target level of neurotransmission assessed with an $[Cl^-]_{in}$ proxy and thus, adds to the hypothesis that neurons may homeostatically regulate synaptic strengths on an input- or synapse-specific basis (Davis and Goodman 1998, Sutton, Ito et al. 2006, Sutton and Schuman 2006, Hou, Zhang et al. 2008, Kim and Tsien 2008, Jakawich, Nasser et al. 2010, Beique, Na et al. 2011, Deeg and Aizenman 2011). This leaves open the possibility that altered synaptic current levels may have been the driver of synaptic scaling in these prior studies of activity-deprivation-induced synaptic scaling. It also supports the idea that a cell-wide "global" synaptic scaling rule may, in fact, be due to a combination of every input synapse to a cell being locally regulated according to its change in transmission level. Together, the work presented in this dissertation, along with the previously referenced studies, provides growing evidence that homeostatic synaptic plasticity may not have a set level of cell-wide or network-wide electrical activity as its homeostatic target as was previously widely assumed.

Future directions

This work provides evidence that inhibitory glutamatergic synaptic strength in the LP-to-PD synapse of the crab *Cancer borealis* is dependent on intracellular chloride, either directly or through a chloride-sensitive pathway. This finding raises many questions, some of which can be addressed in this model system.

First, though these studies are consistent with the hypothesis that the PD neuron might use intracellular chloride concentration as a proxy to establish a target level of synaptic current near synaptic sites, future work will be needed to distinguish whether these changes in synaptic conductance are synapse specific (suggestive of local or quasi-local regulation machinery) or whether they are cell-wide.

One way to test this difference could be done in the *Cancer borealis* pyloric network if other synapses in the circuit exhibit the same synaptic plasticity as I demonstrated at the LP-to-PD synapse. If LP or PY regulate synaptic conductance in the same manner, then it could be possible to determine if both the chemical inputs they receive change in strength by the same factor. For instance, if one were to record synaptic currents and calculate synaptic conductances in the same manner as I have, but from a PY neuron in *Cancer borealis*, this question might be summarily addressed.

As one can see from Figure 1.4, PY receives inhibitory input from both AB and LP in *Cancer borealis*. In lobster, this connectivity diagram is slightly different; the PD neurons make cholinergic inhibitory connections onto PY and LP as well, but the synapses to LP and PY arising from the PD neurons seem to be very weak or absent in *Cancer borealis* (unpublished observations). Therefore, I stress that performing this experiment in *Cancer borealis* may make the experiments more readily interpretable. Again one could take advantage of the relative simplicity of

the pyloric network: there is a single AB neuron and a single LP neuron as the pre-synaptic inputs onto the PYs.

The proposed experimental design is as follows: impale one of the post-synaptic PY neurons with two electrodes and impale the pre-synaptic LP neuron with a single electrode. Hold the PY neuron at a baseline membrane potential in two-electrode voltage clamp with voltage step protocols applied at regular intervals to gather g_{syn}s exactly as I have done in the experimental work presented here. Because one would want to measure the ratio of AB-to-PY g_{syn} to LP-to-PY g_{syn}, one would need to measure average inhibitory post-synaptic currents triggered from spikes emanating from both AB and LP during the voltage step protocol (extracellular PD spikes might suffice for timing).

For this proposed experiment, there would not be any perturbation to the post-synaptic PY, but rather to the pre-synaptic LP neuron. During the perturbation epoch, the LP would be strongly hyperpolarized so as to not allow inhibitory transmission at LP-to-PY sites. Naturally, one would need to relieve LP of the strong hyperpolarization during the voltage step protocol to gather synaptic currents at the different voltage levels and compute a g_{syn} value. As has been observed previously (Nadim, Zhao et al. 2011), strong LP hyperpolarization should not significantly alter the pacemaker cycle period, so inhibitory transmission at AB-to-PY sites should remain unchanged.

Using this experimental design, it may be possible to determine whether the conductances of synaptic connections onto PY are all regulated by a cell-wide established factor or by an input specific mechanism by examining the ratio of AB-to-PY g_{syn} to LP-to-PY g_{syn} over time. I imagine several possible outcomes.

First, there may be no change in either AB-to-PY or LP-to-PY g_{syn}. This could occur if the reduction in inhibitory transmission at LP-to-PY sites was not sufficient to perturb internal chloride levels to activate a regulatory change in g_{syn}, or if, unlike in PD, there happens to be no Cl^--dependent synaptic regulatory mechanism in PY.

The second outcome could be that LP-to-PY g_{syn} changes (the anticipated change would be an increase in LP-to-PY g_{syn} after an acute reduction in LP-to-PY synaptic current) while AB-to-PY g_{syn} does not. This would suggest that regulation occurs as an input specific process and only affects LP-to-PY g_{syn} because that was the only synapse that experienced reduced inhibitory transmission.

A third possible outcome is that both LP-to-PY and AB-to-PY g_{syn}s change in the same way. This would suggest that the need for synaptic conductance adjustments might be made on a cell-wide basis and the reduced chloride entry through LP-to-PY sites triggered a comparable change in g_{syn} at every synapse (as is the general understanding in synaptic scaling).

Of course other possibilities exist in which the synaptic conductances change

in unexpected ways (e.g. if hyperpolarizing LP causes a marked decrease in LP-to-PY g_{syn} instead of the expected increase), or only AB-to-PY conductance changes. These results would be more difficult to interpret and would require further experimentation.

Another future direction would be to address questions about the expected spatial and temporal gradients of chloride that could lead to a compartmentalized synapse-specific regulation mechanism. To begin to answer these questions, two approaches could be employed.

First, a multicompartmental model of the PD neuron could be built based on realistic morphological data in an approach similar to one used for hippocampal cells (Jedlicka, Deller et al. 2011). Such a model could incorporate chloride diffusion dynamics along with the realistic morphology and could be used to establish whether distinct intracellular chloride concentration domains are possible given these parameters.

Another approach could be to attempt to visualize differences in chloride concentration in the living system using genetically encoded biosensors that depend on the cell's transcription and translation machinery to express functional protein sensors (Palmer, Qin et al. 2011). At present there are three appealing genetically encoded chloride indictors. Two of them, Clomeleon (Kuner and Augustine 2000) and Cl-sensor (Markova, Réal et al. 2007, Markova, Mukhtarov et al. 2008), are

molecules consisting of two fused fluorescent proteins that allow for ratiometric estimation of intracellular chloride (Bregestovski, Waseem et al. 2009). A recently developed biosensor, mbYFPQS, features a yellow fluorescent protein variant that is mutated to target the protein to the plasma membrane, allowing for the biosensor to estimate internal chloride concentrations without the risk of unintended leakage or diffusion of the fluorescent protein into a recording electrode (Watts, Suchland et al. 2012).

Therefore, it might be feasible to introduce one of these chloride indicators into PD, potentially through microinjection, to visualize subcellular chloride concentrations and determine if such chloride concentration microdomains exist in PD processes.

Final words

Taken together, this dissertation provides a novel look at how a particular identified inhibitory synapse dynamically responds to perturbation as it happens and presents evidence that this synapse does not homeostatically regulate network activity, but rather post-synaptic chloride concentration. I show that the induced change in synaptic conductance can be triggered by a targeted iontophoretic injection of chloride into the post-synaptic neuron, without disrupting network activity.

In this work, I hope to provide a clearer understanding of how homeostatic synaptic plasticity mechanisms are triggered in the STG and show evidence that the most likely target of the resultant changes to synaptic conductance is the level of inhibitory synaptic current as measured by an internal chloride concentration proxy.

Such a mechanism, if extended to other systems, could confer a greater understanding of how neurons use homeostatic plasticity of inhibitory synapses to establish stable internal chloride concentrations. It could aid in the understanding of how neurons respond dynamically to increases in inhibitory transmission caused by external substances such as benzodiazepines (Rudolph and Mohler 2006), alcohol (Lobo and Harris 2008), or endogenously produced neurosteriods (Belelli and Lambert 2005). Thus, a deeper level of knowledge of this topic has clinical relevance as well, as improper transmembrane distributions of chloride ions are thought to be responsible for neuropathic pain, some forms of epilepsy, and pathological responses to injury (De Koninck 2007).

REFERENCES

Abbott, L. F. and S. B. Nelson (2000). "Synaptic plasticity: taming the beast." Nat Neurosci **3 Suppl**: 1178-1183.

Ayers, J. L. and A. I. Selverston (1977). "Synaptic control of an endogenous pacemaker network." J Physiol (Paris) **73**(4): 453-461.

Ayers, J. L. and A. I. Selverston (1979). "Monosynaptic entrainment of an endogenous pacemaker network: a cellular mechanism for von Holst's magnet effect." Journal of Comparative Physiology A: Neuroethology, Sensory, Neural, and Behavioral Physiology **129**(1): 5-17.

Beique, J. C., Y. Na, D. Kuhl, P. F. Worley and R. L. Huganir (2011). "Arc-dependent synapse-specific homeostatic plasticity." Proc Natl Acad Sci U S A **108**(2): 816-821.

Belelli, D. and J. J. Lambert (2005). "Neurosteroids: endogenous regulators of the GABA(A) receptor." Nat Rev Neurosci **6**(7): 565-575.

Ben-Ari, Y. (2002). "Excitatory actions of gaba during development: the nature of the nurture." Nat Rev Neurosci **3**(9): 728-739.

Ben-Ari, Y., I. Khalilov, K. T. Kahle and E. Cherubini (2012). "The GABA excitatory/inhibitory shift in brain maturation and neurological disorders." Neuroscientist **18**(5): 467-486.

Bergquist, S., D. K. Dickman and G. W. Davis (2010). "A hierarchy of cell intrinsic and target-derived homeostatic signaling." Neuron **66**(2): 220-234.

Blaesse, P., M. S. Airaksinen, C. Rivera and K. Kaila (2009). "Cation-chloride cotransporters and neuronal function." Neuron **61**(6): 820-838.

Bregestovski, P., T. Waseem and M. Mukhtarov (2009). "Genetically encoded optical sensors for monitoring of intracellular chloride and chloride-selective channel activity." Front Mol Neurosci **2**: 15.

Bucher, D., A. A. Prinz and E. Marder (2005). "Animal-to-animal variability in motor pattern production in adults and during growth." J Neurosci **25**(7): 1611-1619.

Burrone, J., M. O'Byrne and V. N. Murthy (2002). "Multiple forms of synaptic plasticity triggered by selective suppression of activity in individual neurons." Nature **420**(6914): 414-418.

Cannon, W. B. (1932). The wisdom of the body, Norton, New York.

Chamma, I., Q. Chevy, J. C. Poncer and S. Levi (2012). "Role of the neuronal K-Cl co-transporter KCC2 in inhibitory and excitatory neurotransmission." Front Cell Neurosci **6**: 5.

Cleland, T. A. (1996). "Inhibitory glutamate receptor channels." Mol Neurobiol **13**(2): 97-136.

Cleland, T. A. and A. I. Selverston (1995). "Glutamate-gated inhibitory currents of central pattern generator neurons in the lobster stomatogastric ganglion." J Neurosci **15**(10): 6631-6639.

Cleland, T. A. and A. I. Selverston (1997). "Dopaminergic modulation of inhibitory glutamate receptors in the lobster stomatogastric ganglion." J Neurophysiol **78**(6): 3450-3452.

Cleland, T. A. and A. I. Selverston (1998). "Inhibitory glutamate receptor channels in cultured lobster stomatogastric neurons." J Neurophysiol **79**(6): 3189-3196.

Coull, J. A., S. Beggs, D. Boudreau, D. Boivin, M. Tsuda, K. Inoue, C. Gravel, M. W. Salter and Y. De Koninck (2005). "BDNF from microglia causes the shift in neuronal anion gradient underlying neuropathic pain." Nature **438**(7070): 1017-1021.

Davis, G. W. and C. S. Goodman (1998). "Genetic analysis of synaptic development and plasticity: homeostatic regulation of synaptic efficacy." Curr Opin Neurobiol **8**(1): 149-156.

Davis, G. W. and C. S. Goodman (1998). "Synapse-specific control of synaptic efficacy at the terminals of a single neuron." Nature **392**(6671): 82-86.

De Koninck, Y. (2007). "Altered chloride homeostasis in neurological disorders: a new target." Curr Opin Pharmacol **7**(1): 93-99.

de Los Heros, P., K. T. Kahle, J. Rinehart, N. A. Bobadilla, N. Vazquez, P. San Cristobal, D. B. Mount, R. P. Lifton, S. C. Hebert and G. Gamba (2006). "WNK3 bypasses the tonicity requirement for K-Cl cotransporter activation via a phosphatase-dependent pathway." Proc Natl Acad Sci U S A **103**(6): 1976-1981.

Deeg, K. E. and C. D. Aizenman (2011). "Sensory modality-specific homeostatic plasticity in the developing optic tectum." Nat Neurosci **14**(5): 548-550.

Desai, N. S., R. H. Cudmore, S. B. Nelson and G. G. Turrigiano (2002). "Critical periods for experience-dependent synaptic scaling in visual cortex." Nat Neurosci **5**(8): 783-789.

Desai, N. S., L. C. Rutherford and G. G. Turrigiano (1999). "Plasticity in the intrinsic excitability of cortical pyramidal neurons." Nat Neurosci **2**(6): 515-520.

Duran, C., C. H. Thompson, Q. Xiao and H. C. Hartzell (2010). "Chloride channels: often enigmatic, rarely predictable." Annu Rev Physiol **72**: 95-121.

Eisen, J. S. and E. Marder (1982). "Mechanisms underlying pattern generation in lobster stomatogastric ganglion as determined by selective inactivation of identified neurons. III. Synaptic connections of electrically coupled pyloric neurons." J Neurophysiol **48**(6): 1392-1415.

Fiumelli, H. and M. A. Woodin (2007). "Role of activity-dependent regulation of neuronal chloride homeostasis in development." Curr Opin Neurobiol **17**(1): 81-86.

Garzon-Muvdi, T., D. Pacheco-Alvarez, K. B. Gagnon, N. Vazquez, J. Ponce-Coria, E. Moreno, E. Delpire and G. Gamba (2007). "WNK4 kinase is a negative regulator of K+-Cl- cotransporters." Am J Physiol Renal Physiol **292**(4): F1197-1207.

Goaillard, J. M., A. L. Taylor, D. J. Schulz and E. Marder (2009). "Functional consequences of animal-to-animal variation in circuit parameters." Nat Neurosci **12**(11): 1424-1430.

Golowasch, J. (1990). Characterization of a Stomatogastric Ganglion Neuron. A Biophysical and a Mathematical Description. PhD, Brandeis University.

Golowasch, J., L. F. Abbott and E. Marder (1999). "Activity-dependent regulation of potassium currents in an identified neuron of the stomatogastric ganglion of the crab Cancer borealis." J Neurosci **19**(20): RC33.

Golowasch, J., M. Casey, L. F. Abbott and E. Marder (1999). "Network stability from activity-dependent regulation of neuronal conductances." Neural Comput **11**(5): 1079-1096.

Gonzalez-Islas, C., N. Chub, M. A. Garcia-Bereguiain and P. Wenner (2010). "GABAergic synaptic scaling in embryonic motoneurons is mediated by a shift in the chloride reversal potential." J Neurosci **30**(39): 13016-13020.

Gonzalez-Islas, C. and P. Wenner (2006). "Spontaneous network activity in the embryonic spinal cord regulates AMPAergic and GABAergic synaptic strength." Neuron **49**(4): 563-575.

Graubard, K., J. A. Raper and D. K. Hartline (1980). "Graded synaptic transmission between spiking neurons." Proc Natl Acad Sci U S A **77**(6): 3733-3735.

Graubard, K., J. A. Raper and D. K. Hartline (1983). "Graded synaptic transmission between identified spiking neurons." J Neurophysiol **50**(2): 508-521.

Haedo, R. J. and J. Golowasch (2006). "Ionic Mechanism Underlying Recovery of Rhythmic Activity in Adult Isolated Neurons." Journal of Neurophysiology **96**(4): 1860-1876.

Harris-Warrick, R. M., E. Marder, A. I. Selverston and M. Moulins (1992). Dynamic biological networks: the stomatogastric nervous system, Mit Press.

Hartman, K. N., S. K. Pal, J. Burrone and V. N. Murthy (2006). "Activity-dependent regulation of inhibitory synaptic transmission in hippocampal neurons." Nat Neurosci **9**(5): 642-649.

Hebb, D. O. (1949). The organization of behavior: A neuropsychological theory, Wiley & Sons.

Henry, F. E., A. J. McCartney, R. Neely, A. S. Perez, C. J. Carruthers, E. L. Stuenkel, K. Inoki and M. A. Sutton (2012). "Retrograde changes in presynaptic function driven by dendritic mTORC1." J Neurosci **32**(48): 17128-17142.

Hou, Q., D. Zhang, L. Jarzylo, R. L. Huganir and H. Y. Man (2008). "Homeostatic regulation of AMPA receptor expression at single hippocampal synapses." Proceedings of the National Academy of Sciences of the United States of America **105**(2): 775-780.

Houston, C. M., D. P. Bright, L. G. Sivilotti, M. Beato and T. G. Smart (2009). "Intracellular chloride ions regulate the time course of GABA-mediated inhibitory synaptic transmission." J Neurosci **29**(33): 10416-10423.

Huberfeld, G., L. Wittner, S. Clemenceau, M. Baulac, K. Kaila, R. Miles and C. Rivera (2007). "Perturbed chloride homeostasis and GABAergic signaling in human temporal lobe epilepsy." J Neurosci **27**(37): 9866-9873.

Ibata, K., Q. Sun and G. G. Turrigiano (2008). "Rapid synaptic scaling induced by changes in postsynaptic firing." Neuron **57**(6): 819-826.

Jakawich, S. K., H. B. Nasser, M. J. Strong, A. J. McCartney, A. S. Perez, N. Rakesh, C. J. Carruthers and M. A. Sutton (2010). "Local presynaptic activity gates homeostatic changes in presynaptic function driven by dendritic BDNF synthesis." Neuron **68**(6): 1143-1158.

Jedlicka, P., T. Deller, B. S. Gutkin and K. H. Backus (2011). "Activity-dependent intracellular chloride accumulation and diffusion controls GABA(A) receptor-mediated synaptic transmission." Hippocampus **21**(8): 885-898.

Johnson, B. R., J. M. Brown, M. D. Kvarta, J. Y. Lu, L. R. Schneider, F. Nadim and R. M. Harris-Warrick (2011). "Differential modulation of synaptic strength and timing regulate synaptic efficacy in a motor network." J Neurophysiol **105**(1): 293-304.

Kahle, K. T., J. Rinehart, A. Ring, I. Gimenez, G. Gamba, S. C. Hebert and R. P. Lifton (2006). "WNK protein kinases modulate cellular Cl- flux by altering the phosphorylation state of the Na-K-Cl and K-Cl cotransporters." Physiology (Bethesda) **21**: 326-335.

Khorkova, O. and J. Golowasch (2007). "Neuromodulators, not activity, control coordinated expression of ionic currents." J Neurosci **27**(32): 8709-8718.

Kilman, V., M. C. van Rossum and G. G. Turrigiano (2002). "Activity deprivation reduces miniature IPSC amplitude by decreasing the number of postsynaptic GABA(A) receptors clustered at neocortical synapses." J Neurosci **22**(4): 1328-1337.

Kilman, V. L. and E. Marder (1996). "Ultrastructure of the stomatogastric ganglion neuropil of the crab, Cancer borealis." J Comp Neurol **374**(3): 362-375.

Kim, J. and R. W. Tsien (2008). "Synapse-specific adaptations to inactivity in hippocampal circuits achieve homeostatic gain control while dampening network reverberation." Neuron **58**(6): 925-937.

Koch, C. and I. Segev (1998). Methods in neuronal modeling: from ions to networks, MIT press.

Kullmann, D. M. (2010). "Neurological channelopathies." Annu Rev Neurosci **33**: 151-172.

Kuner, T. and G. J. Augustine (2000). "A genetically encoded ratiometric indicator for chloride: capturing chloride transients in cultured hippocampal neurons." Neuron **27**(3): 447-459.

LeMasson, G., E. Marder and L. F. Abbott (1993). "Activity-dependent regulation of conductances in model neurons." Science **259**(5103): 1915-1917.

Lissin, D. V., S. N. Gomperts, R. C. Carroll, C. W. Christine, D. Kalman, M. Kitamura, S. Hardy, R. A. Nicoll, R. C. Malenka and M. von Zastrow (1998). "Activity differentially regulates the surface expression of synaptic AMPA and NMDA glutamate receptors." Proc Natl Acad Sci U S A **95**(12): 7097-7102.

Lobo, I. A. and R. A. Harris (2008). "GABA(A) receptors and alcohol." Pharmacol Biochem Behav **90**(1): 90-94.

Luther, J. A., A. A. Robie, J. Yarotsky, C. Reina, E. Marder and J. Golowasch (2003). "Episodic bouts of activity accompany recovery of rhythmic output by a neuromodulator- and activity-deprived adult neural network." J Neurophysiol **90**(4): 2720-2730.

MacLean, J. N., Y. Zhang, B. R. Johnson and R. M. Harris-Warrick (2003). "Activity-independent homeostasis in rhythmically active neurons." Neuron **37**(1): 109-120.

Mamiya, A. and F. Nadim (2004). "Dynamic interaction of oscillatory neurons coupled with reciprocally inhibitory synapses acts to stabilize the rhythm period." J Neurosci **24**(22): 5140-5150.

Manor, Y., F. Nadim, L. F. Abbott and E. Marder (1997). "Temporal dynamics of graded synaptic transmission in the lobster stomatogastric ganglion." J Neurosci **17**(14): 5610-5621.

Marchetti, C., J. Tabak, N. Chub, M. J. O'Donovan and J. Rinzel (2005). "Modeling Spontaneous Activity in the Developing Spinal Cord Using Activity-Dependent Variations of Intracellular Chloride." The Journal of Neuroscience **25**(14): 3601-3612.

Marder, E. (1998). "From biophysics to models of network function." Annu Rev Neurosci **21**: 25-45.

Marder, E. and D. Bucher (2007). "Understanding circuit dynamics using the stomatogastric nervous system of lobsters and crabs." Annu Rev Physiol **69**: 291-316.

Marder, E. and R. L. Calabrese (1996). "Principles of rhythmic motor pattern generation." Physiol Rev **76**(3): 687-717.

Marder, E. and J. S. Eisen (1984). "Transmitter identification of pyloric neurons: electrically coupled neurons use different transmitters." J Neurophysiol **51**(6): 1345-1361.

Marder, E. and J. M. Goaillard (2006). "Variability, compensation and homeostasis in neuron and network function." Nat Rev Neurosci **7**(7): 563-574.

Marder, E. and D. Paupardin-Tritsch (1978). "The Pharmacological Properties of Some Crustacean Neuronal Acetylcholine, Gamma-Aminobutyric Acid, and L-Glutamate Responses." Journal of Physiology-London **280**(Jul): 213-236.

Marder, E. and A. A. Prinz (2002). "Modeling stability in neuron and network function: the role of activity in homeostasis." Bioessays **24**(12): 1145-1154.

Markova, O., M. Mukhtarov, E. Real, Y. Jacob and P. Bregestovski (2008). "Genetically encoded chloride indicator with improved sensitivity." J Neurosci Methods **170**(1): 67-76.

Markova, O., E. Réal, Y. Jacob, M. Mukhtarov and P. Bregestovski (2007). "A genetically encoded indicator for monitoring intracellular chloride." Neurophysiology **39**(4-5): 332-333.

Moroni, M., I. Biro, M. Giugliano, R. Vijayan, P. C. Biggin, M. Beato and L. G. Sivilotti (2011). "Chloride ions in the pore of glycine and GABA channels shape the time course and voltage dependence of agonist currents." J Neurosci **31**(40): 14095-14106.

Nadim, F., S. Zhao and A. Bose (2012). "A PRC description of how inhibitory feedback promotes oscillation stability." Phase Response Curves in Neuroscience: 399-417.

Nadim, F., S. Zhao, L. Zhou and A. Bose (2011). "Inhibitory feedback promotes stability in an oscillatory network." J Neural Eng **8**(6): 065001.

O'Brien, R. J., S. Kamboj, M. D. Ehlers, K. R. Rosen, G. D. Fischbach and R. L. Huganir (1998). "Activity-dependent modulation of synaptic AMPA receptor accumulation." Neuron **21**(5): 1067-1078.

Oprisan, S. A., A. A. Prinz and C. C. Canavier (2004). "Phase resetting and phase locking in hybrid circuits of one model and one biological neuron." Biophys J **87**(4): 2283-2298.

Pacheco-Alvarez, D. and G. Gamba (2011). "WNK3 is a putative chloride-sensing kinase." Cell Physiol Biochem **28**(6): 1123-1134.

Palmer, A. E., Y. Qin, J. G. Park and J. E. McCombs (2011). "Design and application of genetically encoded biosensors." Trends Biotechnol **29**(3): 144-152.

Pratt, K. G. and C. D. Aizenman (2007). "Homeostatic regulation of intrinsic excitability and synaptic transmission in a developing visual circuit." J Neurosci **27**(31): 8268-8277.

Prinz, A., D. Bucher and E. Marder (2004). "Similar network activity from disparate circuit parameters." Nature Neuroscience **7**(12): 1345-1352.

Prinz, A. A., C. P. Billimoria and E. Marder (2003). "Alternative to hand-tuning conductance-based models: construction and analysis of databases of model neurons." J Neurophysiol **90**(6): 3998-4015.

Prinz, A. A., V. Thirumalai and E. Marder (2003). "The functional consequences of changes in the strength and duration of synaptic inputs to oscillatory neurons." J Neurosci **23**(3): 943-954.

Ransdell, J. L., S. S. Nair and D. J. Schulz (2012). "Rapid homeostatic plasticity of intrinsic excitability in a central pattern generator network stabilizes functional neural network output." J Neurosci **32**(28): 9649-9658.

Rinehart, J., N. Vazquez, K. T. Kahle, C. A. Hodson, A. M. Ring, E. E. Gulcicek, A. Louvi, N. A. Bobadilla, G. Gamba and R. P. Lifton (2011). "WNK2 kinase is a novel regulator of essential neuronal cation-chloride cotransporters." J Biol Chem **286**(34): 30171-30180.

Rivera, C., H. Li, J. Thomas-Crusells, H. Lahtinen, T. Viitanen, A. Nanobashvili, Z. Kokaia, M. S. Airaksinen, J. Voipio, K. Kaila and M. Saarma (2002). "BDNF-induced TrkB activation down-regulates the K+-Cl- cotransporter KCC2 and impairs neuronal Cl- extrusion." J Cell Biol **159**(5): 747-752.

Roffman, R. C., B. J. Norris and R. L. Calabrese (2012). "Animal-to-animal variability of connection strength in the leech heartbeat central pattern generator." J Neurophysiol **107**(6): 1681-1693.

Rudolph, U. and H. Mohler (2006). "GABA-based therapeutic approaches: GABAA receptor subtype functions." Curr Opin Pharmacol **6**(1): 18-23.

Schulz, D. J., J. M. Goaillard and E. Marder (2006). "Variable channel expression in identified single and electrically coupled neurons in different animals." Nat Neurosci **9**(3): 356-362.

Schulz, D. J., J. M. Goaillard and E. E. Marder (2007). "Quantitative expression profiling of identified neurons reveals cell-specific constraints on highly variable levels of gene expression." Proc Natl Acad Sci U S A **104**(32): 13187-13191.

Soden, M. E. and L. Chen (2010). "Fragile X protein FMRP is required for homeostatic plasticity and regulation of synaptic strength by retinoic acid." J Neurosci **30**(50): 16910-16921.

Soto-Trevino, C., K. A. Thoroughman, E. Marder and L. F. Abbott (2001). "Activity-dependent modification of inhibitory synapses in models of rhythmic neural networks." Nat Neurosci **4**(3): 297-303.

Stein, W. (2009). "Modulation of stomatogastric rhythms." J Comp Physiol A Neuroethol Sens Neural Behav Physiol **195**(11): 989-1009.

Stellwagen, D. and R. C. Malenka (2006). "Synaptic scaling mediated by glial TNF-alpha." Nature **440**(7087): 1054-1059.

Succol, F., H. Fiumelli, F. Benfenati, L. Cancedda and A. Barberis (2012). "Intracellular chloride concentration influences the GABAA receptor subunit composition." Nat Commun **3**: 738.

Sutton, M. A., H. T. Ito, P. Cressy, C. Kempf, J. C. Woo and E. M. Schuman (2006). "Miniature neurotransmission stabilizes synaptic function via tonic suppression of local dendritic protein synthesis." Cell **125**(4): 785-799.

Sutton, M. A. and E. M. Schuman (2006). "Dendritic protein synthesis, synaptic plasticity, and memory." Cell **127**(1): 49-58.

Thirumalai, V., A. A. Prinz, C. D. Johnson and E. Marder (2006). "Red pigment concentrating hormone strongly enhances the strength of the feedback to the pyloric rhythm oscillator but has little effect on pyloric rhythm period." J Neurophysiol **95**(3): 1762-1770.

Thoby-Brisson, M. and J. Simmers (1998). "Neuromodulatory inputs maintain expression of a lobster motor pattern-generating network in a modulation-dependent state: evidence from long-term decentralization in vitro." J Neurosci **18**(6): 2212-2225.

Thoby-Brisson, M. and J. Simmers (2000). "Transition to endogenous bursting after long-term decentralization requires De novo transcription in a critical time window." J Neurophysiol **84**(1): 596-599.

Thoby-Brisson, M. and J. Simmers (2002). "Long-term neuromodulatory regulation of a motor pattern-generating network: maintenance of synaptic efficacy and oscillatory properties." J Neurophysiol **88**(6): 2942-2953.

Tobin, A. E. and R. L. Calabrese (2005). "Myomodulin increases Ih and inhibits the NA/K pump to modulate bursting in leech heart interneurons." J Neurophysiol **94**(6): 3938-3950.

Turrigiano, G. G. (1999). "Homeostatic plasticity in neuronal networks: the more things change, the more they stay the same." Trends Neurosci **22**(5): 221-227.

Turrigiano, G. G. (2012). "Homeostatic synaptic plasticity: local and global mechanisms for stabilizing neuronal function." Cold Spring Harb Perspect Biol **4**(1): a005736.

Turrigiano, G. G., L. F. Abbott and E. Marder (1994). "Activity-dependent changes in the intrinsic properties of cultured neurons." Science **264**(5161): 974-977.

Turrigiano, G. G., G. LeMasson and E. Marder (1995). "Selective regulation of current densities underlies spontaneous changes in the activity of cultured neurons." J Neurosci **15**(5 Pt 1): 3640-3652.

Turrigiano, G. G., K. R. Leslie, N. S. Desai, L. C. Rutherford and S. B. Nelson (1998). "Activity-dependent scaling of quantal amplitude in neocortical neurons." Nature **391**(6670): 892-896.

Turrigiano, G. G. and E. Marder (1993). "Modulation of identified stomatogastric ganglion neurons in primary cell culture." J Neurophysiol **69**(6): 1993-2002.

Turrigiano, G. G. and S. B. Nelson (2004). "Homeostatic plasticity in the developing nervous system." Nat Rev Neurosci **5**(2): 97-107.

Verissimo, F. and P. Jordan (2001). "WNK kinases, a novel protein kinase subfamily in multi-cellular organisms." Oncogene **20**(39): 5562-5569.

Wardle, R. A. and M. M. Poo (2003). "Brain-derived neurotrophic factor modulation of GABAergic synapses by postsynaptic regulation of chloride transport." J Neurosci **23**(25): 8722-8732.

Watts, S. D., K. L. Suchland, S. G. Amara and S. L. Ingram (2012). "A sensitive membrane-targeted biosensor for monitoring changes in intracellular chloride in neuronal processes." PLoS One **7**(4): e35373.

Weaver, A. L. and S. L. Hooper (2003). "Follower neurons in lobster (Panulirus interruptus) pyloric network regulate pacemaker period in complementary ways." J Neurophysiol **89**(3): 1327-1338.

Weaver, A. L. and S. L. Hooper (2003). "Relating network synaptic connectivity and network activity in the lobster (Panulirus interruptus) pyloric network." J Neurophysiol **90**(4): 2378-2386.

Wilhelm, J. C., M. M. Rich and P. Wenner (2009). "Compensatory changes in cellular excitability, not synaptic scaling, contribute to homeostatic recovery of embryonic network activity." Proc Natl Acad Sci U S A **106**(16): 6760-6765.

Wilhelm, J. C. and P. Wenner (2008). "GABAA transmission is a critical step in the process of triggering homeostatic increases in quantal amplitude." Proc Natl Acad Sci U S A **105**(32): 11412-11417.

Zhao, S., A. F. Sheibanie, M. Oh, P. Rabbah and F. Nadim (2011). "Peptide neuromodulation of synaptic dynamics in an oscillatory network." J Neurosci **31**(39): 13991-14004.